



FCTUC FACULDADE DE CIÊNCIAS
E TECNOLOGIA
UNIVERSIDADE DE COIMBRA

DEPARTAMENTO DE
ENGENHARIA MECÂNICA

JWL parameters optimization for isentropic THOR prediction and confined underwater blasting generators experiments

Dissertação apresentada para a obtenção do grau de Mestre em Engenharia Mecânica na Especialidade de Energia e Ambiente.

Autor

Joana Ester Vaz Ambrósio

Orientador

José Leandro Simões de Andrade Campos

Júri

Presidente **Doutor Pedro de Figueiredo Vieira Carvalheira**
Professor Auxiliar da Universidade de Coimbra

Doutor José Carlos Miranda Góis
Professor Auxiliar da Universidade de Coimbra

Vogais **Doutor Ricardo António Lopes Mendes**
Professor Auxiliar da Universidade de Coimbra
Doutor José Leandro Simões de Andrade Campos
Professor Associado da Universidade de Coimbra

Coimbra, Setembro, 2013

Aos meus pais e irmã.

Agradecimentos

O trabalho que aqui se apresenta só foi possível graças à colaboração e apoio de algumas pessoas, às quais não posso deixar de prestar o meu reconhecimento.

Por isso, gostaria de começar por agradecer ao meu orientador de tese, Professor Doutor José Leandro Simões de Andrade Campos, pela ajuda que proporcionou, pela oportunidade prática enriquecedora, pela partilha do seu vasto conhecimento e por toda a disponibilidade que demonstrou sempre ao longo do trabalho. Agradeço também aos restantes intervenientes que possibilitaram a realização deste trabalho, ao Sr. João Moreira e Sr. Fernando pelas suas disponibilidades e colaboração na parte prática, e ao Bruno Tavares pela partilha de informação e ao Paulo Santos pelo seu apoio a nível computacional.

Gostaria de agradecer também a todos os meus colegas de laboratório, Jaqueline Marques, Joana Quaresma, João Pimenta e ao Rui Ferreira pelo apoio e pelos momentos de humor e interajuda, bem como a todos os restantes amigos e amigas pela preocupação e apoio que demonstraram. Élia obrigada pelo incentivo e conselhos.

Queria também agradecer a toda a minha família pela ajuda, apoio, compreensão e suporte que me deram ao longo do curso. Rita obrigada pela paciência e ajuda.

A todos, um sincero obrigado.

Abstract

Underwater blasting operations have been, during last decades, subject of research and development of maritime blasting operations, including torpedo studies. Aquarium tests, for the measurement of blasting energy of industrial explosives, are based in studies of confined underwater blast wave generators (WBWG). The current work present the study of the behavior of WBWG, based in two different water plastic containers (25 litres and 1000 litres), having in the center a detonator inside a cylindrical explosive charge. The explosive charges used were ammonium nitrate with fuel oil (ANFO) emulsion and pentaerythritol tetranitrate (PETN) detonating cords (12 g/m). Summarily the theoretical background was review. The explosives detonation properties were predicted using a thermochemical computer code, named THOR. For the expansion of the detonation products of the explosives was applied JWL EoS. JWL fundamentals were review and his parameters were determined and optimized correlating THOR predictions and JWL EoS to a minimum difference with an auxiliary quadratic function. In order to calculate the JWL coefficients, a new numerical method was used. It was based in the evolution of adiabate and isentrope curves, obtained by THOR code, using a function of the Microsoft Excel ® Solver, assuming a few assumptions for Grüneisen coefficient (from the exponential of the adiabatic curve; from the exponential of the isentrope curve at a limit adimensional volume; from the exponential of the total expansion of isentrope curve and, at last; deducted from Handley, 2011). The best results were obtained using the Grüneisen coefficient from the exponential of the total expansion of isentrope curve, which were $\omega = 0.328$ for ANFO emulsion and $\omega = 0.356$ for PETN.

The dimensions and design configurations of the experimental WBWG were presented and also a blast type experiment for 3 g of PETN (detonator No. 8 plus 2.4 g charge of PETN detonation cord) was described. Autodyn 2D and 3D simulations of WBWG were performed using a cubic meter water container (1000 litres) for both explosive. The obtained results show the possibility of having these explosive charges without destruction of WBWG containers. Since water pressure levels, close to plastic walls, under maximum admissible charges, are closed to 6 MPa. It was always observed the elastic deformation of containers wall, under the water shock reflections, changing

from its original cubic shape to a transient spherical one. Additionally the execution procedures of THOR code, Microsoft Excel ® Solver and the interface of Autodyn simulations material input data was presented.

Keywords: WBWG, experimental underwater explosions, ANFO emulsion, PETN detonating cord, thermochemical computer code THOR, optimize JWL EoS parameters, Autodyn predictions of WBWG.

Resumo

As operações de detonação submarinas têm sido, durante as últimas décadas, alvo de pesquisa e desenvolvimento das operações de detonação marítimas, incluindo testes de torpedo, bem como, em testes em piscinas para a medição de energia de detonação de explosivos industriais. O estudo dos geradores de demolição por carga submersa (*WBWG*) tiveram por base nestes conceitos. Com o presente trabalho pretendo apresentar o estudo do comportamento de *WBWG*, com base em dois tipos de recipientes de plástico com água (25 litros e 1000 litros), contendo no seu interior exactamente no centro um detonador dentro de uma carga explosiva cilíndrica. As cargas explosivas usadas foram uma emulsão de nitrato de amónio com *fuel oil* (ANFO) e cordão detonante (12 g/m) de pentrite (PETN). Muito resumidamente uma revisão bibliográfica foi realizada. As propriedades de detonação dos explosivos foram previstas utilizando um programa termoquímico, designado por THOR. Para a expansão dos produtos de detonação dos explosivos foi aplicado uma equação de estado JWL. Foi realizado uma revisão aos conceitos fundamentais desta equação e os seus coeficientes foram determinados e optimizados correlacionando as previsões do THOR e a equação de estado (*EOS*) JWL para a mínima diferença através de uma função quadrática auxiliar. Por forma a calcular os coeficientes de JWL um novo método foi usado. Este baseia-se na evolução das curvas adiabáticas e isentrópicas obtidas pelo THOR, utilizando uma função do Microsoft Excel® Solver, assumindo algumas suposições para o coeficiente Grüneisen (a partir do exponencial da curva adiabática; do exponencial da curva isentrópica para um volume adimensional limite; do exponencial da curva isentrópica para todos os valores da expansão, e por último; deduzido por Handley, 2011). Os melhores resultados obtidos foram pela utilização do coeficiente Grüneisen do exponencial da curva isentrópica para todos os valores da expansão, onde $\omega = 0.328$ para a emulsão de ANFO e $\omega = 0.356$ para PETN.

As dimensões e o *design* da configuração de “*WBWG*” experimental foram apresentadas, juntamente com a descrição de uma experiência de detonação tipo utilizando 3 g de PETN (detonador No.8 mais 2.4 g de cordão detonante de PETN). Foi realizada uma simulação a 2D e 3D de “*WBWG*” usando o programa Autodyn para um contentor de

metro cúbico cheio de água (1000 litros) para ambos os explosivos. Os resultados obtidos mostram a possibilidade de ter este tipo de cargas explosivas sem a destruição do “WBWG” contentor. Uma vez que, os níveis de pressão na água, perto das paredes plásticas, sob a maior carga admissível, ronda os 6 MPa. Foi sempre possível observar a deformação elástica das paredes do contentor, as reflexões do choque subaquático, alterando a sua forma cúbica original para uma espiral transiente.

Adicionalmente os procedimentos executados para o THOR, para o Microsoft Excel ® Solver e para a interface do programa de simulação Autodyn “material input data” foram apresentados.

Palavras-chave: WBWG, explosões experimentais submarinas, emulsão de ANFO, cordão detonante de PETN, *programa termoquímico THOR*, optimização dos parâmetros JWL *EoS*, previsões de *WBWG* pelo Autodyn.

Contents

List of Figures.....	xi
List of tables	xvii
Abbreviations and Symbols.....	xix
Symbols	xix
Abbreviations	xx
1. Introduction	1
1.1. Description of the dissertation	4
2. Theoretical Background	5
2.1. Theory of detonation.....	5
2.2. Shock polar	8
2.3. Underwater blast wave generators	9
2.4. General equations	9
3. Applied Model and Results	11
3.1. THOR fundamentals	11
3.2. THOR approach.....	13
3.2.1. CJ detonation regime prediction.....	13
3.2.2. The adiabatic dynamic regime.....	16
3.2.3. Isentrope regime	18
4. Jones-Wilkins-Lee Equation of State	23
4.1. JWL fundamentals	24
4.1.1. Isentropic expansion of ideal gas described on an adiabatic process	24
4.1.2. Isentrope expansion on condensed materials.....	24
4.1.3. JWL approximation	25
4.2. JWL EoS approach	31
4.2.1. ANFO emulsion correlations.....	34
4.2.2. PETN correlations	41
5. Dimension and Design Configurations.....	49
6. Simulations and Experimental Results	59
6.1. Autodyn simulations	60
6.1.1. ANFO emulsion Autodyn simulations inside WBWG	61
6.1.2. PETN Autodyn simulations inside WBWG	63
6.2. Experimental results	66
6.2.1. ANFO emulsion experimental results	66
6.2.2. PETN experimental results.....	67
7. Synthesis and Conclusions	77
References	79
Appendix A - THOR execution procedure.....	83
Appendix B - Microsoft Excel Solver execution procedure	89
Appendix C - Autodyn material data input	93

LIST OF FIGURES

Figure 2.1. Simulation of propagation scheme of explosive detonation used to derive the Rankine-Hugoniot relations.	5
Figure 2.2. Drawing of the Hugoniot and the Crussard curves and between them the Rayleigh lines in the pressure-particle velocity (P-v) plane.....	7
Figure 2.3. Increased pressure profile as a function of time.....	10
Figure 3.1. THOR structure of calculation.	12
Figure 3.2. Behavior of the composition of the detonation products with the chemical stoichiometric ratios.	14
Figure 3.3. Interface of the program THOR – emulsion information.	15
Figure 3.4. Interface of the program - PETN information.....	16
Figure 3.5. Evolution of predicted adiabatic dynamic curve (P as a function of adimensional volume (v/v_{CJ}), where $v_{CJ} = 0.681 \text{ cm}^3/\text{g}$).....	17
Figure 3.6. Evolution of predicted adiabatic dynamic curve (P as a function of adimensional volume (v/v_{CJ}), where $v_{CJ} = 0.678 \text{ cm}^3/\text{g}$).....	18
Figure 3.7. Evolution of predicted limited isentrope curve (P as a function of adimensional volume (v/v_{CJ}), where $v_{CJ} = 0.681 \text{ cm}^3/\text{g}$).	19
Figure 3.8. Isentrope curve unlimited adimensional volume values given by THOR simulation (P as a function of adimensional volume (v/v_{CJ}), where $v_{CJ} = 0.681 \text{ cm}^3/\text{g}$).....	20
Figure 3.9. Evolution of predicted limited isentrope curve (P as a function of adimensional volume (v/v_{CJ}), where $v_{CJ} = 0.678 \text{ cm}^3/\text{g}$).	20
Figure 3.10. Isentrope curve unlimited adimensional volume values given by THOR simulation (P as a function of adimensional volume (v/v_{CJ}), where $v_{CJ} = 0.678 \text{ cm}^3/\text{g}$).....	21
Figure 4.1. DP evolution of PETN from THOR simulation – on the left to a limited expansion; and to the right for unlimited expansion.	31
Figure 4.2. The adiabatic and isentrope limited expansion curves for PETN DP – in the left, using the Grüneisen coefficient withdraw from the adiabatic curve; in the right , using the Grüneisen coefficient withdraw from the isentrope unlimited expansion.....	32
Figure 4.3. The adiabatic and isentrope limited expansion curves for PETN DP, both in double logarithmic $Y=Y(x)$ plot – in the left, using the Grüneisen coefficient withdraw from the adiabatic curve; in the right , using the Grüneisen coefficient withdraw from the isentrope unlimited expansion.	32

Figure 4.4. Evolution of predicted adiabatic and isentrope curves for limited expansion (“Isen-adiab for limited expansion”) - (P as a function of adimensional volume (v/v_{CJ}) if a double logarithmic scale). 34

Figure 4.5. Evolution of predicted adiabatic and isentrope curves for unlimited expansion (“Isen-adiab for unlimited expansion”) - (P as a function of adimensional volume (v/v_{CJ}) if a double logarithmic scale). 35

Figure 4.6. Adiabatic and limited isentrope curves, at 2.242 Grüneisen coefficient of the experimental curve, JWL - res. 1.0. (logarithmic scale). 35

Figure 4.7. Adiabatic and unlimited isentrope curves, at 2.242 Grüneisen coefficient of the experimental curve, JWL - res. 1.1. (logarithmic scale). 36

Figure 4.8. Adiabatic and limited isentrope curves, at 1.086 Grüneisen coefficient of the experimental curve, JWL - res. 2.0. (logarithmic scale). 37

Figure 4.9. Adiabatic and unlimited isentrope curves, at 1.086 Grüneisen coefficient of the experimental curve, JWL - res. 2.1. (logarithmic scale). 37

Figure 4.10. Adiabatic and limited isentrope curves, at 0.328 Grüneisen coefficient of the experimental curve, JWL - res. 3.0. (logarithmic scale). 38

Figure 4.11. Adiabatic and unlimited isentrope curves, at 0.328 Grüneisen coefficient of the experimental curve, JWL - res. 3.1. (logarithmic scale). 38

Figure 4.12. Adiabatic and limited isentrope curves, at 2.12 Grüneisen coefficient and at 8.33 GPa C parameter, from Caroline, 2011, for the experimental curve, JWL - res. 4.0. (logarithmic scale). 39

Figure 4.13. Adiabatic and unlimited isentrope curves, at 2.12 Grüneisen coefficient and at 8.33 GPa C parameter, from Caroline, 2011, for the experimental curve, JWL - res. 4.1. (logarithmic scale). 40

Figure 4.14. Evolution of predicted adiabatic and isentrope curves for limited expansion (“Isen-adiab for limited expansion”) - (P as a function of adimensional volume (v/v_{CJ}) if a double logarithmic scale). 41

Figure 4.15. Evolution of predicted adiabatic and isentrope curves for unlimited expansion (“Isen-adiab for unlimited expansion”) - (P as a function of adimensional volume (v/v_{CJ}) if a double logarithmic scale). 42

Figure 4.16. Adiabatic and limited isentrope curves, at 1.602 Grüneisen coefficient of the experimental curve, JWL - res. 1.0. (logarithmic scale). 42

Figure 4.17. Adiabatic and unlimited isentrope curves, at 1.602 Grüneisen coefficient of the experimental curve, JWL - res. 1.1. (logarithmic scale). 43

Figure 4.18. Adiabatic and limited isentrope curves, at 0.825 Grüneisen coefficient of the experimental curve, JWL - res. 2.0. (logarithmic scale). 43

Figure 4.19. Adiabatic and unlimited isentrope curves, at 0.825 Grüneisen coefficient of the experimental curve, JWL - res. 2.1. (logarithmic scale). 44

Figure 4.20. Adiabatic and limited isentrope curves, at 0.356 Grüneisen coefficient of the experimental curve, JWL - res. 3.0. (logarithmic scale). 44

Figure 4.21. Adiabatic and unlimited isentrope curves, at 0.356 Grüneisen coefficient of the experimental curve, JWL - res. 3.1. (logaritm scale).	45
Figure 4.22. Adiabatic and limited isentrope curves, at 1.63 Grüneisen coefficient and at 27.56 GPa C parameter, from Caroline, 2011, for the experimental curve, JWL - res. 4.0. (logaritm scale).	46
Figure 5.1. On the left the plastic cubic meter container and on the right the 25 litres container.	49
Figure 5.2. Explosive support structure for the experimental tests. On the top the alluminium tube having the small charge at the end. On the bottom the ones for the 25 lt jerry cans – on the right a plate adapter, and on the left a vertical plastic tube.	50
Figure 5.3. Experimental pressure set-up – hydrostatic pressure transmission.....	51
Figure 5.4. 3100 Series Pressure Transmitter, 4-20 mA and its connection circuit.	52
Figure 5.5. Pressure sensores calibration curves of Sensor A (left) and Sensor B (right). .	52
Figure 5.6. Plastic 25 litres container, charged with explosive, on the pressure set-up plate.	53
Figure 5.7. New experimental pressure set up – hydrostatic pressure transmission.	53
Figure 5.8. Scheme of the relation between the reference points of the wall, on the left, and the light electrical circuit measure points, on the right, to the experimental distance set up used.	54
Figure 5.9. Scheme of the light electrical circuit of the experimental distance set up.	55
Figure 5.10. Scheme of the light electrical circuit of the experimental distance set up used.	56
Figure 5.11. Experimental light electrical circuit set up.....	56
Figure 5.12. Plastic 1000 litres container, with the pressure set-up plate and the distance set-up.	57
Figure 5.13. Control room.	57
Figure 5.14. Blast type experiment – 2.4 g of PETN plus detonator No. 8 and 25L container.	58
Figure 5.15. Final state of the blast type experiment – 2.4 g of PETN plus detonator No. 8 and 25L container.	58
Figure 6.1. 3D Autodyn simulation scheme for both explosives – properties were visualized by the faces generated in the vertival axial line of the charge.	60
Figure 6.2. Simulation of propagation scheme of detonation of emulsion explosive.	61
Figure 6.3. Simulation of detonation of emulsion explosive at its end (2D).....	62
Figure 6.4. Simulation 3D of expansion products of detonation of emulsion explosive, when its adimensional volume reaches the value of 165 v/v ₀ (3D simulation - left), when touch water tank wall (3D simulation - center) and when is moving to the corners zone (3D simulation - right).	62

Figure 6.5. 3D simulation of pressure evolution inside water container. 62

Figure 6.6. Simulation of propagation scheme of detonation of emulsion explosive. 63

Figure 6.7. Simulation of detonation of emulsion explosive at its end (2D)..... 63

Figure 6.8. Pressure measurement at point #1 and #2 for the 2D simulation on the right. The points are identify on the left picture and correspond to the extrem of the explosive, one measure on the center, Point #1, and other on the edge, Point #2. 64

Figure 6.9. Simulation 3D of expansion products of detonation of emulsion explosive, when its adimensional volume reaches the value of 165 v/v₀ (3D simulation - left), when touch water tank wall (3D simulation - center) and when is moving to the corners zone (3D simulation - right). 64

Figure 6.10. Pressure reflection measurements, at point #3 on the bottom and point #4 on the top for the 3D simulation. The points are identify on the center picture and correspond to the corner of the water container, one measure in the middle, Point #3, and other on the top, Point #4..... 64

Figure 6.11. 3D simulation of pressure evolution inside water container. 65

Figure 6.12. Deformed aluminium support tube, as a function of used charge (5 g left, 10 g center and 15 g right and their group). 66

Figure 6.13. External deformation of plastic container and observed reflections for the 3 tested charges (5 g left, 10 g center and 15 g right). 67

Figure 6.14. Prediction of the Water shock polar in P-u_p plane. 68

Figure 6.15. Prediction of the PETN shock polar in P-u_p plane. This prediction correlates different PETN densities from experimental data. 68

Figure 6.16. Prediction of the Water - PETN shock polar in P-u_p plane..... 69

Figure 6.17. Peak pressure P [GPa] evolution as a function of radius r [m], from central charge – PETN vs Water. 70

Figure 6.18. Video frames from first class of tests, using standard detonator as charge, inside a 25 litres water container..... 71

Figure 6.19. Measurement of the pressure of the first test conducted on 25 litres container. Signal obtained by using a pressure sensor 0-10 bar and a oscilloscope, Tektronix TDS 320, as his periphery recording equipment. 71

Figure 6.20. Video frames from second class of tests, using standard detonator more 2.4 g of PETN as charge, inside a 25litres water container (420 fps sequence). 72

Figure 6.21. Measurement of the pressure of the secound class of tests conducted on 25 litres container. Signal obtained by using a pressure sensor 0-10 bar and a oscilloscope, Tektronix TDS 320, as his periphery recording equipment. 72

Figure 6.22. Video frames from second class of tests, using standard detonator more 3 g of PETN as charge, inside a 25litres water container (1000 fps sequence)..... 73

Figure 6.23. Final imges of the 25 litres container – on the left the first class of tests and on the center and right the second class of the tests respectively. 74

Figure 6.24. Video frames from the external deformation of plastic container on the detonation initial states, using 7.2 g PETN plus standard detonator as charge, inside a 1000 litres water container (initial point left, detonation point right).....	75
Figure 6.25. Video frames from the external deformation of plastic container on the final states before the water comes out, using 7.2 g PETN plus standard detonator as charge, inside a 1000 litres water container.	75
Figure 6.26. Measurement of the pressure of 7.2 g PETN on 1000 litres containers. Signal obtained by using a pressure sensor 0-16 bar and a oscilloscope, Tektronix TDS 320, as his periphery recording equipment.	75
Figure 6.27. Video frames from the light panel , using 7.2 g PETN plus standard detonator as charge, inside a 1000 litres water container.	76
Figure A.1. An example of the interface of the reaction information of the program THOR using PETN.	84
Figure A.2. An example of the interface of the thermochemical database of the program THOR – selecting PETN.	85
Figure A.3. NASA Thermo Build interface.	86
Figure A.4. An example of the interface of the Preview / Calculate of the program THOR – for PETN in the Isentrope condition.	87
Figure A.5. An example of the interface of the data given by the THOR – for PETN in the detonation condition.	87
Figure A.6. An example of the interface of the data given by the THOR – for PETN in the isentrope condition.	88
Figure A.7. An example of the interface of the data given by the THOR – for PETN in the adiabatic dynamic.	88
Figure B.1. Interface of the Excel options of the menu "file".	89
Figure B.2. Supplement menu of the interface Excel options from the menu "file".....	90
Figure B.3. Interface of the Microsoft Excel – JWL parameters calculation.	90
Figure B.4. Interface of the Solver implementation.	91
Figure B.5. Interface of an example of the possible restrictions used on the Solver parameters box.	92
Figure C.1. Interface of the Autodyn material data input – water in the left and PETN on the right.....	93

LIST OF TABLES

Table 3.1. Behavior of the composition of the detonation products with the chemical stoichiometric ratios Composition of the products compounds used on the THOR code.	14
Table 3.2. Initial and detonation products properties predicted using THOR code.	15
Table 3.3. Initial and detonation products properties predicted using THOR code.	16
Table 4.1. The JWL coefficients and detonation energies determined in the Suceska work and derived from cylinder test data.	34
Table 4.2. The Grüneisen coefficient and the JWL C parameter calculated by Caroline assumption – ANFO emulsion.	39
Table 4.3. Calculated JWL coefficients from the different test – ANFO emulsion.	40
Table 4.4. The Grüneisen coefficient and the JWL C parameter calculated by Caroline assumption –PETN.	45
Table 4.5. Calculated JWL coefficients from the different test – PETN.	46
Table 5.1. Main components and global characteristics of classical emulsion explosive. ...	50
Table 5.2. Global characteristics of classic PETN explosive.	51
Table A.1. Composition of the mixtures used on the THOR code.	83

ABBREVIATIONS AND SYMBOLS

Symbols

α – dissipation exponent

γ – ratio of specific heat capacities for an ideal gas

Γ – Mie-Grüneisen gamma

Γ_T – THOR great gamma

Γ_G – Mie-Grüneisen gamma

θ – time constant that describes exponential pressure drop with time [s]

v – specific volume $n = 1/\rho$ [m^3/kg]

v_0 – initial specific volume [m^3/kg]

v_{CJ} – specific volume at the CJ state [m^3/kg]

ρ – density [kg/m^3]

ρ_0 – initial density [kg/m^3]

ρ_{CJ} – density at the CJ state [kg/m^3]

σ – Stefan-Boltzmann constant [$\text{J}/\text{s m}^2 \text{K}^4$]

$\phi(S)$ – function of entropy [J/kg]

ω – Mie-Grüneisen gamma

A – maximum detonation products pressure [Pa]

A – JWL parameter [Pa]

B – JWL parameter [Pa]

C – JWL parameter [Pa]

c_0 – sound speed [m/s]

c_p – specific heat capacity at constant pressure [$\text{J}/\text{kg K}$]

c_v – specific heat capacity at constant volume [$\text{J}/\text{kg K}$]

$c_{v,\text{CJ}}$ – specific heat capacity at constant volume and at the CJ state [$\text{J}/\text{kg K}$]

D – detonation velocity [m/s]

D_{CJ} – detonation velocity at CJ state [m/s]

E – internal energy [J/kg]

G – Gibbs free energy [J/K]

H – enthalpy [J]
I – impulse [Pa.s]
 \dot{m} – mass flux of material through the shock wave [kg / s m²]
N – politropic index
P – pressure [Pa]
r – explosive expansion radius [m]
r₀ – radius of explosive charge [m]
R – molar gas constant [J / mol K]
R₁ – JWL parameter
R₂ – JWL parameter
s – adimensional constant of the material
S – entropy [J / K]
t – time [s]
T – temperature [K]
T₀ – initial temperature [K]
T_{CJ} – temperature at CJ state [K]
u_p – particle velocity [m / s]
u_{p,CJ} – particle velocity at CJ state [m / s]
U_s – shock velocity [m / s]
V – volume [m³]

Abbreviations

ANFO – Ammonium Nitrate with Fuel Oil

BKW – Becken-Kistiakowsky-Wilson

BWG – Blast Wave Generator

CJ – Chapman-Jouget

DEM – “Departamento de Engenharia Mecânica” - Mechanical Engineering

Department

DP – Detonation Products

EoS – Equation of State

FCTUC – “Faculdade de Ciências e Tecnologia da Universidade de Coimbra” -
Faculty of Science and Technology of Coimbra University

HE – High Explosives

JWL – Jones-Wilkins-Lee

PETN – PentaErythritol TetraNitrate

RH – Rankine - Hugoniot

VN – Von Neumann Spike

WBWG – UnderWater Blast Wave Generator

1. INTRODUCTION

Nowadays, the explosives have been common used in operations of demolition of structures as well other civil matters. However, it also has been increasing the number of accidents related with accidental explosions and from criminal attacks. The problem of security, generated by the use of explosive charges in historic buildings, implies the analysis of the transmission of a shock wave in non-homogeneous environment, which increasingly needs models correlated with experimental data. During the last decades a new method of underwater blasting operations has been researched and developed, and for that, aquarium tests has been established for the measurement of blasting energy of industrial explosives and confined underwater blast wave generators (WBWG). The program, recently approved, of security to explosions of historic buildings, complements modeling and experimental trials, like experimental destruction of walls with the resource of explosive charges placed in a container of water, which will be the focus of this work.

As we know the detonation of an explosive results in the production and violent release of compressed gases. The produced energy rapidly propagates through the environment (air or water), causing changes in pressure, forming a shock wave, which propagates over the sound speed. This wave front, with high dynamic pressure and supersonic velocity, is known as the shock wave that gives blasting an enormous power of collapse. The original blast wave generators (BWG), from the direct application of explosion in air of high explosives, have the inconvenient of hot polluted gases products, a reduced area of induced pressure, the possibility of generation of high velocity fragments and the existing of a very intense sound wave. Since physical properties of water and air are different, the characteristics of the shock waves (in air and water) are different principally due to the differences of density and shock wave velocity (shock impedance). Density of water is about 800 times greater than density of air; the sound velocity in water is 1500 m/s and in air ~ 340 m/s (4.5 times faster). Shock wave in water is 4.5 times faster than in air; pressure impulse in shock wave in water is 15-20 times higher than in air. After the detonation of an underwater explosive charge, the detonation products expand generating shock wave in water and forming a gas bubble. Gas bubble expands and pressure inside the bubble decreases. However, when charges are detonated, it can be

observed several cycles of contractions and expansions that generate, by this way, pulsating movement of gas bubble and additional compression waves in the water. This kind of evolutions is very important in large volumes. In our particular case, using small charges, these phenomena must be reduced or even eliminated. Our interest is to use water just as a pressure dissipative media. For that, this work was based on a previous work developed by Tavares, et al., 2012 for predicting and comparing with experimental results of confined underwater blasting generators (WBWG). Two different industrial explosives, ANFO emulsion and PETN, placed in the center of the container were now applied to these kinds of experiments.

Brief general concepts about his kind of explosives: according with the history, in the 60s, because was cheaper and provides a large amount of blasting energy the mixture of granular ammonium nitrate with fuel oil (ANFO) start to be usually used on mining industry. The ammonium nitrate is mixed with a fuel to create a water-in-oil type emulsion. In this emulsion the ammonium nitrate solution are covered entirely in fuel, creating a close relationship between the fuel and the oxidizer, providing a water-proofing property on the explosive, since the oil is immiscible with water. For that reason the ammonium nitrate emulsions became nowadays common used in the industry, like Orica for example (Morley, 2011); in 1891, Penthrite was first synthesized by Bernhard Tollens and P. Wigand by nitration of pentaerythritol. The production of PETN started in 1912, when it was patented by the German government and used in World War I. This explosive is known as one of the most powerful high explosives, with a very reduced critical diameter. Due to its highly symmetrical structure, PETN is resistant to attack by many chemical reagents; it is practically insoluble in water, but soluble in some other organic solvents, acetone for example.

Detonation predictions used an adapted equation of state (EoS) of detonation products (DP). Then thermal energy release at the Chapman-Jouget (CJ) point during detonation can be calculated. There are a number of EoS's of DP that result from different assumptions concerning detonated material conditions. The Jones-Wilkins-Lee (JWL) equation of state (EoS) is widely used in reactive hydro simulations due to his simplicity to describe thermodynamics of DP final expansion, assuming no more reactions inside DP. This EoS can be used in different forms (two or three terms) according with the level of accuracy in the pressure-volume domain that applications need and it is also possible to

increase mathematical complexity of HE EoS, but it does not guarantee increased accuracy for practical problems of interest. Increasing the numbers of parameters is often justified based on improved physics descriptions, but can also mean increased calibration complexity, as happens with the modified JWL EoS (JWL_B). For example, Tang, P.K. for modeling the overdriven release experiments of PBX 9501 proved JWL_B to be more suitable than standard JWL EoS (Tang, 1997). However, often it is questionable whether the increased complexity of mathematical JWL is of value, increasing the number of calibration parameters could mean no increase in complexity and ensures greater accuracy for practical problems of interest. In this work will be used and determined the JWL equation of state with only three parameters, in the classic form:

$$P = A \cdot \exp\left(-R_1 \cdot \frac{v}{v_{CJ}}\right) + B \cdot \exp\left(-R_2 \cdot \frac{v}{v_{CJ}}\right) + C \cdot \left(\frac{v}{v_{CJ}}\right)^{-(\omega+1)}.$$

Predictions properties of DP need a thermochemical computer code, named THOR, with four calculating clusters. The first is related to the thermal equation of state (EoS) that allows the calculation of the *PVT* state of the detonation products, the second calculating cluster is related to the energetic equation of state, H_L , corresponding to the internal energy calculation using thermochemical data and polynomial expressions of Gordon and McBride, 1971, 1994, applied to intermediate and final products, the third cluster is related to the conservation equations - mass, atomic species, momentum and energy, being the thermodynamic equilibrium achieved for $G=G_{\min}(P,T,x_i)$. The last cluster corresponds to the reaction regime, which is, in this particular case, Chapman-Jouguet (CJ) detonation. Despite the use of THOR code to prediction the DP necessities to determine JWL EoS there are many others like PANDA (Kerley, et al., 1993), CHEETAH (Fried, et al., 1994), EXPO5 (Suceska, 2007) and most more.

The simulation phenomenological problem remains until the time/displacement originated by the expansion of detonation products. LS-DYN (MSC.Software, 2005), and Autodyn (ANSYS, 2006), are explicit 3D codes able to integrate results in a phenomenological way, using parameters and constants predicted before. After the determination of the JWL EoS parameters it was performed a detonation simulation for the two explosives using the program Autodyn. This simulation study the expanding process of detonation products of the explosives and that helps to determine the pressures that we are dealing with and the consequences of the surroundings for a specific quantity of the

explosive used. This program was performed for 2D and 3D simulation for each explosive used; it provided the simulation of the underwater explosion of the explosives, predicting space/time/intensity of underwater shock wave and its multiple reflections at the external wall of the container. And also for modeling these effects (nonlinear dynamics), the program Autodyn ANSYS code uses the JWL EoS expressed in the classic form.

1.1. Description of the dissertation

After the present Chapter 1 (Introduction) where was presented the general concepts, the objectives and structure of the present work the following texts have:

- a) Chapter 2 (Theoretical background) – is presented a brief background of the concepts used;
- b) Chapter 3 (Applied model and results) – is presented the model used to predict the detonations products. THOR fundamentals are described and the prediction results are presented;
- c) Chapter 4 (Jones-Wilkins-Lee equation of state) – is presented the JWL equation of state used, its fundamentals are described and its parameters are determined using the THOR predictions;
- d) Chapter 5 (Dimensions and design configurations) – is presented a brief description of the experimental assembly of underwater blast wave generator performed on explosive charges placed in water container;
- e) Chapter 6 (Simulations and experimental results) – is presented a simulation using Autodyn of the experimental assembly and all the results achieved are analyzed, as the previous simulations as the experimental tests;
- f) Chapter 7 (Synthesis and Conclusions) – is presented a conclusion of all the work done and new ideas for future work are suggested;
- g) References – are presented all the bibliographic references used for the current work;
- h) Appendix A – is the description of THOR execution procedures;
- i) Appendix B – is the Microsoft Excel Solver execution procedures;
- j) Appendix C – is an example of the Autodyn database.

2. THEORETICAL BACKGROUND

2.1. Theory of detonation

An explosion of a chemical explosive is defined by a very quick release of all potential energy accumulated in the explosive. This quick release known as shock wave causes a rapid increase in pressure and volume propagating through the surroundings. Theoretical model of detonation, represented by the picture below, assumes a shock front propagating in un-reacted explosive, followed by a reaction zone, where combustion occurs.

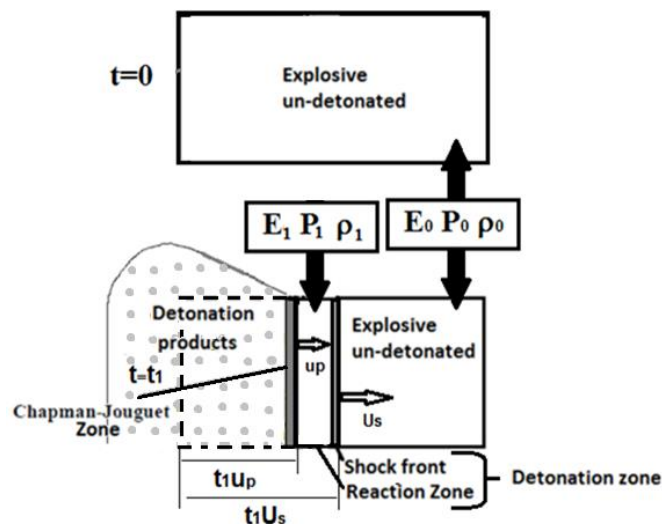


Figure 2.1. Simulation of propagation scheme of explosive detonation used to derive the Rankine-Hugoniot relations.

Studying a theoretical one-dimensional detonation it can be assumed that detonation wave travels through the explosive material from left to right (Figure 2.1). The shock front is followed by the chemical reaction zone. Behind the reaction zone are located the dense and hot gases from the detonation products, DP. This decomposition process that generates the DP is approximately adiabatic, since the high reaction rate does not allow heat exchanges with the outside, because these are rather slower. The increase the volume of the gases of the products generates an increase of the pressure, generating a shock wave inside surrounding material (that in this case will be water).

At $t = 0$ the explosive stays unreacted, and instantly the detonation starts, CJ zone. The Chapman-Jouguet zone represents the ideal detonation zone, where the

propagation velocity is equal to the sound velocity through the DP. It is assumed that the explosion energy is instantaneously released in a discontinuous shock front across which the conservation conditions of Rankine-Hugoniot (RH). (The velocity of the detonation wave was assumed to be the minimum velocity compatible with the hydrodynamic conservation equations, defining a unique steady-state detonation velocity).

Assuming that the detonation moves at a constant particle velocity, u_p , resulting in a shock velocity, U_s , of the front of the compressed material. The velocity is greater than the velocity of the detonation point resulting in growing area (volume in 3D) of the compressed material. . At the time t_1 there are both compressed material and undisturbed unreacted material inside the explosive and if the CJ zone and the detonation zone are assumed to be unity, the first of three RH equations is derived by conservation of masses.

$$\dot{m} = \rho_0 \cdot U_s = \rho_1 \cdot (U_s - u_p), \quad (2.1)$$

where \dot{m} is the mass flux of material passing through the shock wave.

Next RH is derived by starting that the change in momentum is equal to the impulse caused by outer forces. Momentum is defined by the product of mass and velocity, in this case at time t_1 the compressed fluid has the mass $\rho_1 \cdot (U_s - u_p) \cdot t_1$ and at $t = 0$, the momentum is zero. The impulse is defined by the product of the change in pressure at the different states, P_1 and P_0 , and at the time. This gives the conservation of momentum as

$$(P_1 - P_0) = \rho_0 \cdot U_s \cdot u_p = \rho_1 \cdot (U_s - u_p) \cdot u_p . \quad (2.2)$$

Conservation of energy is the fundamental point when deriving the third RH equation. Generally the conservation of energy means that the work done by the outer forces equals the change in internal energy plus the change in kinetic energy, which in this case yields

$$\rho_0 \cdot U_s \cdot (E_1 - E_0) = P_1 \cdot u_p - \frac{1}{2} \cdot \rho_0 \cdot U_s \cdot u_p^2 , \quad (2.3)$$

where E_1 and E_0 are the internal energy at the two different states. If this equation is rewritten by the previews equations of mass and momentum conservation the following relation is achieved

$$(E_1 - E_0) = \frac{1}{2} \cdot (P_1 + P_0) \cdot (v_0 - v_1) , \quad (2.4)$$

here v_0 and v_1 are the specific volumes at different states, defined by $v = 1/\rho$.

From these three RH conservation equations we identify eight parameters; u_p , U_s , ρ_0 , ρ_1 , P_1 , P_0 , E_1 and E_0 . Which the three initial conditions represented by the index 0 are known and remain five unknown parameters for only three equations. In order to solve shock problems, two more relationships are needed. One relation is called the equation of state (EoS) and is presented in more details in the upcoming chapter 4, and the last one is related with the specification of the boundary conditions.

The Hugoniot curve could be described as a relation between, for example, mass and momentum conservation equations describing pressure and specific volume when going from one state to another.

This curve contains all the possible states that the explosive can reach during shock. When detonation occur in ideal theory the pressure over the shock wave front changes with a discontinuous jump described by drawing a straight line between the initial and final states, the Rayleigh line which is given by

$$P = \rho_0 \cdot U_s^2 \cdot \left(1 - \frac{\rho_0}{\rho_1}\right), \tag{2.5}$$

where P is the detonation pressure, i. e., the pressure of the shock wave front, ρ_0 and ρ_1 are the densities at different states, initial and final, respectively, and U_s is the velocity of the shock wave in the explosive material (it can be also denominated as the detonation velocity, D), has as main feature being constant and independent of the energy and the way how the detonation is initiated.

Follow the graphic representation of these assumptions on a P-v plane:

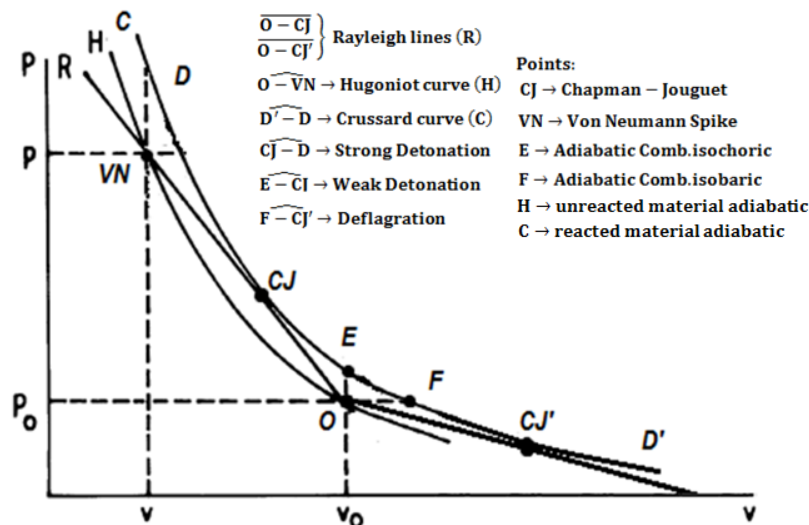


Figure 2.2. Drawing of the Hugoniot and the Crussard curves and between them the Rayleigh lines in the pressure-particle velocity (P-v) plane.

The Hugoniot curve represents the adiabatic unreacted curve and the Crussard curve represents the detonation products. The Rayleigh line is a tangent to the Crussard curve giving the CJ point.

2.2. Shock polar

From experimental observations was development a linear relation between the shock wave velocity U_s and the particle velocity u_p at high range of pressures for describe the shocks in solids, called the shock polar or the shock Hugoniot in the $U_s - u_p$ plane.

$$U_s = c_0 + s \cdot u_p + q \cdot u_p^2 , \quad (2.6)$$

where c_0 , s and q are constants of the material that can be determined experimentally. c_0 is the sound velocity of the undisturbed surrounding and s and q are adimensional constant.

The above relation can be simplified in

$$U_s = c_0 + s \cdot u_p , \quad (2.7)$$

since $(q \cdot u_p^2) \cong 0$.

When combined with the Hugoniot equations for the conservation of mass and momentum, can be used to determine the shock Hugoniot in the $P - u_p$ plane, where u_p is the particular velocity:

$$(P_1 - P_0) = U_s \cdot \rho_0 \cdot u_p = (c_0 + s \cdot u_p) \rho_0 \cdot u_p = \rho_0 \cdot c_0 \cdot u_p + s \cdot \rho_0 \cdot u_p^2 . \quad (2.8)$$

The shock Hugoniot describes the locus of all possible thermodynamic states a material can exist in behind a shock, projected onto a two dimensional state-state plane. It is therefore a set of equilibrium states and does not specifically represent the path through which a material undergoes transformation.

2.3. Underwater blast wave generators

Several studies concern aquarium tests for the measurement of blasting energy of industrial explosives. Confined underwater blast wave generators (WBWG) then appear as an industrial application of reduced size aquarium test procedures. The confined WBWG, applying the extremely high rate conversion of the explosive detonation energy into the kinetic energy of a thick water confinement, allows a wide range of the produced blast impulse and surface area distribution. It also avoids the generation of high velocity fragments and reduces atmospheric sound wave. This kind of WBWG find an wide application in special anti-terrorist operations as an effective mean for breaching doors, walls, roofs or reinforced Windows (Plaksin, et al., 2007). More recently, the recent studies of WBWG open the possibility of collecting detonation products, specially condensed materials, from small explosive charges placed in the center of a water confinement, without the destruction of water container (Tavares, et al., 2012). The present study shows the behavior of WBWG, based in water plastic containers, having in the center a cylindrical explosive charge.

2.4. General equations

The detonation wave is a wave which thus creates a state of high temperature and pressure, which causes the means of containment truly devastating effect. The structure of the pressure wave transmitted to the medium is characterized by the appearance of a ridge almost instantaneous pressure, followed by an impulsion, which are decreasing as they move away from the point of initial formation.

Based on basic general conservation equations Suceska, 2007 recreated that phenomenon that helps to define quantities and design values of experiments. He created an equation that correlates the pressure level, ΔP , as a function of distance radius r related to the original radius of explosive charge, r_0 , with a dissipation exponent, α , and the maximum products detonation pressure value, A (Suceska, 2007).

In aquarium experimental trials he concluded that the dissipation exponent in water was $\alpha = 1.5$, and for TNT of initial $\rho = 1600 \text{ kg/m}^3$, $A = 37 \text{ GPa}$.

$$\Delta p = A \cdot \left(\frac{r_0}{r}\right)^\alpha \quad (2.9)$$

The pressure profile, as a function of time (vd. Figure 2.3), can be expressed by equation (2.10) when $t < \theta$, and by equation (2.11) when $\theta < t < 5 \cdot \theta$ up to $10 \cdot \theta$, being $\theta = B_1 \cdot \left(\frac{r}{r_0}\right)^\beta \cdot \frac{r_0}{c_0}$ (for TNT of initial $\rho = 1600 \text{ kg/m}^3$, $B_1 = 1.4$ and $\beta = 0.24$). The θ is so-called time constant or characteristic P width of peak (it describes exponential pressure drop with time, and it is the P width value at which maximum pressure decreases to value p_{max}/e - (Suceska, 2007).

$$p(t) = \Delta p^{-t/\theta}, \quad (2.10)$$

$$p(t) = \Delta p \cdot 0.368 \cdot \frac{\theta}{t}. \quad (2.11)$$

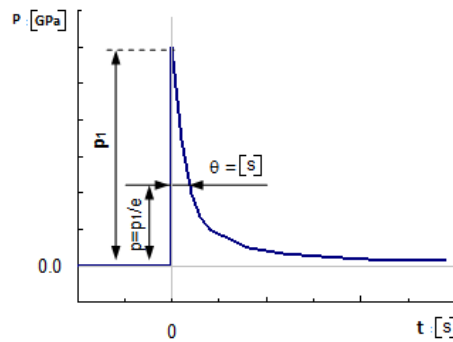


Figure 2.3. Increased pressure profile as a function of time.

In a similar way the pressure impulse, I , can be expressed by eq. (2.12) and (2.13) for the two considered cases, respectively:

$$I = \int_0^t p dt = 1.10^5 \cdot [\Delta p \cdot \theta \cdot (1 - e^{-t/\theta})], \quad (2.12)$$

$$I = \int_0^t p dt = 1.10^5 \cdot \left[\Delta p \cdot \theta \cdot \left(0.632 - 0.368 \cdot \ln \frac{t}{\theta} \right) \right]. \quad (2.13)$$

These basic equations, representing a very simple unidimensional approach, are very useful to define boundary values of explosive charges to be used in WBWG.

3. APPLIED MODEL AND RESULTS

To predict detonation properties of used explosives, thermochemical computer code, named THOR was used, and ANFO (Ammonium Nitrate with Fuel Oil) emulsion and PETN (PentaErythritol TetraNitrate) were the selected explosives. And with this program code was performed the theoretical prediction of DP and thermodynamic properties of the explosives compositions for the CJ detonation with the adiabatic dynamic and isentropic conditions.

3.1. THOR fundamentals

THOR is a program for the prediction of combustion and detonation processes of energetic mixtures. It requires a large database (THOR database) that contains the thermochemical characteristics of the reactants and possible products of the reaction. Supported with Gordon and McBride polynomial coefficients to evaluate the energetic state of the detonation/ combustion products.

This kind of program predict the products compounds, pressure and temperature detonation values, assuming the existence of thermodynamic equilibria of detonation products, i.e., the mechanical ($dP = 0$), chemical ($d\mu_i = 0$) and thermal ($dT = 0$) equilibria for the minimum value for its Gibbs free energy. The THOR code has been developed and optimized and several kinds of EoS were developed, like for example BKW, Boltzmann and JCZ3. Obtained results prove the importance of calculated products composition and the influence of $\Gamma_T = \left. \frac{dH}{dE} \right|_s$ value, where the great gamma with index T represents the THOR great gamma related to the detonation products, that is equal to the fraction between the variation of enthalpy, dH , and the variation of internal energy dE at constant entropy, S. (Durães, et al., 1995). Demonstrate this assumption we have:

$$\Gamma_T = \left. \frac{dH}{dE} \right|_s = \frac{\frac{\partial H}{\partial T} \cdot dT + \frac{\partial H}{\partial P} \cdot dP}{\frac{\partial E}{\partial T} \cdot dT + \frac{\partial E}{\partial V} \cdot dV} = \frac{c_p \cdot dT + h \cdot dP}{c_v \cdot dT + l \cdot dV} \quad (3.1)$$

Assuming the detonation products doesn't change phase, the pressure is constant ($h \cdot dP = 0$), and also, the specific volume is constant, so $l \cdot dV = 0$. Therefore:

$$\Gamma_T = \frac{c_p \cdot dT}{c_v \cdot dT} = \frac{c_p}{c_v} = \gamma \quad (3.2)$$

The great gamma, Γ_T , is equal to the fraction of the calorific heat at constant pressure, c_p , and at constant specific volume, c_v and equal to the gamma, γ .

For the present work, the new EoS developed by (Durães, et al., 1995), H_L , was used to calculate equilibrium compositions of gas and solid species, as a function of initial composition of energetic system, based on the same assumptions of a Boltzmann EoS, $PV/RT = \sigma(V, T, X_i)$, being $\sigma = 1 + x + 0.625x^2 + 0.287x^3 - 0.093x^4 + 0.014x^5$ with $x(V, T, X_i) = \Omega / (V \cdot T^{3/\alpha})$ and $\Omega = \sum(X_i \omega_i)$, but on physical intermolecular potential of gas components instead of correlations from final experimental results. This EoS takes $\alpha = 13.5$ to the exponent of the intermolecular potential. The selection of components is dependent of atomic initial composition. The code allows the possibility of estimating various sets of reaction products, obtained successively by the decomposition of the original reacting compound, as a function of the released energy.

The following image represents the THOR structure of calculation.

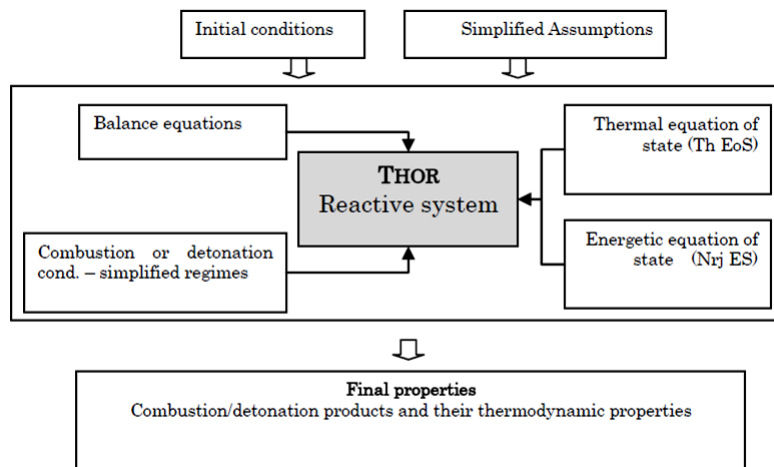


Figure 3.1. THOR structure of calculation.

The Figure 3.1 shows the THOR code with four calculation clusters, adapting it for the current work we have:

- 1- The thermal EoS that allows the calculation of the detonation products;
- 2- The energetic EoS, corresponding to the internal energy calculation, $E = \sum x_i e_i(T) + \Delta e$, $e_i(T)$, using thermochemical database, NASA Thermo Build tables, and polynomial expressions of Gordon and McBride (1971, 1974) applied to intermediate and final products;

3- The conservation equations – mass, atomic species, momentum and energy, being the thermodynamic equilibrium achieved for $G = G_{min}(P, T, x_i)$, applying to the condensed phase the model proposed by Tanaka, 1983, or the equivalent function proposed by Gordon and McBride, 1994;

4- The reaction regime, Chapman-Jouguet (CJ) detonation, with the adiabatic dynamic curve and the isentrope curve. It can be also determined, being P constant, the isobar adiabatic combustion (equal initial and final total enthalpy $H_b^{T_b} = H_0^{T_0}$) and the isochor adiabatic combustion ($E_b^{T_b} = E_0^{T_0}$).

3.2. THOR approach

On the Appendix A is described according with the THOR calculation clusters and the respectively assumptions. The next steps are presented the THOR approach for both explosive used and the tree combustions regimes taken are described in detail.

3.2.1. CJ detonation regime prediction

3.2.1.1. ANFO emulsion DP simulation data

Since the emulsion of ANFO is not a pure compound, it was performed an initial study about the stoichiometric of his mixture. It reveals to be extremely important for achieving the detonation products curve. The next graphic shows the behavior of the detonation products for different chemical stoichiometric ratios created by only changing the quantity of fuel oil on the mixture, starting with 0.05 mol to 0.1 mol with an interval of 0.005 mol.

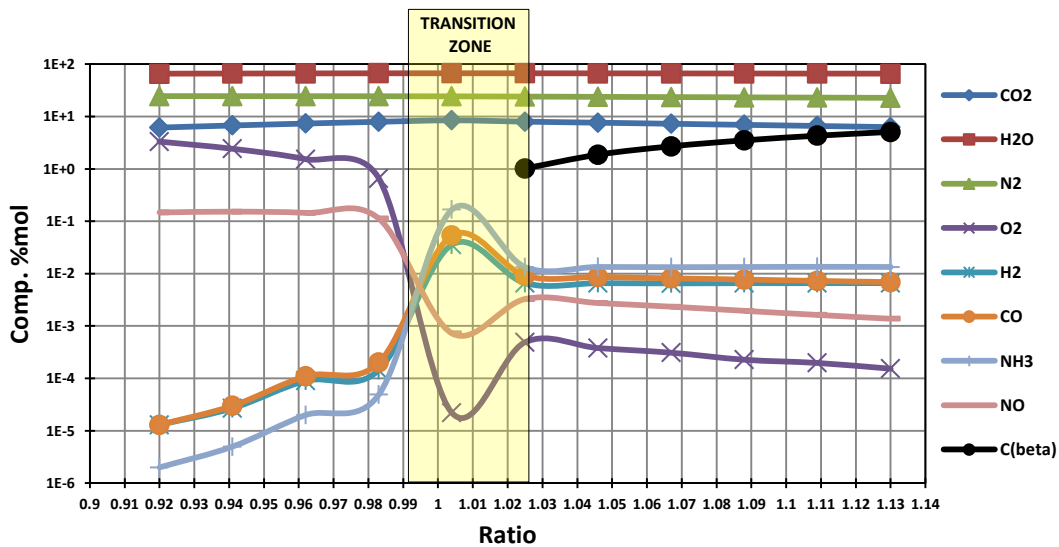


Figure 3.2. Behavior of the composition of the detonation products with the chemical stoichiometric ratios.

As it can be seen at Figure 3.2 there is a transition for equivalence ratio $r \cong 1$, where the basic detonation products change (CO₂, H₂O, O₂, N₂ for poor mixture $r < 1$, to CO₂, H₂O, H₂ and N₂ for rich mixture $r > 1$).

Table 3.1. Behavior of the composition of the detonation products with the chemical stoichiometric ratios
Composition of the products compounds used on the THOR code.

Temperature [K]	1988.493	2060.269	2130.029	2198.964	2248.927	2230.57	2210.473	2190.253	2171.098	2151.767	2132.683
Detonation Velocity [km/s]	7.5274	7.4538	7.3819	7.315	7.2669	7.2394	7.219	7.1965	7.1783	7.1578	7.1373
Pressure [kbar]	81.016	83.002	84.926	86.764	88.046	86.898	85.798	84.717	83.653	82.609	81.581
γ	1.22	1.22	1.22	1.21	1.21	1.21	1.21	1.21	1.21	1.21	1.21
Ratio	0.92	0.941	0.962	0.983	1.004	1.025	1.046	1.067	1.088	1.109	1.13

This study reveals that the increase of the quantity of fuel oil is directly proportional to the increase of the chemical stoichiometric ratio and temperature, but inversely proportional with the decrease the detonation velocity. At the 0.98 ratio, approximately, the formation of the detonation products starts to be instable. At 1.025 ratios the C_β starts to be formed and the other products start to stabilize. And so, an ideal zone for studying the DP was establish and it must be on a stable zone that is before the ideal stoichiometric ratio 1 or in the zone of 1.025 to 1.05 ratios when the C_β is formed. But when the carbon solid is formed, C_β, the pressure decreases and originating an equilibrium of Gibbs Free Energy for other kind of products composition (different from $r < 1$ zone). So, was assumed a stable point before the ideal stoichiometric ratio for study the DP curve, 0.92 ratios.

The numerical calculation, using THOR code, was performed assuming a mixture of 87.351 % of ammonium nitrate (NH_4NO_3), 3.771 % of fuel oil ($\text{C}_{10}\text{H}_{17.963}$), 0.031 % of air ($\text{N}_{1.5788}\text{O}_{0.4212}$) (corresponding to the sensitizing air microballons) and 8.847 % of water (H_2O), and an equilibrium composition of detonation products of CO_2 , H_2O , N_2 , H_2 , OH , CO , NH_3 , O_2 , NO , H , $\text{C}(\text{gas})$, N , O , C_α , C_β , CH_2O_2 components. Detonation properties calculated by THOR code were presented in Table 3.2.

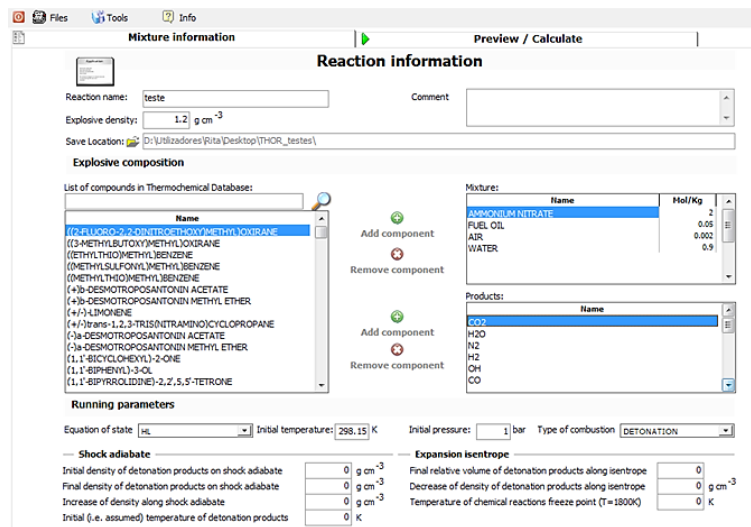


Figure 3.3. Interface of the program THOR – emulsion information.

Table 3.2. Initial and detonation products properties predicted using THOR code.

Initial conditions	CJ conditions	
Density $\rho=1112.13$ kg/m^3	$V_{\text{CJ}}D=5480.89$ m/s	$T = 1988.493$ K
$E_o=-5619.53$ kJ/kg	PressureCJ $=8.102$ GPa	$G = -1.44E+04$ kJ/kg
$T = 298.15$ K	$a_{\text{CJ}} = 4151.74$ m/s	$\gamma = 1.22$
Pressure $=10^5$ Pa	$u_{\text{CJ}} = 1329.12$ m/s	$\Gamma_T = 3.12$

3.2.1.2. PETN DP simulation data

For PETN system it was assumed an mixture of 99.959% of PentaErythritol TetraNitrate ($\text{C}_5\text{H}_8\text{N}_4\text{O}_{12}$) and 0.041% of air ($\text{N}_{1.5788}\text{O}_{0.4212}$) and an equilibrium composition of CO_2 , H_2O , N_2 , H_2 , OH , CO , NH_3 , O_2 , NO , H , $\text{C}(\text{gas})$, N , O , C_α , C_β , CH_2O_2 . Detonation properties calculated by THOR code were presented in Table 3.3.

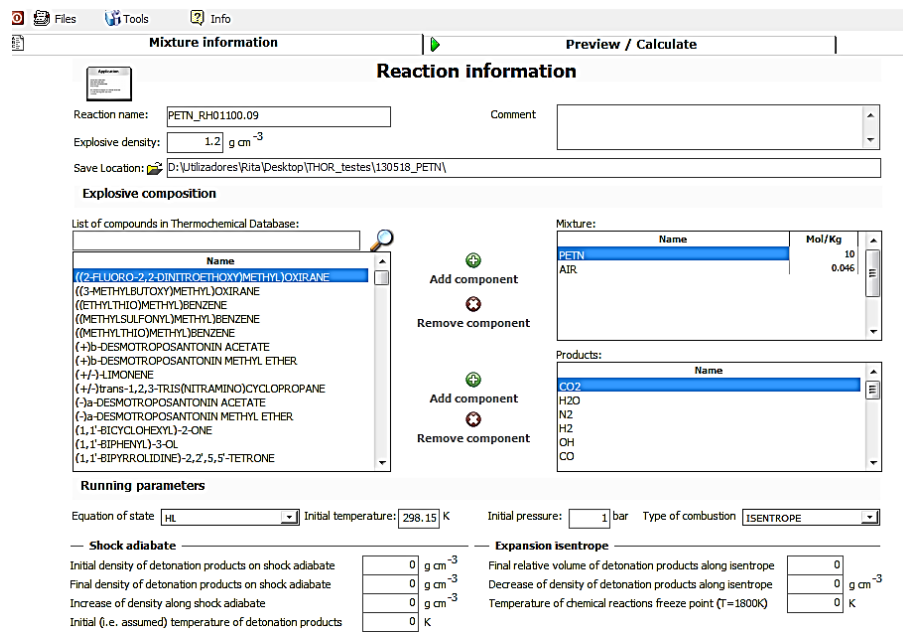


Figure 3.4. Interface of the program - PETN information.

Table 3.3. Initial and detonation products properties predicted using THOR code.

Initial conditions	CJ conditions	
Density $\rho = 1100 \text{ kg/m}^3$	$V_{CJ}D = 5329.27 \text{ m/s}$	$T = 3847.111 \text{ K}$
$E_o = -1682.85 \text{ kJ/kg}$	Pressure $CJ = 8.725 \text{ GPa}$	$G = -2.59E+04 \text{ kJ/kg}$
$T = 298.15 \text{ K}$	$a_{CJ} = 4057.08 \text{ m/s}$	$\gamma = 1.1$
Pressure = 10^5 Pa	$u_{CJ} = 1488.29 \text{ m/s}$	$\Gamma_T = 2.63$

3.2.2. The adiabatic dynamic regime

The adiabatic dynamic approached by THOR, according with CJ point, is applied to the general expression $dQ = 0$ obtained by dH or dE variation.

3.2.2.1. ANFO emulsion DP simulation data

The obtained results using THOR code for the adiabatic curve related to CJ point is represented in the following figure.

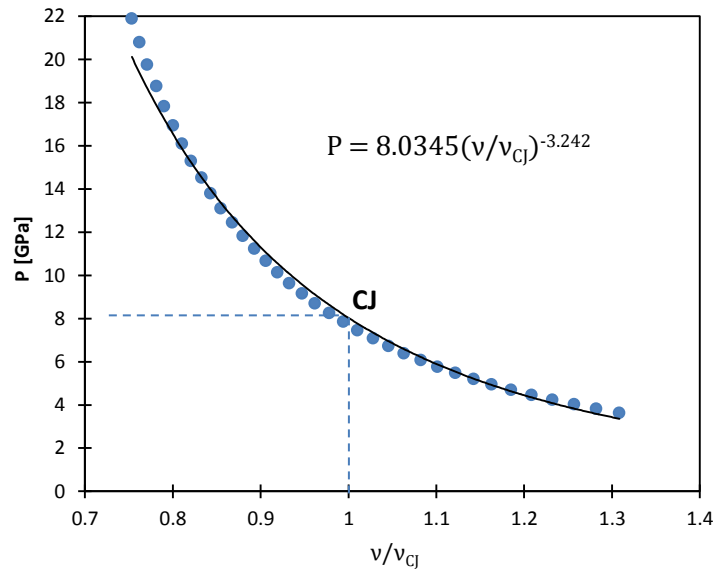


Figure 3.5. Evolution of predicted adiabatic dynamic curve (P as a function of adimensional volume (v/v_{CJ}), where $v_{CJ} = 0.681 \text{ cm}^3/\text{g}$).

As it can be seen, the numerical results from THOR code represent the adiabatic dynamic curve in Pressure vs. adimensional volume, (P vs (v/v_{CJ})). The pressure was converted in GPa and the initial volume, v_0 , assumed was at CJ point, $v_{CJ} = 0.681 \text{ cm}^3/\text{g}$. Using a power trend line in adiabatic dynamic curve, we concluded an exponent of -3.242.

3.2.2.2. PETN DP simulation data

The obtained results using THOR code for the adiabatic curve related to CJ point is represented in the following figure.

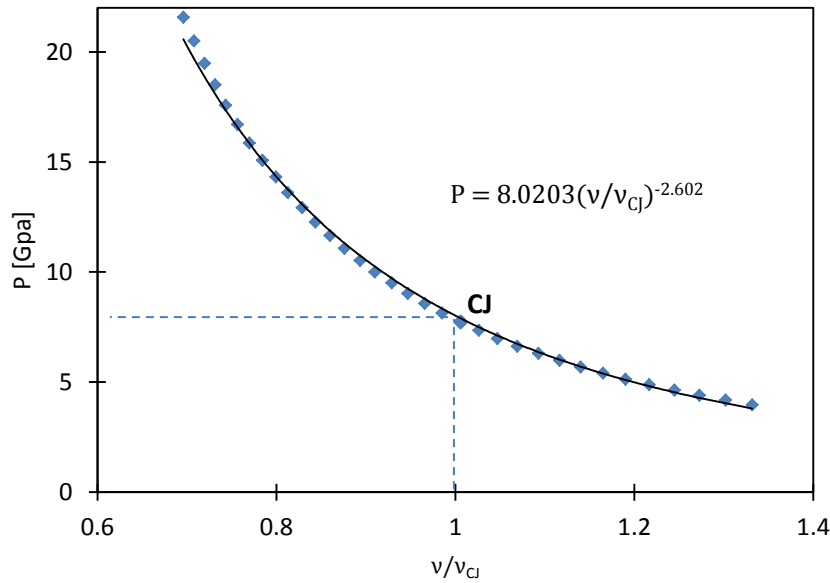


Figure 3.6. Evolution of predicted adiabatic dynamic curve (P as a function of adimensional volume (v/v_{CJ}), where $v_{CJ} = 0.678 \text{ cm}^3/\text{g}$).

For the PETN, like was said before for the emulsion, the adiabatic dynamic curve provided from THOR was represented in Pressure vs. adimensional volume, (P vs (v/v_{CJ})), the pressure was converted in GPa and the initial volume, v_0 , assumed was at CJ point, $v_{CJ} = 0.678 \text{ cm}^3/\text{g}$. Using a power trend line in adiabatic dynamic curve, we concluded an exponent of -2.602 .

3.2.3. Isentrope regime

For the Isentrope regime, the THOR platform determines, according with the CJ point, the evolution of the system entropy through the Gibbs Free Energy. In a brief summary the Gibbs Free Energy is the energy released or absorbed in reversible chemical processes. Is the total variation of entropy that came with a chemical reaction, proceeding slowly and at temperature and pressure constants. It is given by:

$$\Delta S_{universe} = \Delta S_{neighbor} + \Delta S_{system} \leftrightarrow \Delta S_{universe} = -\frac{\Delta H}{T_{system}} + \Delta S_{system} . \quad (3.3)$$

Multiplying with $-T$:

$$-T \cdot \Delta S_{universe} = \Delta H_{system} - T \cdot \Delta S_{system} , \quad (3.4)$$

Gibbs defined the function free energy so that $-T\Delta S_{universe}$ was equal to the free energy variation of the system:

$$\Delta G_{system} = -T \cdot \Delta S_{universe} = \Delta H_{system} - T \cdot \Delta S_{system} . \quad (3.5)$$

Simplifying the Gibbs free energy can be express as

$$G = H - T.S \text{ or } G = E + P.V - T.S . \quad (3.6)$$

Since at the isentrope state we have

$$dS = 0 , \quad (3.7)$$

and knowing the Gibbs Free Energy, G, the entropy, S will be given by THOR database

$$dTS = d(H - G) \leftrightarrow dS = \frac{d(H - G)}{dT} \leftrightarrow \Delta S = \frac{\Delta(H - G)}{\Delta T} . \quad (3.8)$$

3.2.3.1. ANFO emulsion DP simulation data

The experimental results of the isentrope curve, related to CJ point, are represented in the following Figures. These experimental data was study in two forms: the first one at a limit values (until a 4.97 adimensional volume) and the last one for all values obtained.

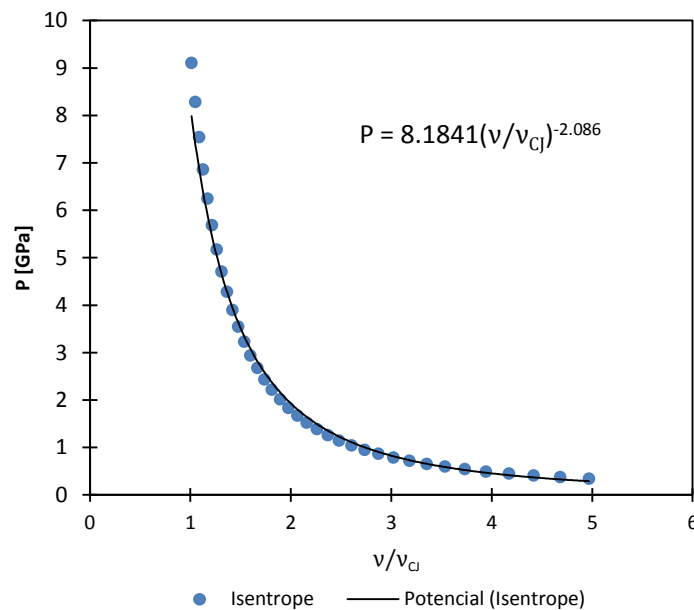


Figure 3.7. Evolution of predicted limited isentrope curve (P as a function of adimensional volume (v/v_{CJ}), where $v_{CJ} = 0.681 \text{ cm}^3/\text{g}$).

For the isentrope curve limited expansion, using a power trend line, we have an exponent of -2.086 (until 4.97 adimensional volume, v/v_{CJ}), and in the case of isentrope curve unlimited expansion an exponent of -1.328, as shows the next figure.

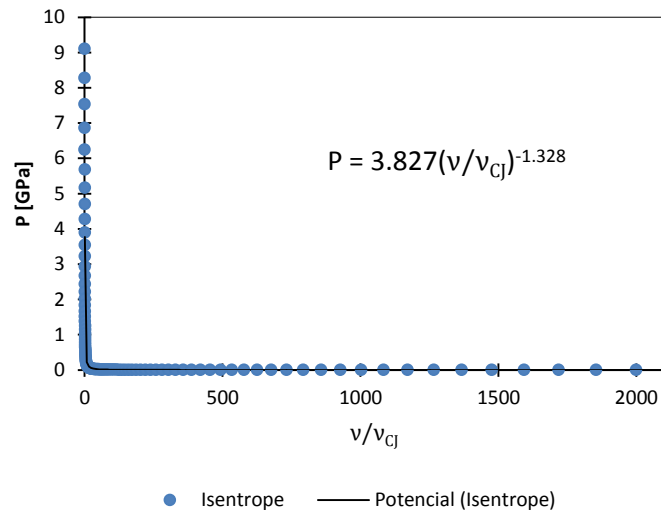


Figure 3.8. Isentrope curve unlimited adimensional volume values given by THOR simulation (P as a function of adimensional volume (v/v_{CJ}), where $v_{CJ} = 0.681 \text{ cm}^3/\text{g}$).

3.2.3.2. PETN DP simulation data

The isentrope curve obtained results by THOR code was study in two forms: the first one at a limit expansion (until a 14.29 adimensional volume) and the last one for an unlimited expansion.

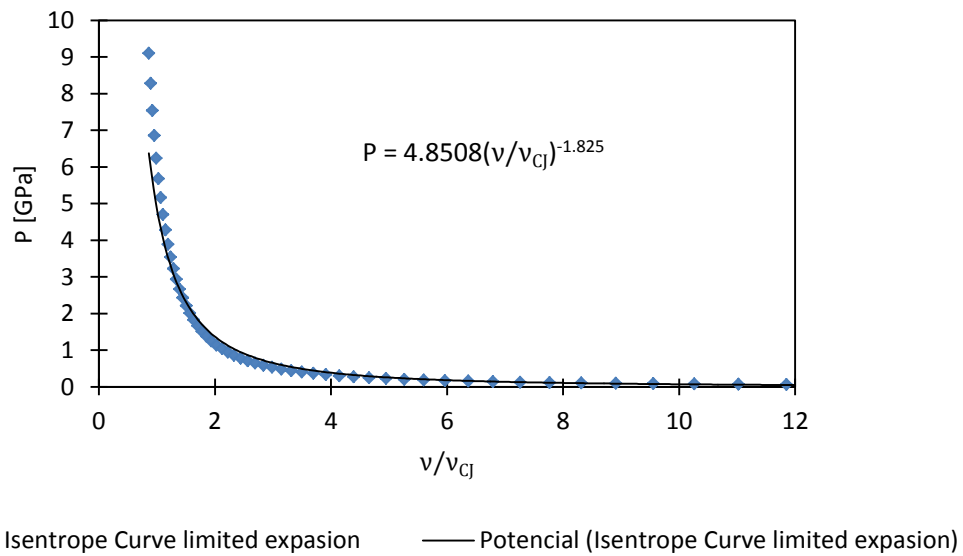
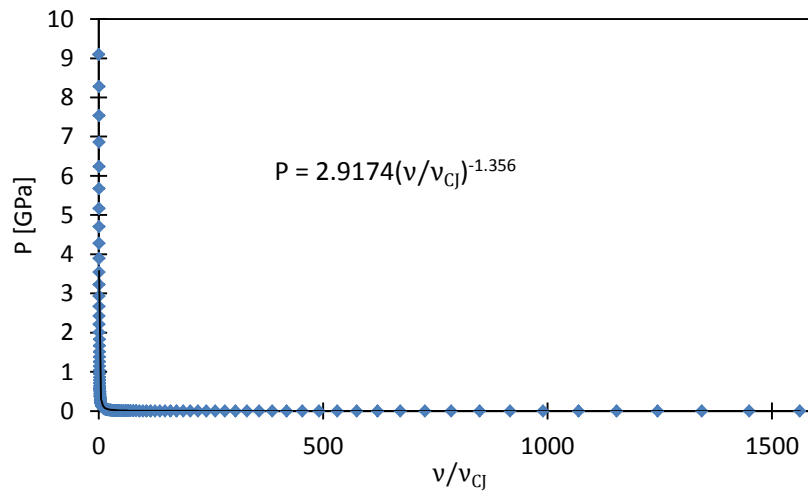


Figure 3.9. Evolution of predicted limited isentrope curve (P as a function of adimensional volume (v/v_{CJ}), where $v_{CJ} = 0.678 \text{ cm}^3/\text{g}$).



◆ Isentrope Curve unlimited expansion — Potencial (Isentrope Curve unlimited expansion)

Figure 3.10. Isentrope curve unlimited adimensional volume values given by THOR simulation (P as a function of adimensional volume (v/v_{CJ}), where $v_{CJ} = 0.678 \text{ cm}^3/\text{g}$).

The numerical approach power trend line shows, in the case of isentrope curve limited expansion the exponent of -1.825, and for the isentrope curve unlimited expansion the exponent of -1.356.

4. JONES-WILKINS-LEE EQUATION OF STATE

The equation of state (EoS) that is going to be used to represent the detonation products (DP) of high explosives (HE) will be the Jones-Wilkins-Lee (JWL) EoS. JWL EoS describes the relationship among the volume and pressure of DP (and in some cases, also with energy, for example C coefficient deduced by Handley, 2011). This EoS is a mathematical expression widely used due to its simplicity in hydrodynamic calculations and has been developed and its structure modified according with the explosive used. And so, this EoS has been used in different forms (two, three terms) according to the level of accuracy in the pressure-volume domain that applications need. For the current study the JWL EoS with three terms for describing the DP was used.

$$P_S(v) = A. \exp\left(-R_1 \cdot \frac{v}{v_{CJ}}\right) + B. \exp\left(-R_2 \cdot \frac{v}{v_{CJ}}\right), \quad (4.1)$$

or

$$P_S(v) = A. \exp\left(-R_1 \cdot \frac{v}{v_{CJ}}\right) + B. \exp\left(-R_2 \cdot \frac{v}{v_{CJ}}\right) + C. \left(\frac{v}{v_{CJ}}\right)^{-(\omega+1)}, \quad (4.2)$$

where A , B , and C are pressure constants [Pa] and R_1 , and R_2 adimensional coefficients.

The JWL model assumes that the detonation of an explosive may be completely described in the pressure-volume space. It also assumes that the detonation explosives compresses instantly from the room temperature and pressure up to the Rayleigh line to the CJ point. Then it expands down the isentrope given by the JWL EoS.

The JWL EoS formula, although very popular and useful, cannot provide *a priori* this prediction because it needs to be fit to experimental data for each new explosive composition. And for many years this has been one of the principal objectives on explosive research, the prediction of EoS for the DP without the need of experimental data. Nowadays, for this common problem theoretical “chemical” EoS models have been providing reasonable predictions of detonation properties. And so, the JWL EoS parameters can be accurately adjusted to fit on this experimental data.

4.1. JWL fundamentals

On gas detonations processes we can use the widely known thermodynamic properties of isentropic expansion ideal gases but on solids detonation process we need to enter also with compression properties of the solids to describe the expansion of the DP.

4.1.1. Isentropic expansion of ideal gas described on an adiabatic process

A polytropic process is a thermochemical process that obeys the relation:

$$P \cdot V^n = C, \quad (4.3)$$

where the P is the pressure, V is the specific volume, n the polytropic index that is a real number, and C is a constant. This equation can be used to accurately characterize processes of certain systems, notably the compression or expansion (including with heat transfer) of a gas and in some cases liquids and solids.

In the case of an isentropic ideal gas, γ is the ratio of specific heats $= \frac{C_p}{C_v}$, known as the adiabatic index or as adiabatic exponent. This ratio gives the important relation for an isentropic (quasistatic, reversible, adiabatic process) process of a simple compressible calorically perfect ideal gas

$$P \cdot V^\gamma = \text{constant}, \quad (4.4)$$

where P is the pressure and V is the volume. And so, the adiabatic exponent can be written as:

$$\gamma = - \left. \frac{\partial \ln(P)}{\partial \ln(V)} \right|_S. \quad (4.5)$$

4.1.2. Isentrope expansion on condensed materials

In 1912 Eduard Grüneisen forms the Grüneisen model that correlates the relation between the pressure and the volume of a solid at a given temperature. This model determines the pressure in a shock-compressing solid.

The Grüneisen model is expressed as

$$\Gamma_G = V \cdot \left. \left(\frac{dP}{dE} \right) \right|_V, \quad (4.6)$$

where V is the volume, P is the pressure, E is the internal energy, and $\Gamma_{Grüneisen}$ is the Grüneisen coefficient which represents the thermal pressure from a set of vibration atoms. Integrating the Grüneisen's model we can correlate Γ_G independently of pressure and internal energy

$$(P - P_0) = (E - E_0) \cdot \frac{\Gamma_G}{V}, \quad (4.7)$$

where P_0 and E_0 are at a reference state usually assumed to be the state at which the temperature is 0 K. In that case they are independent of temperature and the values of these quantities can be estimated from Hugoniot equations.

It is necessary remember that this Mie-Grüneisen coefficient, Γ_G , is different from the great gamma used by THOR, Γ_T . The Mie-Grüneisen parameter is a relation between the pressure, P , energy E , and the volume, V , of the solid at a given temperature and it is used to determine the pressure in a shock-compressed solid, and in the other hand, the great gamma used by THOR related the detonation products and it is a relation between the variation of enthalpy, dH , and the variation of internal energy, dE , at constant entropy, S .

4.1.3. JWL approximation

G. Baudin and R. Serradeill, (Baudin, et al., 2010), describe the JWL EoS as a pure empirical EoS, in generally, with a non-physical Grüneisen coefficient considered constant. The fundamentals achieved for the formulation of the empirical JWL EoS were based on the following assumptions: (i) follows the Chapman-Jouguet (CJ) model, where both Rayleigh line, reactive shock Crussard curve, isentropic expansion and CJ point assumptions can be assumed as one. They are both related in the following way: the Rayleigh line is tangent with the reactive shock Crussard curve and the isentropic expansion, giving the CJ point in the pressure-volume plane. The CJ point represents the point where the ideal detonation starts; (ii) the DP expansion isentropic from any point on the Crussard curve is almost coincident with the Crussard curve in the pressure-particle velocity ($P - u$) plane. This relationship along the Crussard curve of the pressure-particle velocity can be expressed as a universal curve in the $P - u$ plane and is usually used to determine the thermodynamic state at DP-metal interface.

The Crussard curve describes the fully reactive shock states from room pressure and temperature given by the equation that follow:

$$P = \rho_0 \cdot D \cdot u_p, \quad (4.8)$$

where P is the pressure, ρ_0 is the initial density, D is the detonation velocity, and u_p is the particle velocity.

The ambient pressure P_0 is neglected comparing to the pressure along the Crussard curve and at the CJ state, we have:

$$P_{CJ} = \rho_0 \cdot D_{CJ} \cdot u_{pCJ}, \quad (4.9)$$

where P_{CJ} is the pressure at CJ point, D_{CJ} is the detonation velocity at CJ point, and u_{pCJ} is the particle velocity at CJ point.

The ratio between the two previous equations, P/P_{CJ} we have:

$$\frac{P}{P_{CJ}} = \frac{\rho_0}{\rho_0} \cdot \frac{D}{D_{CJ}} \cdot \frac{u}{u_{CJ}} \leftrightarrow \frac{P}{P_{CJ}} = \frac{D}{D_{CJ}} \cdot \frac{u}{u_{CJ}}. \quad (4.10)$$

As (Baudin, et al., 2010), mention, for a wide range of ideal HE, using the Becker-Kistiakowsky-Wilson (BKW) thermochemical simulations, demonstrated by Gimenez, the detonation velocity D can be represented by the following ‘universal’ relationship:

$$\frac{D}{D_{CJ}} = a \cdot \left(\frac{u}{u_{CJ}} \right)^{-1} + b + c \cdot \left(\frac{u}{u_{CJ}} \right), \quad (4.11)$$

where a, b, c are constant parameters.

Introducing this equation in the previous one, we obtained:

$$\frac{P}{P_{CJ}} = \frac{u}{u_{CJ}} \cdot \left[a \cdot \left(\frac{u}{u_{CJ}} \right)^{-1} + b + c \cdot \left(\frac{u}{u_{CJ}} \right) \right] \leftrightarrow \frac{P}{P_{CJ}} = a + b \cdot \left(\frac{u}{u_{CJ}} \right) + c \cdot \left(\frac{u}{u_{CJ}} \right)^2. \quad (4.12)$$

The first assumption of the CJ model, express the next relation between CJ isentrope of DP and the Crussard curve, represented respectively by indices S and C:

$$(dP/dv)_S = (dP/dv)_C, \quad (4.13)$$

where v is the specific volume.

Since the relation of this two is almost coincident, $(dP/dv)_S \approx (dP/dv)_C$, we can express the equation demonstrated by Gimenez, along the CJ isentrope as:

$$\frac{P_S}{P_{CJ}} \approx a + b \cdot \left(\frac{u}{u_{CJ}} \right) + c \cdot \left(\frac{u}{u_{CJ}} \right)^2, \quad (4.14)$$

and

$$\frac{u_{CJ}}{P_{CJ}} \cdot \frac{dP_S}{du} = b + 2c \cdot \left(\frac{u}{u_{CJ}} \right). \quad (4.15)$$

On the isentrope we have:

$$\left(\frac{dP_S}{du} \right)^2 = -\frac{dP_S}{dv} = -(\rho \cdot c)^2. \quad (4.16)$$

Therefore, the previous equations lead to a differential equation which can be integrated expressing in the following way:

$$P_S(v) = A \cdot \exp\left(-R \cdot \frac{v}{v_0}\right) + B, \quad (4.17)$$

where A, R and B are pressure constant parameters given by:

$$A = (P_{CJ} - P_\infty) \cdot e^R, \quad (4.18)$$

$$B = P_{CJ} \cdot \left(a - \frac{b^2}{4a \cdot c} \right), \quad (4.19)$$

$$R = a \cdot c \cdot \frac{\rho_{CJ}}{\rho_0} \cdot \left(\frac{\rho_0 \cdot D_{CJ}^2}{P_{CJ}} - 1 \right). \quad (4.20)$$

This relation is similar with the first exponential term of JWL and B can be neglected since this term represents a few percent of the pressure. Increasing DP expansion the exponential term decreases toward 0 and adding the ideal gas pressure-volume tendency ensures a correct behavior at large expansion. For improving this equation performance a second exponential term is added, leading to a new equation known as JWL isentrope:

$$P_S(v) = A \cdot \exp\left(-R_1 \cdot \frac{v}{v_0}\right) + B \cdot \exp\left(-R_2 \cdot \frac{v}{v_0}\right) + C \cdot \left(\frac{v}{v_0} \right)^{-(\omega+1)}. \quad (4.21)$$

Where the Mie- Grüneisen formulation is represented as a variation at temperature and specific volume:

$$e = e_S(v) + \frac{v}{\Gamma'_G} \cdot (P - P_S(v)), \quad (4.22)$$

$$P_S(v) = - (de_S(v) / dv), \quad (4.23)$$

$$\Gamma'_G = \omega = \text{constant}, \quad (4.24)$$

where Γ'_G is the Grüneisen coefficient defined as $\Gamma'_G = -(\partial \log T / \partial \log v)_S$, $e_S(v)$ is the internal energy along the CJ isentrope, $P_S(v)$ is the pressure evolutions along the CJ isentrope.

This analysis validates the pressure-volume JWL relationship chosen to represent the reference curves for DP. Although, assuming a constant Grüneisen coefficient is a restrictive assumption.

Because of that they describe a new derivation of JWL EoS with a less restrictive assumption for the Grüneisen coefficient to represent both large expansions and near CJ states suggested by W. C. Davis. Similarly to the previous one, they developed a complete EoS for unreacted solid HE, using Hugoniot curve instead the Crussard curve. Therefore the expansion isentrope from any point of the Hugoniot curve was almost coincident with the Hugoniot curve in the P-u plane. This assumption, applied for compression/release of inert material gives an exponential form EoS similar to exponential terms of the JWL EoS. The functions $P(v, s)$, $T(v, s)$ and the Mie- Grüneisen formulation $P(v, e) = P_S(v) + (\Gamma'_G(s)/v) \cdot (e - e_S(s))$ derives from this fundamentals equation via the Maxwell thermodynamic equations $T = (\partial e / \partial s)|_V$ and $P = -(\partial e / \partial v)|_S$. This model allows the computation of the DP entropy and temperature.

Taver and Urtiew try to approximate the JWL EoS correlating the adiabatic exponential with the Grüneisen coefficient, Γ_G , that will be represented as ω ($\Gamma_G = \omega$):

$$\Gamma_G = \omega = V \cdot \left(\frac{\partial P}{\partial E} \right) \Big|_V, \quad (4.25)$$

$$\gamma = - \frac{\partial \ln(P)}{\partial \ln(V)} \Big|_S, \quad (4.26)$$

$$\omega = \gamma - 1, \quad (4.27)$$

$$P = A \cdot \exp(-R_1 \cdot V) + B \cdot \exp(-R_2 \cdot V) + C \cdot (V)^{-(\omega+1)}, \quad (4.28)$$

where P represents the pressure [Mbar], V represents the specific volume, T the temperature, ω the Grüneisen coefficient, γ the adiabatic exponent and A, B, C, R_1 ,

and R_2 are constants. This last expression (4.27) is very useful when it is correlated results from THOR predictions (fixing Γ_T and γ) to calculate ω value.

Taking the Crussard curve as the objective of the present study a new possibility of the JWL EoS where studied and presented by Caroline using HMX-based plastic-bonded explosives.

Caroline (Handley, 2011) in her thesis describe another form to JWL EoS for detonation products assuming a Grüneisen EoS reference to the gaseous reaction products and with an isentrope as the reference curve and $\Gamma(v) = w$:

$$P = \left(1 - \frac{\omega}{R_1} \cdot \frac{v_0}{v}\right) \cdot A \cdot \exp\left(-R_1 \cdot \frac{v}{v_0}\right) + \left(1 - \frac{\omega}{R_2} \cdot \frac{v_0}{v}\right) \cdot B \cdot \exp\left(-R_2 \cdot \frac{v}{v_0}\right) + \frac{\omega \cdot e}{v}, \quad (4.29)$$

which has constant Grüneisen coefficient $\omega = \Gamma$ and a reference curve which is apparently $e = 0$. However for the CJ isentrope:

$$p_S(v) = A \cdot \exp\left(-R_1 \frac{v}{v_0}\right) + B \cdot \exp\left(-R_2 \frac{v}{v_0}\right) + C \left(\frac{v}{v_0}\right)^{-(1+\omega)}. \quad (4.30)$$

$$\Gamma = \left. \frac{dP}{dE} \right|_V \times V = \omega. \quad (4.31)$$

Integrating the JWL the equation for the energy on the isentrope at any relative volume is obtained ($e_S(v)$):

$$e_S(v) = \int_{\infty}^v p_S(v) dv, \quad (4.32)$$

$$e_S(v) = \frac{v_0}{R_1} \cdot A \cdot \exp\left(-R_1 \cdot \frac{v}{v_0}\right) + \frac{v_0}{R_2} \cdot B \cdot \exp\left(-R_2 \cdot \frac{v}{v_0}\right) + \frac{v_0 \cdot C}{\omega} \cdot \left(\frac{v}{v_0}\right)^{-\omega}. \quad (4.33)$$

Since at infinite volume the energy on isentrope equals zero, detonation energy is:

$$e_d(v \rightarrow \infty) = -[e_S(CJ) - e_{DP}] = e_0. \quad (4.34)$$

On the third term of JWL EoS the C parameter was deduced by the energy released of the detonation products at a constant volume:

$$C = \frac{\omega \cdot \Phi_{CJ}}{v_0}, \quad (4.35)$$

where Φ_{CJ} is given by the next expression:

$$\Phi_{CJ} = \int_{T_0}^{T_{CJ}} c_v dT = c_v \cdot [T_{CJ} - T_0], \quad (4.36)$$

then,

$$C = \frac{\omega \cdot c_v \cdot [T_{CJ} - T_0]}{v_0} \quad (4.37)$$

Caroline deduce, primarily, the C constant by the energy released of the detonation products at a constant volume, then the Grüneisen coefficient that can be expressed as $\Gamma = \Gamma_0 - \Gamma_1 \cdot (v/v_0)$, and then A and B constants, and finally R_1 , R_2 constants. With these deductions she comforted with difficulties to produce reasonable maximum and minimum values for JWL reaction products EoS parameters. Although, since she tested HMX it reveals to be unnecessary changing the form of the JWL EoS according with its little reaction. "The binder JWL could only have an effect in regions where the binder reacts significantly". However, uncertainties in the thermal properties of the DP where thought to be greater than in the EoS. And so if the thermal properties, i. e., effects of uncertainties in the values of T_{CJ} and $C_{v_{CJ}}$ on the reaction products, had been revealed to be affecting the final results, the JWL would do so either. Despise the JWL EoS could reveal some restrictions on several specific conditions according with the explosive used, like is "inappropriate in problems where the reaction Kinetics depend explicitly on temperature", mentioned by Kerley, Caroline managed to have a good relationship of DP using the same EoS.

Often it is questioned where the increased mathematical complexity over JWL is of value, as increased numbers of parameters can mean increased calibration complexity and does not guarantee increased accuracy for practical problems of interest.

In order to calculate the JWL coefficients, a new numerical method was used. It was based in the evolution of adiabate and isentrope curves, obtained by THOR code, using a function of the Microsoft Excel®, assuming a few assumptions:

- (1) the Grüneisen coefficient from the exponential of the adiabatic curve;
- (2) the Grüneisen coefficient from the exponential of the isentrope curve at a limit adimensional volume;
- (3) the Grüneisen coefficient from the exponential of the total expansion of isentrope curve and, at last;
- (4) the Grüneisen coefficient and the parameter C of JWL deduced by Caroline (Handley, 2011).

The graphics that follow in JWL approach subchapter correlate graphically the theoretical curve, given by THOR code, to the predicted curve JWL for the different results.

4.2. JWL EoS approach

All the experimental data about the CJ detonation, adiabatic dynamic, and isentrope regimes achieved from THOR was transferred to Microsoft Excel. In this new platform the all the database was treated in order to find the JWL parameters.

Like was mention before, tree curves were described, one for the adiabatic dynamic and two for the isentrope. In the isentrope was study a curve with a limited expansion where was assumed a stable DP expansion, and a curve with all the expansion data given by THOR. The JWL EoS was approximated to all curves using different Grüneisen parameters. From each curve was retrieved a Grüneisen coefficient. And from each Grüneisen coefficient was achieved the JWL parameters approximating the experimental curve with the theoretical curve given by THOR. Was also performed another JWL parameters approximation to the isentrope curves according with Caroline assumptions.

The perfect fitting of the Adiabatic Dynamic with Isentrope curves, according with CJ point, represents the evolution of the DP for the respective explosives used (ANFO emulsion and PETN). The next figure represents the DP curve of the PETN for a limit expansion and to all values obtained by the THOR simulation.

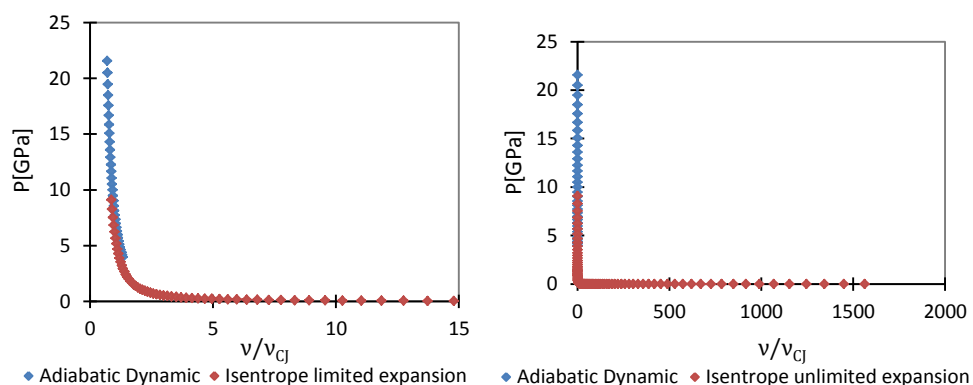


Figure 4.1. DP evolution of PETN from THOR simulation – on the left to a limited expansion; and to the right for unlimited expansion.

When both theoretical and experimental curve are approximated on their original forms is difficult to see the correct experimental curve, JWL EoS, since the small variation of its parameters (A , B , C , R_1 , R_2 and ω) are hard to observe. His graphical visualization can lead to approximation errors. Therefore both curves are converted in double logarithmic $Y = Y(x)$ plot. As an example, the following figures shows, initially, the approximation of the JWL EoS to the DP curve at a limited expansion using, as base of calculation, two different Grüneisen coefficients, adiabatic and isentropie unlimited expansion, for the PETN. And then, the same curves converted in double logarithmic $Y = Y(x)$ plot, and we now we can observe the differences of both approximation. The graphic visualization of both graphics, initially, seem to have a similar and good approximation, but when both graphics are converted at a logarithmic scale we can distinguish which graphic represents the better approximation for the JWL EoS (in this case the graphic from de right).

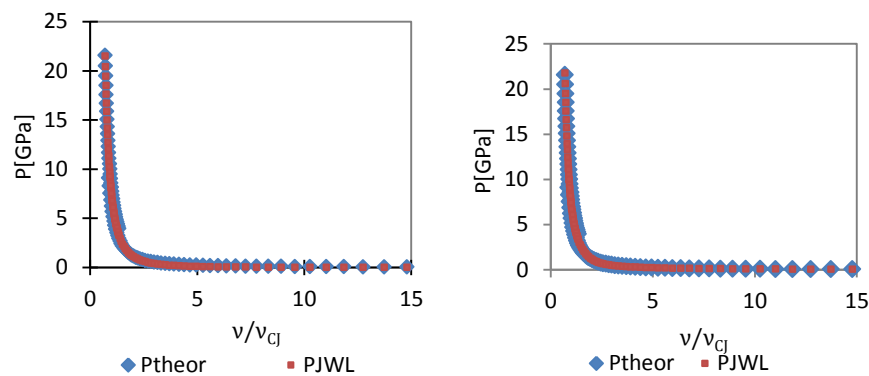


Figure 4.2. The adiabatic and isentropie limited expansion curves for PETN DP – in the left, using the Grüneisen coefficient withdraw from the adiabatic curve; in the right , using the Grüneisen coefficient withdraw from the isentropie unlimited expansion.

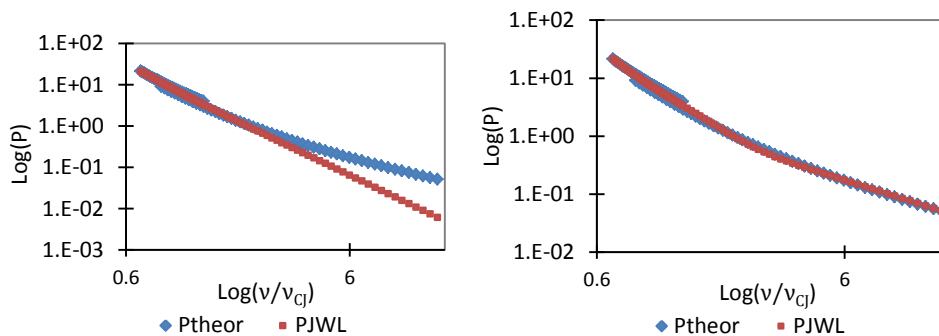


Figure 4.3. The adiabatic and isentropie limited expansion curves for PETN DP, both in double logarithmic $Y=Y(x)$ plot – in the left, using the Grüneisen coefficient withdraw from the adiabatic curve; in the right , using the Grüneisen coefficient withdraw from the isentropie unlimited expansion.

As the JWL expression used demonstrates itself, the double exponential intent to approximate the curve to detonation products experimental data, and the third term correlated with compressing phenomenon of solids:

$$P_S(v) = A \cdot \exp\left(-R_1 \cdot \frac{v}{v_{CJ}}\right) + B \cdot \exp\left(-R_2 \cdot \frac{v}{v_{CJ}}\right) + C \cdot \left(\frac{v}{v_{CJ}}\right)^{-(\omega+1)}. \quad (4.38)$$

For find the JWL parameters was used a function of the platform Excel, called Solver, and assumed a few assumptions:

- The exponent $(\omega + 1)$ from the JWL EoS can be correlated to Grüneisen coefficient by $\omega = \Gamma - 1$, and will be study in the four scenarios presented by Γ assumptions;
- The Γ is the exponential coefficient of the power trand lines, adiabatic dynamics curve, isentrope curve with limit adimensional values and unlimit adimensional values and final one from THOR correlated with Caroline assumptions, respectively;
- Imposing restrictive values on the function solver for the different JWL parameters according with the bibliography data base in order to validate procedures;

For determine the JWL EoS parameters was used the Microsoft Excel ® which a supplement function called Solver. The Excel Solver is used to optimize linear and nonlinear problems. Therefore in this work this supplement of the Microsoft Excel is used for minimize the difference between both curves, theoretical from THOR experimental database and experimental, JWL EoS, modifying the JWL parameters in order to match both of them, with an auxiliary quadratic function that correlates the difference values of both functions points. And so, the Solver is going to minimize that difference providing an optimize values for the JWL parameters. In Appendix B - Microsoft Excel Solver execution procedure is described.

Before performing calculations, a reflexion of previous waves was done, consulting Table 4.1. created by Suceska that correlates the JWL parameters and detonation energies for different kinds of explosives.

Table 4.1. The JWL coefficients and detonation energies determined in the Suceska work and derived from cylinder test data.

Explosive	Density [g/cm ³]	Legend	A [Mbar]	B [Mbar]	C [Mbar]	R ₁	R ₂	ω	E ₁ (CJ) [kJ/cm ³]	E ₀ [kJ/cm ³]
HMX	1.894	(1)	20.12840	1.071023	0.10137	7.09118	3.1816	1.299	15.64	-10.91
		(2)	8.580805	0.07546531	0.00781274	4.306	0.80	0.30	16.23	-11.00
HMX	1.188	(1)	6.95936	0.35241	0.0436676	7.72829	2.97463	0.9533	7.92	-5.89
		(2)	2.182000	0.04959433	0.01977170	4.379	1.10	0.55	8.67	-6.40
HNS	1.655	(1)	10.06145	0.51930	0.052554	6.78240	2.94139	1.002	9.89	-7.19
		(2)	4.237580	0.03131467	0.01704155	4.332	1.00	0.40	10.33	-7.50
HNS	1.001	(1)	2.51429	0.161932	0.024348	7.14928	2.97477	0.8287	4.71	-3.61
		(2)	1.388149	0.02779832	0.00694139	4.657	1.00	0.35	4.62	-3.60
PETN	1.763	(1)	17.22837	0.841286	0.0880185	7.36127	3.14138	1.1964	13.89	-9.92
		(2)	10.32158	0.9057014	0.0372735	6.000	2.60	0.57	14.91	-10.80
PETN	1.503	(1)	12.89617	0.591259	0.065047	7.483667	3.13618	1.0526	10.92	-8.03
		(2)	3.510723	0.05705547	0.0121624	4.075	0.90	0.35	11.91	-8.50
PETN	1.263	(1)	6.28059	0.295271	0.044381	6.94494	2.78259	0.8644	8.68	-6.57
		(2)	2.281744	0.05104579	0.01412013	4.240	1.05	0.35	9.63	-7.20
NM	1.130	(1)	4.233131	0.178524	0.0394769	6.952815	2.74858	0.96283	6.84	-5.13
		(2)	2.977799	0.05954922	0.01108004	5.026	1.10	0.49	6.57	-4.95
TNT	1.632	(1)	10.05503	0.477044	0.050447	6.67859	2.94404	1.0030	9.46	-6.88
		(2)	5.244089	0.04900052	0.00626131	4.579	0.85	0.23	9.68	-7.10
Comp B	1.717	(1)	13.93734	0.818032	0.0769913	7.114145	3.24020	1.17868	12.33	-8.79
		(3)	4.96376	0.03944	0.01288	4.06244	0.94846	0.35	12.48	-8.50
Cyclotol	1.754	(1)	12.00982	0.520719	0.068580	6.264679	2.59003	1.0592	13.37	-9.55
		(3)	5.60038	0.05131	0.01361	4.12004	0.99514	0.35	13.49	-9.20

Legend:
 (1) derived from EXPLOS results
 (2) derived from cylinder test (values taken from Souers and Kury)⁽²⁾
 (3) derived from cylinder test (values taken from Hornberg)⁽³⁾

4.2.1. ANFO emulsion correlations

According with THOR program follow the evolution of predicted adiabatic and isentrope curves for limited expansion (“Isen-adiab for limited expansion”), adiabatic and isentrope curves for unlimited expansion (“Isen-adiab for unlimited expansion”) - (P as a function of adimensional volume (v/v_{CJ}) if a double logarithmic scale).

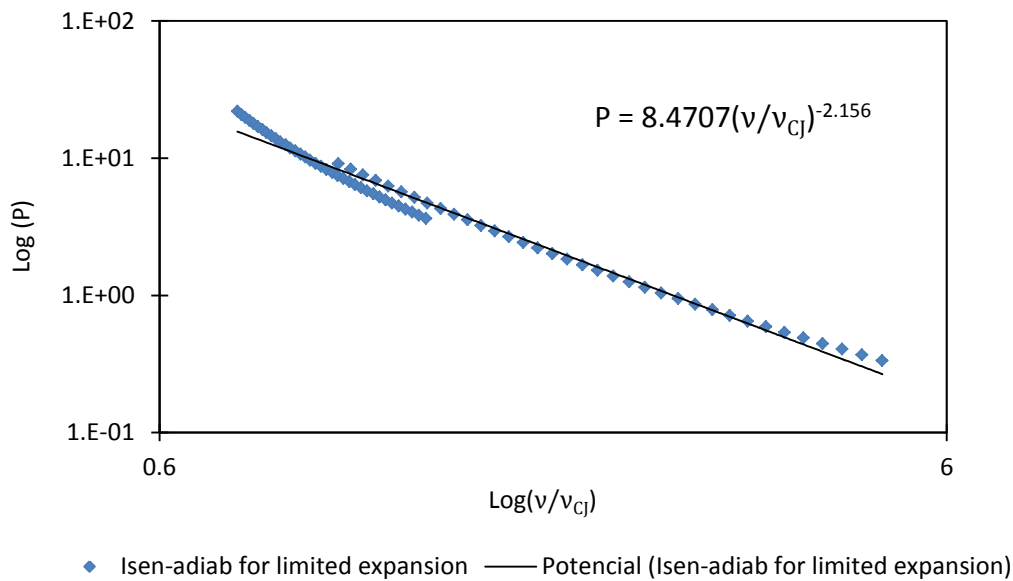
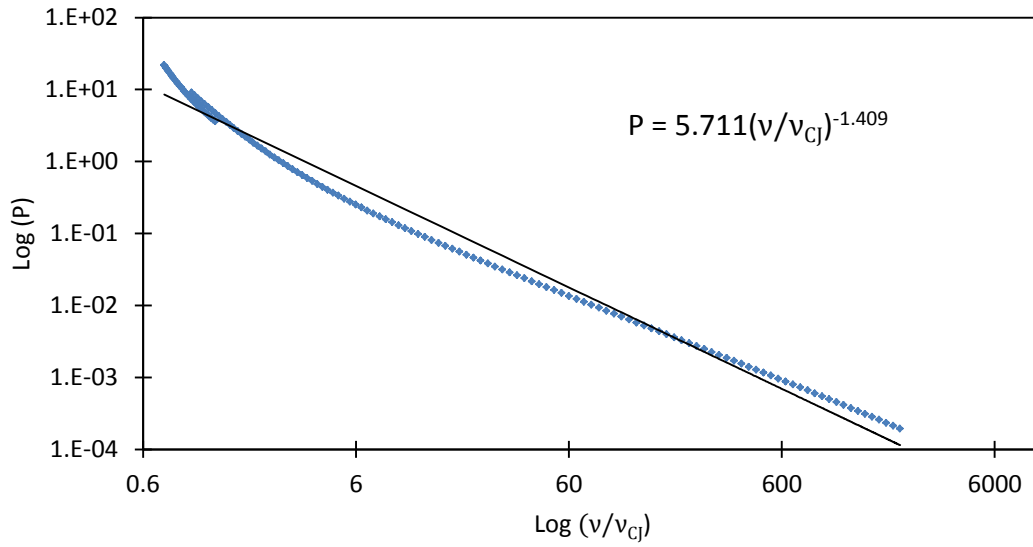


Figure 4.4. Evolution of predicted adiabatic and isentrope curves for limited expansion (“Isen-adiab for limited expansion”) - (P as a function of adimensional volume (v/v_{CJ}) if a double logarithmic scale).



◆ Isen-adiab for unlimited expansion — Potential (Isen-adiab for unlimited expansion)

Figure 4.5. Evolution of predicted adiabatic and isentrope curves for unlimited expansion (“Isen-adiab for unlimited expansion”) - (P as a function of adimensional volume (v/v_{CJ}) if a double logarithmic scale).

All the graphics results are presented on a conclusion table presented below.

a) the evolution of adiabat and isentrope curves based on the Grüneisen coefficient from the exponential of the adiabatic curve, $\omega = 2.242$.

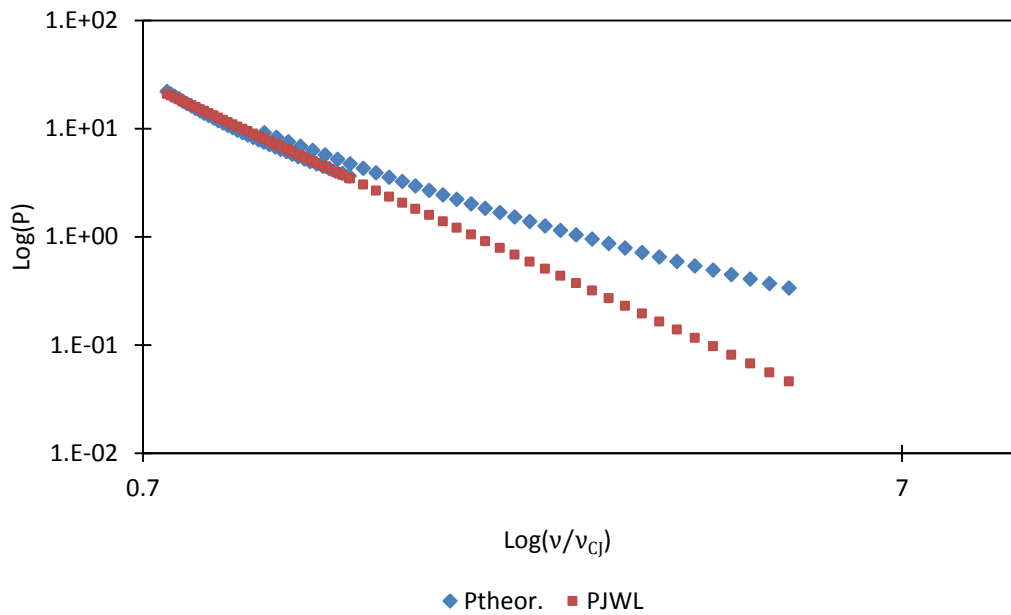


Figure 4.6. Adiabatic and limited isentrope curves, at 2.242 Grüneisen coefficient of the experimental curve, JWL - res. 1.0. (logarithmic scale).

For the graphic result 1.0., “res. 1.0.” the restriction imposive were all influenciated with previous approximation where only Grüneisen coefficient is restricted to his current value and all the parameters to a positive value (applied to al graphic results); then all parameters were approximated to a more valible value. And so the final restritions were $\omega = 2.242$; $A \leq 1000 \text{ GPa}$; $R_1 \leq 12$; $B \leq 60 \text{ GPa}$; $R_2 \leq 4$.

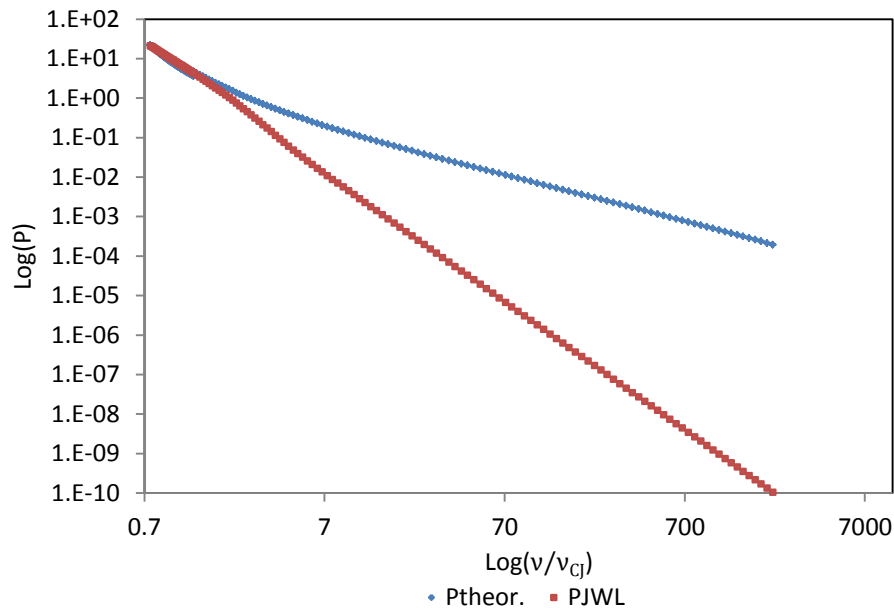


Figure 4.7. Adiabatic and unlimited isentrope curves, at 2.242 Grüneisen coefficient of the experimental curve, JWL - res. 1.1. (logaritm scale).

For the graphic result 1.1., “res. 1.1.” the restriction imposive were $\omega = 2.242$; $12 \leq A \leq 56 \text{ GPa}$; $4 \leq R_1 \leq 10$; $B \geq 10 \text{ GPa}$; $1 \leq R_2 \leq 4$; $C \leq 12 \text{ GPa}$.

b) the evolution of adiabat and isentrope curves based on the Grüneisen coefficient from the exponential of the limited isentrope curve, $\omega = 1.086$.

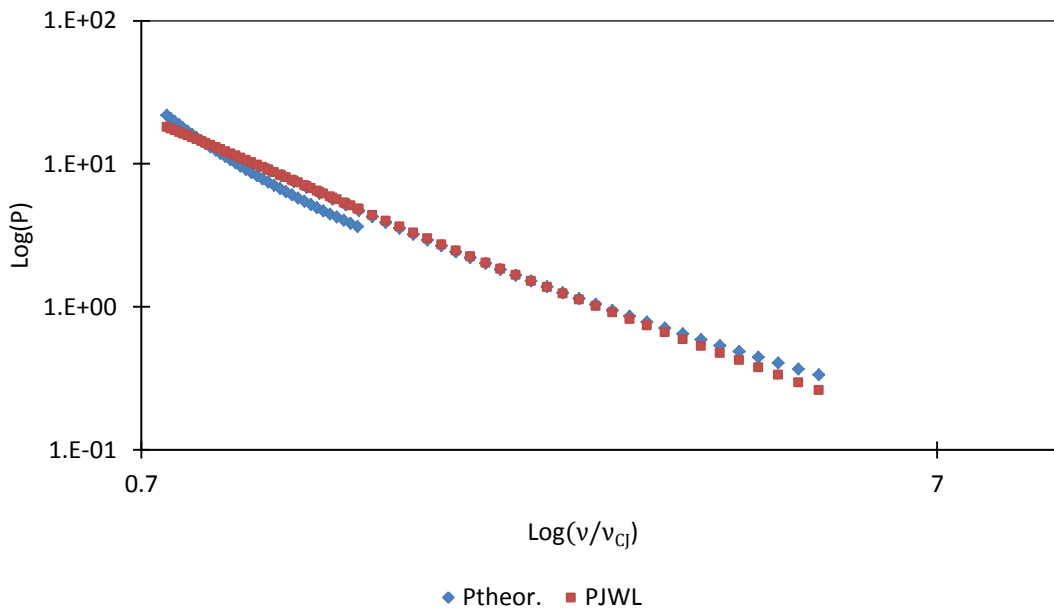


Figure 4.8. Adiabatic and limited isentrope curves, at 1.086 Grüneisen coefficient of the experimental curve, JWL - res. 2.0. (logarithmic scale).

For the graphic result 2.0., “res. 2.0.” the restriction imposed were $\omega = 1.086$.

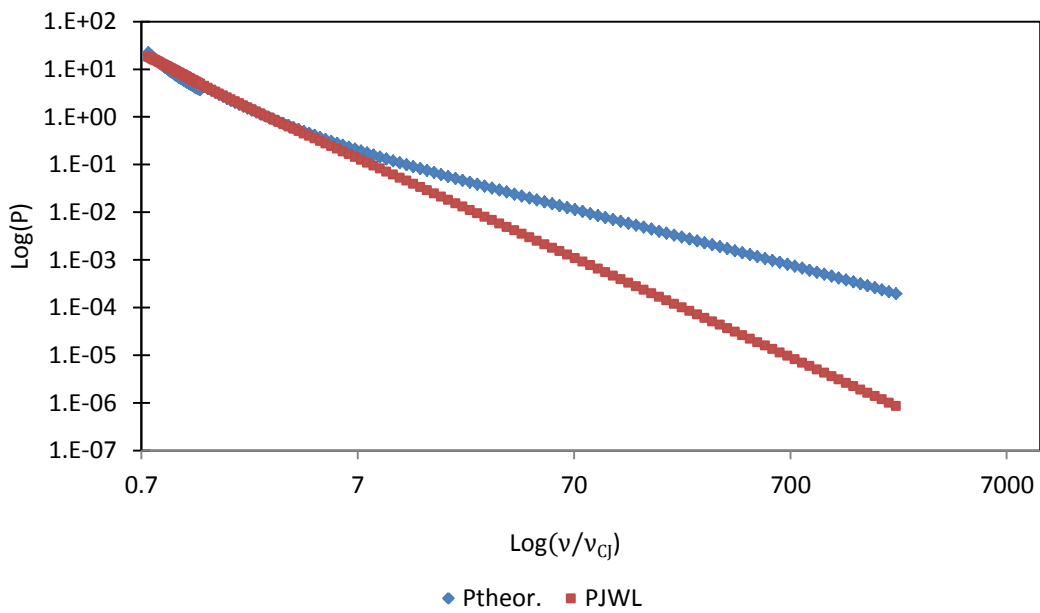


Figure 4.9. Adiabatic and unlimited isentrope curves, at 1.086 Grüneisen coefficient of the experimental curve, JWL - res. 2.1. (logarithmic scale).

For the graphic result 2.1., “res. 2.1.” the restriction imposed were $\omega = 1.086$;
 $A \leq 80 \text{ GPa}$; $R_1 \leq 10$; $B \geq 80 \text{ GPa}$; $R_2 \leq 10$;

c) the evolution of adiabat and isentrope curves based on the Grüneisen coefficient from the exponential of the unlimited isentrope curve, $\omega = 0.328$.

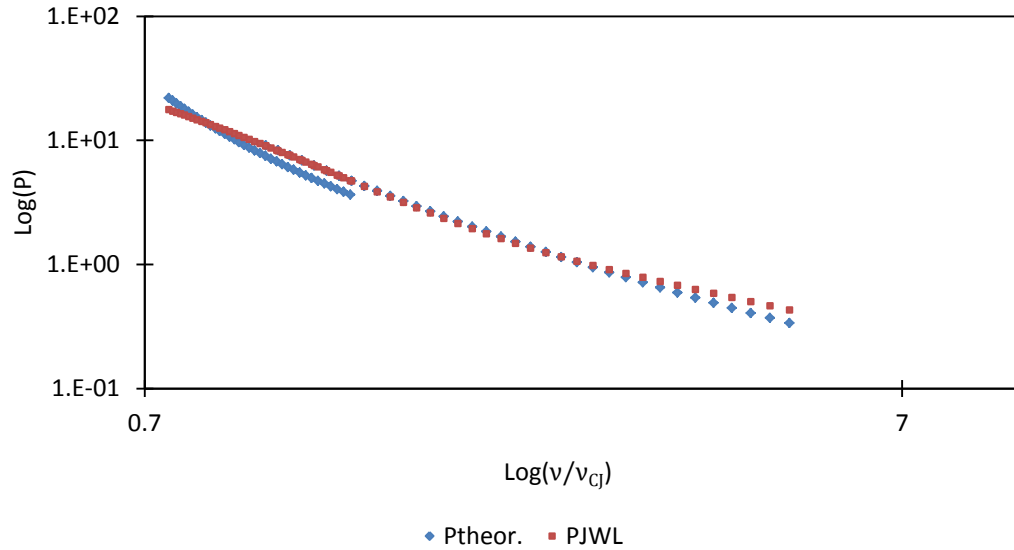


Figure 4.10. Adiabatic and limited isentrope curves, at 0.328 Grüneisen coefficient of the experimental curve, JWL - res. 3.0. (logarithmic scale).

For the graphic result 3.0., “res. 3.0.” the restriction impose were $\omega = 0.328$.

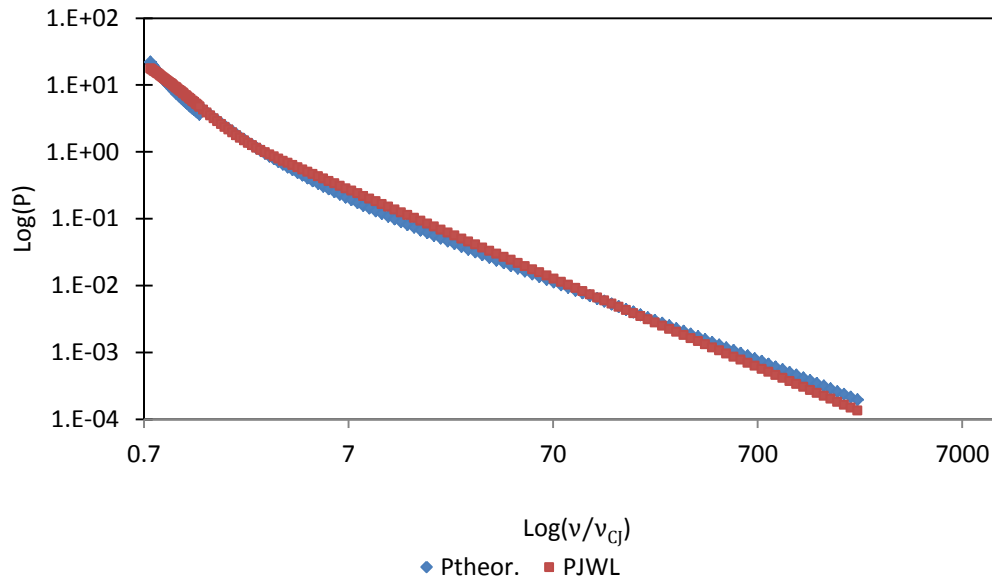


Figure 4.11. Adiabatic and unlimited isentrope curves, at 0.328 Grüneisen coefficient of the experimental curve, JWL - res. 3.1. (logarithmic scale).

For the graphic result 3.1., “res. 3.1.” the restriction impose were $\omega = 0.328$; $A \leq 80 \text{ GPa}$; $R_1 \leq 10$; $B \geq 80 \text{ GPa}$; $R_2 \leq 10$. Being until now the best correlation.

d) the evolution of adiabat and isentrope curves based on the Grüneisen coefficient and the parameter C of JWL deduced by Caroline (Handley, 2011), $\omega = 2.12$.

From Caroline assumptions follow a table with all values obtained for the calculation of the C parameter:

Table 4.2. The Grüneisen coefficient and the JWL C parameter calculated by Caroline assumption – ANFO emulsion.

$\Gamma_{THOR} = 3.12$	$Cv_{CJ} = 2090 \text{ J/kgK}$	Final results
$T_0 = 298.15 \text{ K}$	$v_0 = 0.899 \text{ cm}^3/\text{g}$	$\omega = 2.12$
$T_{CJ} = 1988.493 \text{ K}$	$\phi_{CJ} = 353.3 \times 10^4 \text{ J/kg}$	$C = 8.33 \text{ GPa}$

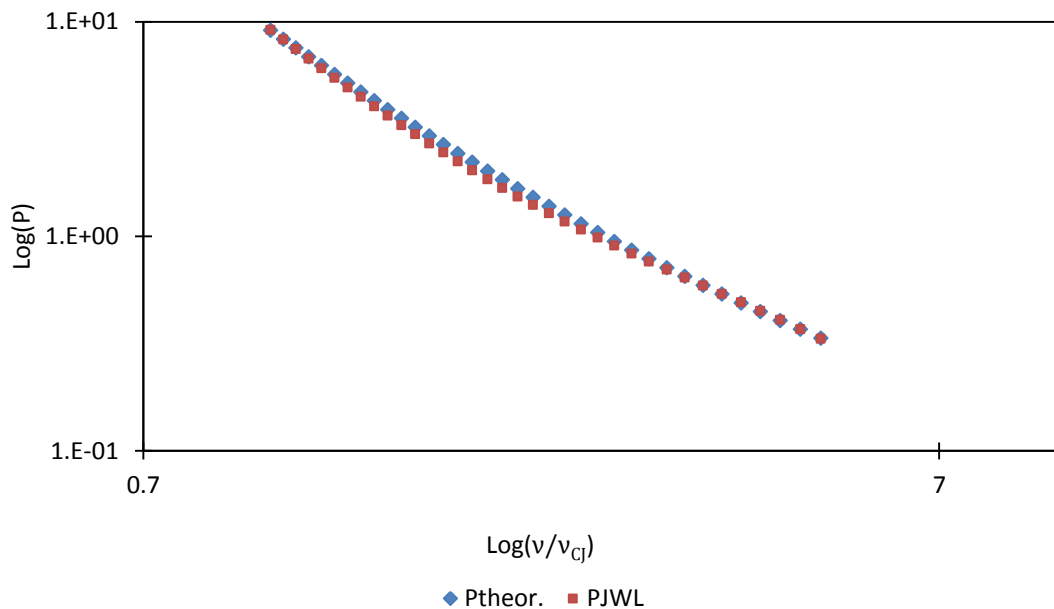


Figure 4.12. Adiabatic and limited isentrope curves, at 2.12 Grüneisen coefficient and at 8.33 GPa C parameter, from Caroline, 2011, for the experimental curve, JWL - res. 4.0. (logarithmic scale).

For the graphic result 4.0., “res. 4.0.” the restriction imposed were $\omega = 2.12$; $C = 8.33 \text{ GPa}$; $12 \leq A \leq 56 \text{ GPa}$; $4 \leq R_1 \leq 10$; $B \geq 10 \text{ GPa}$; $1 \leq R_2 \leq 4$.

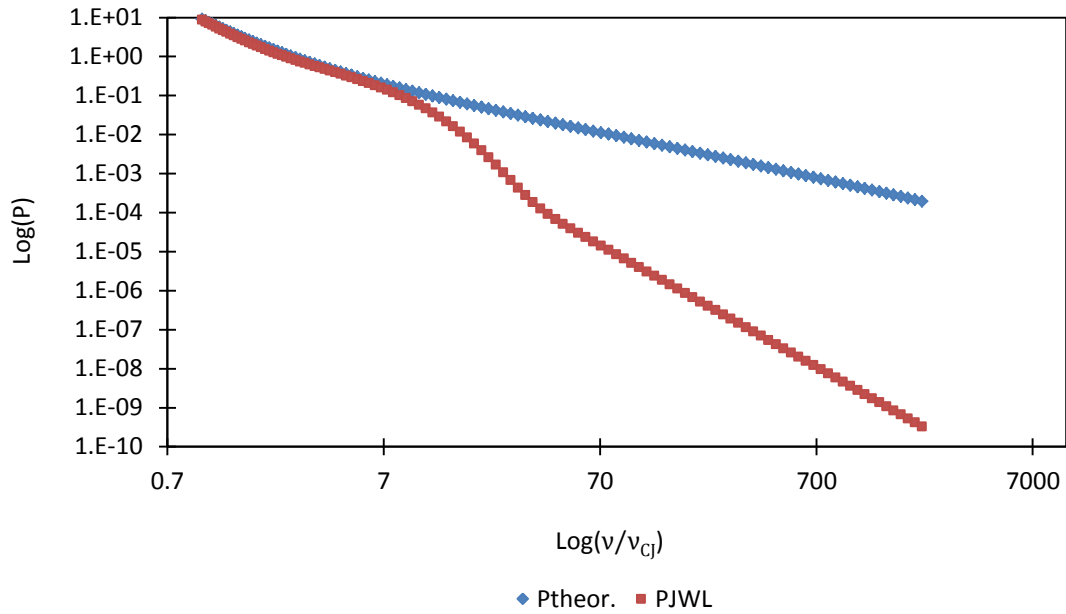


Figure 4.13. Adiabatic and unlimited isentrope curves, at 2.12 Guneisen coefficient and at 8.33 GPa C parameter, from Caroline, 2011, for the experimental curve, JWL - res. 4.1. (logarithmic scale).

For the graphic result 4.1., “res. 4.1.” the restriction impose were $\omega = 2.12$; $C = 8.33 \text{ GPa}$; $A \leq 1000 \text{ GPa}$; $R_1 \leq 12$; $B \geq 80 \text{ GPa}$.

Caroline only applied hers assumptions to a limited adimensional volume less than 10, because after that occurs great products expansion resulting from multiple reactions between products. For the ANFO emulsion the Caroline assumption was performed in both conditions (limited expansion and unlimited expansion), and was concluded that for great adimensional volume expansion is not suitable. Therefore the JWL approach on PETN was only performed to a limited adminisional volume values.

Table 4.3. Calculated JWL coefficients from the different test – ANFO emulsion.

Test	ω	C	A	R1	B	R2	Deflection
		GPa	GPa		GPa		$\Sigma [P_{theor.}-PJWL]^2$
1.0	2.242	8.286	2.716	10.433	0.722	10.333	40.824
1.1	2.242	6.689	56	5.897	14.733	1.747	77.313
2.0	1.086	7.429	56	4	21.999	3.211	91.775
2.1	1.086	7.734	56	3.825	18	3.825	93.453
3.0	0.328	3.6	90	5	90	2.879	99.027
3.1	0.328	3.6	90	5	90	2.879	99.090
4.0	2.12	8.331003	10	3.8	1.23	0.3	0.772
4.1	2.12	8.331003	10	8	1	0.29	0.958

For the current results can be concluded that the most suitable JWL parameters for describing the DP is the res. 3.1., $\omega = 0.328$; $C = 3.6 \text{ GPa}$; $A = 90 \text{ GPa}$; $R_1 = 5$; $B = 90 \text{ GPa}$; $R_2 = 2.9$. Although the deflection between both curves (theoretical and experimental) be the higher it presents a better graphical approximation so as for the limited expansion products as for the unlimited expansion products.

4.2.2. PETN correlations

According with THOR program follow the evolution of predicted adiabatic and isentrope curves for limited expansion (“Isen-adiab for limited expansion”), adiabatic and isentrope curves for unlimited expansion (“Isen-adiab for unlimited expansion”) - (P as a function of adimensional volume (v/v_{CJ}) if a double logarithmic scale).

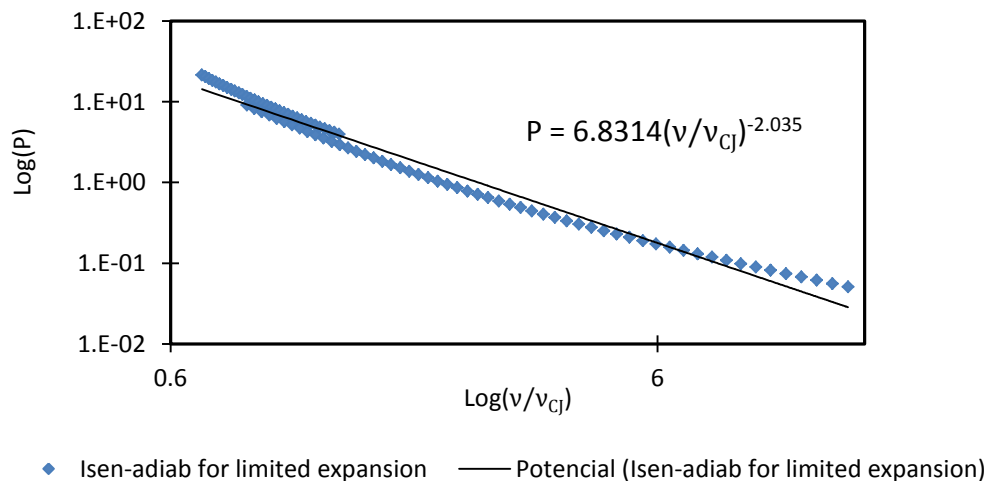


Figure 4.14. Evolution of predicted adiabatic and isentrope curves for limited expansion (“Isen-adiab for limited expansion”) - (P as a function of adimensional volume (v/v_{CJ}) if a double logarithmic scale).

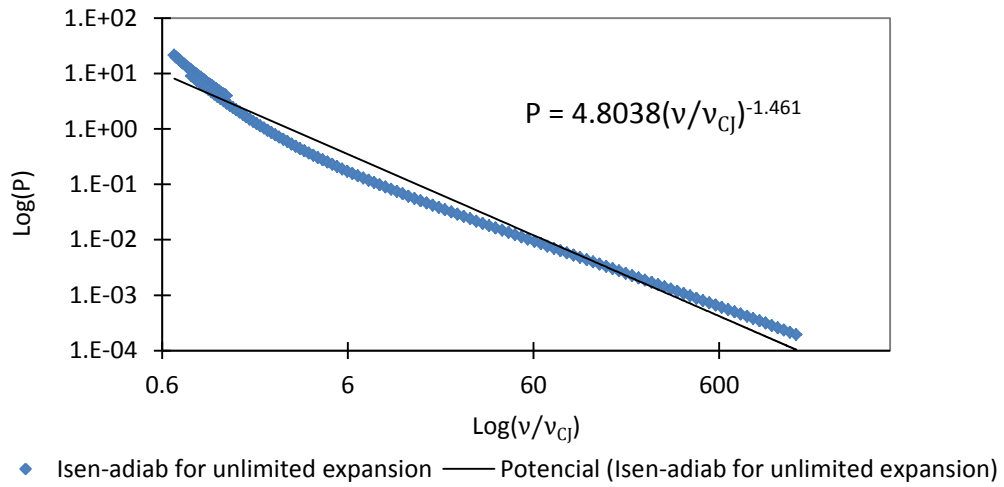


Figure 4.15. Evolution of predicted adiabatic and isentrope curves for unlimited expansion (“Isen-adiab for unlimited expansion”) - (P as a function of adimensional volume (v/v_{CJ}) if a double logarithmic scale).

All the graphics results are presented on a conclusion table presented below.

a) the evolution of adiabat and isentrope curves based on the Grüneisen coefficient from the exponential of the adiabatic curve, $\omega = 1.602$.

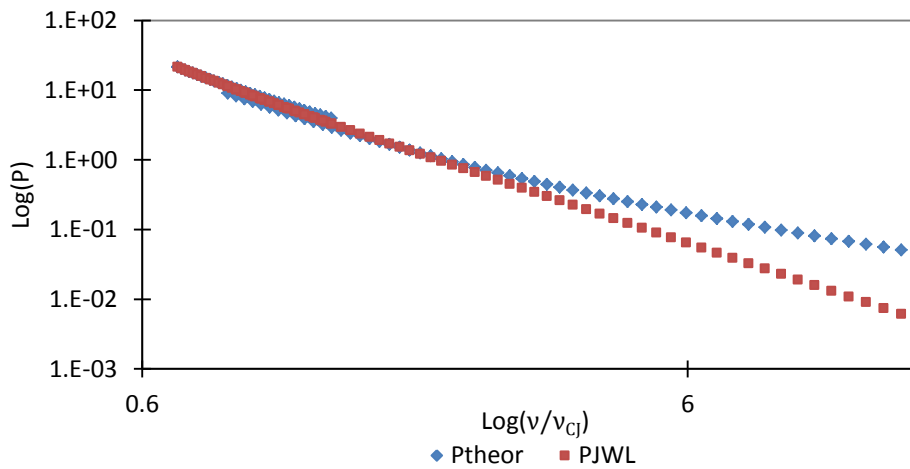


Figure 4.16. Adiabatic and limited isentrope curves, at 1.602 Grüneisen coefficient of the experimental curve, JWL - res. 1.0. (logarithmic scale).

For the graphic result 1.0., “res. 1.0.” the restriction impose were $\omega = 1.602$;
 $A \leq 1000 \text{ GPa}$; $R_1 \leq 12$; $30 \text{ GPa} \leq B \leq 200 \text{ GPa}$; $R_2 \leq 5$.

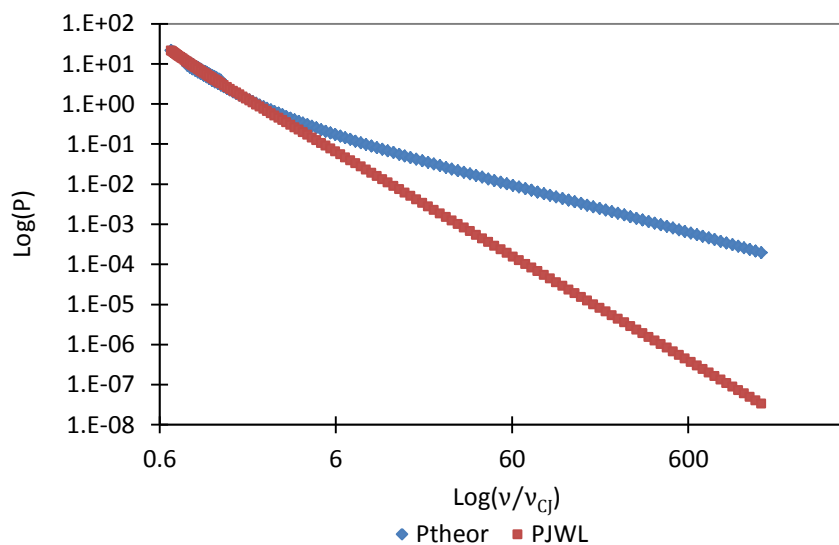


Figure 4.17. Adiabatic and unlimited isentrope curves, at 1.602 Grüneisen coefficient of the experimental curve, JW - res. 1.1. (logarithmic scale).

For the graphic result 1.1., “res. 1.1.” the restriction imposed were $\omega = 1.602$;
 $A \leq 1000 \text{ GPa}$; $R_1 \leq 12$; $30 \text{ GPa} \leq B \leq 200 \text{ GPa}$; $R_2 \leq 5$.

b) the evolution of adiabat and isentrope curves based on the Grüneisen coefficient from the exponential of the limited isentrope curve, $\omega = 0.825$.

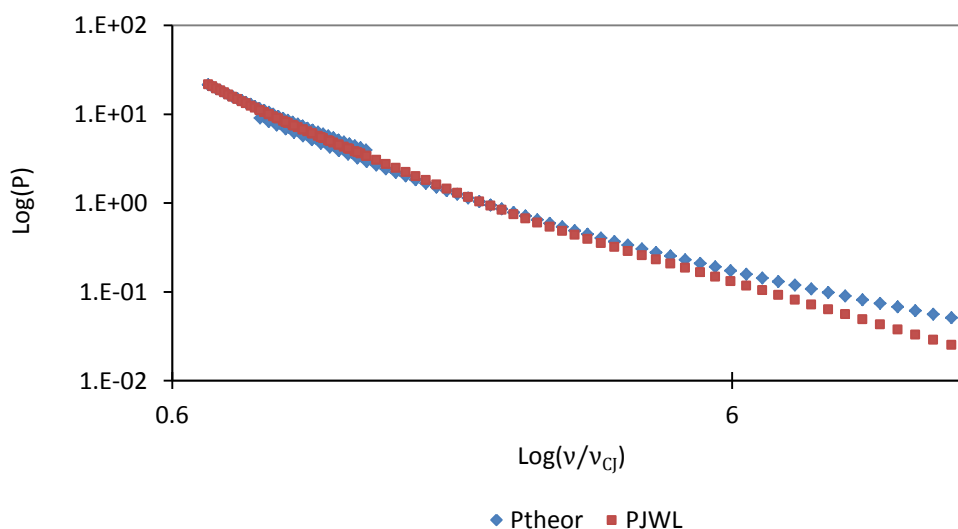


Figure 4.18. Adiabatic and limited isentrope curves, at 0.825 Grüneisen coefficient of the experimental curve, JW - res. 2.0. (logarithmic scale).

For the graphic result 2.0., “res. 2.0.” the restriction imposed were $\omega = 0.825$;
 $A \leq 2800 \text{ GPa}$; $R_1 \leq 12$; $B \leq 200 \text{ GPa}$; $R_2 \leq 5$.

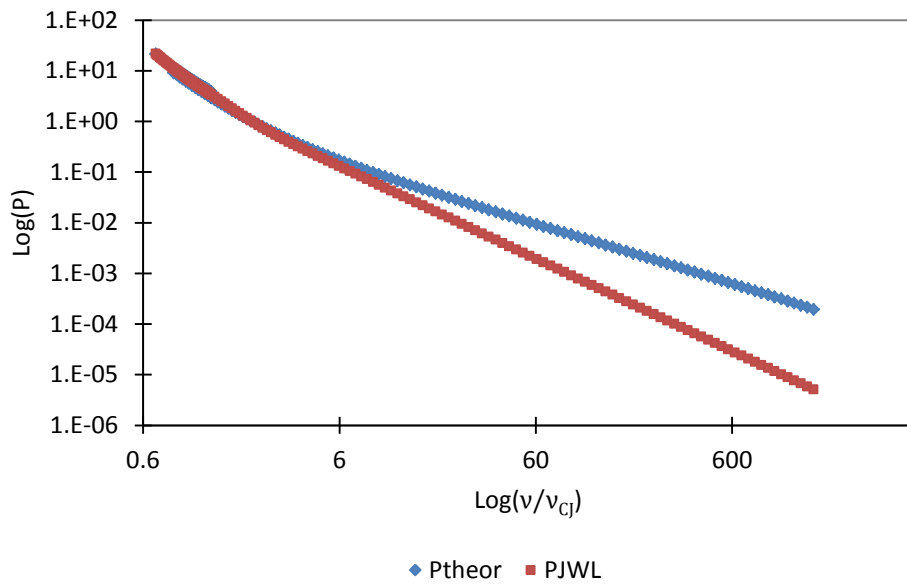


Figure 4.19. Adiabatic and unlimited isentrope curves, at 0.825 Grüneisen coefficient of the experimental curve, JWL - res. 2.1. (logarithmic scale).

For the graphic result 2.1., “res. 2.1.” the restriction impose were $\omega = 0.825$;
 $A \leq 2800 \text{ GPa}$; $R_1 \leq 12$; $B \leq 200 \text{ GPa}$; $R_2 \leq 5$.

c) the evolution of adiabat and isentrope curves based on the Grüneisen coefficient from the exponential of the unlimited isentrope curve, $\omega = 0.356$.

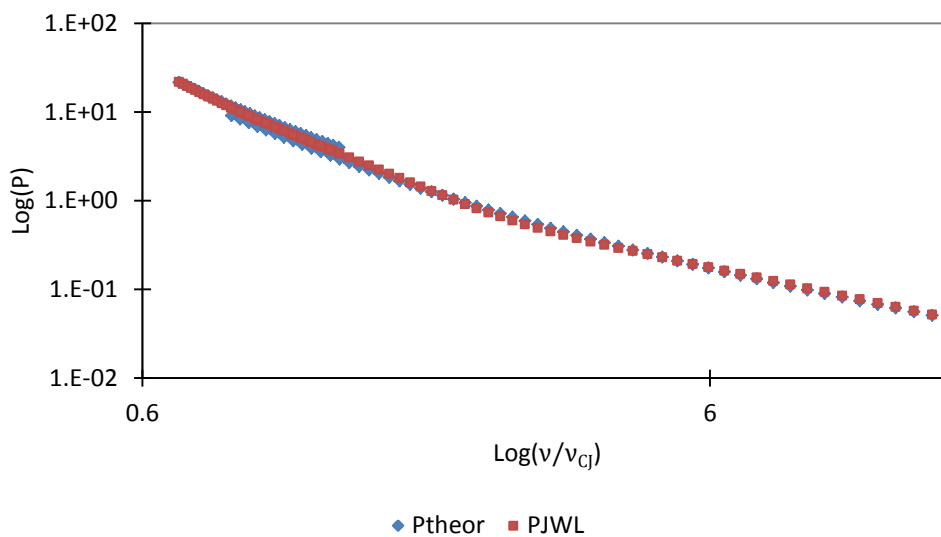


Figure 4.20. Adiabatic and limited isentrope curves, at 0.356 Grüneisen coefficient of the experimental curve, JWL - res. 3.0. (logarithmic scale).

For the graphic result 3.0., “res. 3.0.” the restriction impose were $\omega = 0.356$;
 $A \leq 2800 \text{ GPa}$; $R_1 \leq 12$; $B \leq 200 \text{ GPa}$; $R_2 \leq 5$.

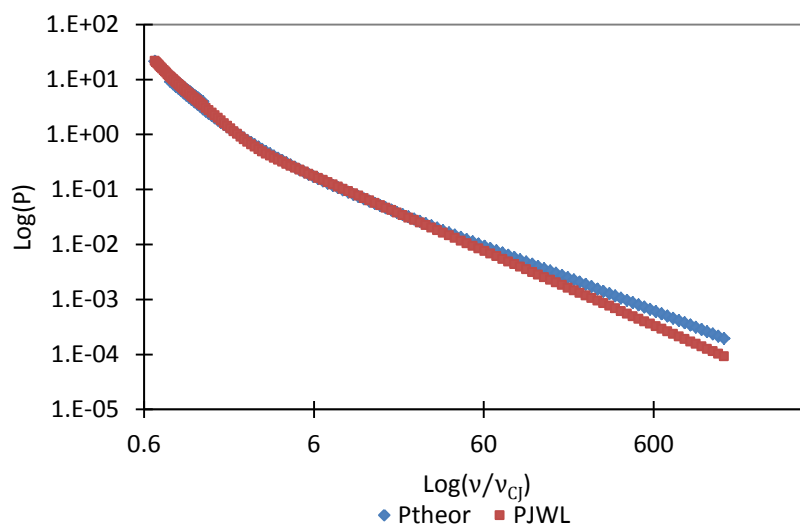


Figure 4.21. Adiabatic and unlimited isentrope curves, at 0.356 Grüneisen coefficient of the experimental curve, JW - res. 3.1. (logarithmic scale).

For the graphic result 3.1., “res. 3.1.” the restriction imposed were $\omega = 0.356$; $A \leq 2800 \text{ GPa}$; $R_1 \leq 12$; $B \leq 200 \text{ GPa}$; $R_2 \leq 5$. Being until now the best correlation.

d) the evolution of adiabat and isentrope curves based on the Grüneisen coefficient and the parameter C of JW deduced by Caroline (Handley, 2011), $\omega = 1.63$.

From Caroline assumptions follow a table with all values obtained for the calculation of the C parameter:

Table 4.4. The Grüneisen coefficient and the JW C parameter calculated by Caroline assumption –PETN.

$\Gamma_{THOR} = 2.63$	$Cv_{CJ} = 4330 \text{ J/kgK}$	Final results
$T_0 = 298.15 \text{ K}$	$v_0 = 0.909 \text{ cm}^3/\text{g}$	$\omega = 1.63$
$T_{CJ} = 3847.111 \text{ K}$	$\phi_{CJ} = 153.7 \times 10^5 \text{ J/kg}$	$C = 27.56 \text{ GPa}$

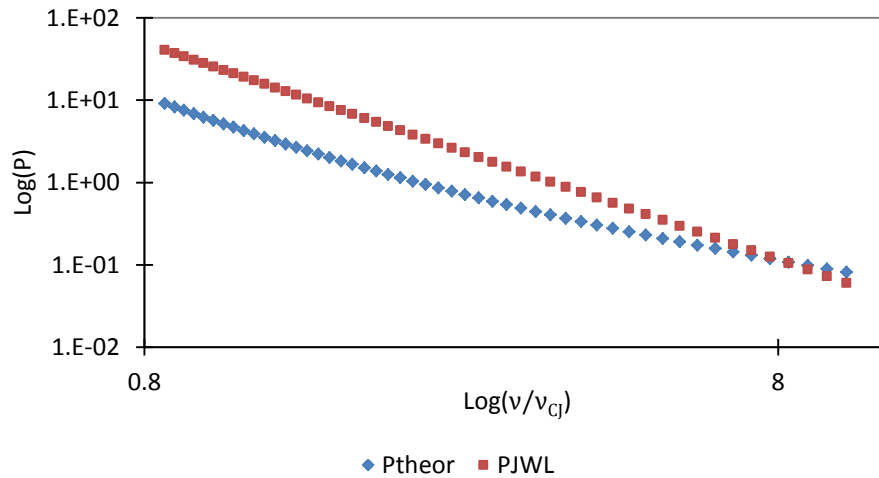


Figure 4.22. Adiabatic and limited isentrope curves, at 1.63 Grüneisen coefficient and at 27.56 GPa C parameter, from Caroline, 2011, for the experimental curve, JWL - res. 4.0. (logarithmic scale).

For the graphic result 4.0., “res. 4.0.” the restriction imposed were $\omega = 1.63$; $C = 27.56 \text{ GPa}$; $R_1 \leq 12$; $R_2 \leq 12$.

For PETN the Caroline assumption is not suitable even for the limited adimensional volume values.

Table 4.5. Calculated JWL coefficients from the different test – PETN.

Test	ω	C	A	R1	B	R2	Deflection
		GPa	GPa		GPa		$\Sigma [P_{theor.} - P_{JWL}]^2$
1.0	1.602	6.81	800	8.29	50	5	26.93
1.1	1.602	6.81	1000	8.29	30	5	26.4
2.0	0.825	3.44	2486.75	8.2	41.54	2.59	25.5
2.1	0.825	3.44	2467.53	8.19	41.48	2.592	25.508
3.0	0.356	1.99	2354.65	7.93	47.78	2.385	25.421
3.1	0.356	1.99	2343.62	7.92	47.62	2.383	25.421
4.0	1.63	27.56	10	12	10	12	576

For the current results can be concluded that the most suitable JWL parameters for describing the DP is the res. 3.1., $\omega = 0.356$; $C = 2 \text{ GPa}$; $A = 2343.6 \text{ GPa}$; $R_1 = 7.9$; $B = 47.6 \text{ GPa}$; $R_2 = 2.4$ the deflection between both curves (theoretical and experimental) is the lower and it presents a better graphical approximation so as for the limited expansion products as for the unlimited expansion products.

In general, the presented results of both explosives show the strong influence of the JWL parameters on the DP curves:

- The Grüneisen parameter influence the initial curve inclination;
- The C parameter influence directly the localization of the curve initial point;
- The A and B parameters are sequentially the next curve inclination;
- The R_1 and R_2 parameters influences the bending of curve itself.

5. DIMENSION AND DESIGN CONFIGURATIONS

Present configuration (Tavares, et al., 2012), (Ambrósio, et al., 2013) was designed to describe a simple BWG. Two types of water containers were used, one with 25 litres, polyethylene container (25x27x38 cm), Figure 5.1 right, and another one with 1000 litres, high density polyethylene (HDPE) cubic meter container (enclosed in aluminium thin tube net grid – Figure 5.1 left). There were also used two types of explosives, ANFO emulsion and PETN detonation cord.

The selected explosives were placed in the center of their respective containers using a 20 mm diameter tube either for the 1000 litres container as for the 25 litres container (Figure 5.2).

The explosive charges that were used were:

- 5, 10 and 15 g charge of ANFO emulsion within the 1000 litres container;
- 0.8 g equivalent charge of PETN corresponding to the standard detonator No. 8 within the 25 litres container;
- detonator No. 8 plus 2.4 g charge of PETN detonation cord (20 cm) also within the 25 litres container, and;
- 7.2 g charge of PETN plus the standard detonator (60 cm) within the 1000 litres container.

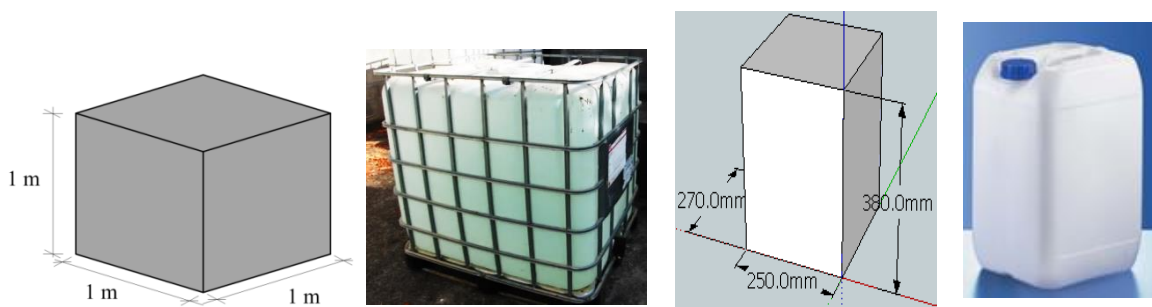


Figure 5.1. On the left the plastic cubic meter container and on the right the 25 litres container.



Figure 5.2. Explosive support structure for the experimental tests. On the top the alluminium tube having the small charge at the end. On the bottom the ones for the 25 lt jerry cans – on the right a plate adapter, and on the left a vertical plastic tube.

During the underwater explosions’ blasting action produced by the explosive-charge, there is a few percentage of explosive material that is shut down from the effective detonation process, but this is not the only source of losses in the BWG performance.

The chemical energy of an underwater explosion is partitioned between the “bubble” energy of gaseous detonation products, the water non-dissipated internal energy, part of shock energy dissipated in surrounding water to heat and the water kinetic energy. Sternberg & Hurvitz, 1976, studied the distribution of the explosive chemical energy at underwater detonations. Obtained results prove the quasi linearity of shock behavior inside water (Plaksin and Campos, 2007).

The composition of emulsion explosive is presented in Table 5.1 and the composition of PETN - PentaErythritol TetraNitrate (a very well defined chemical component) is presented in Table 5.2.

Table 5.1. Main components and global characteristics of classical emulsion explosive.

NAME	COM. NAME	REF.	GLOBAL FORM.	DENS. [g/cm3]		COLOR	PHYS. STATE
				Bulk	Effective		
Ammonium Nitrate	Porous Am. Nit.	AN	NH ₄ NO ₃	0.69-0.74	1.725	white	solid
Oil	Diesel Oil	Oil SAE 30	-	0.9		yellow	liquid
Microcristal Wax	Galp P1	Galp P1	-	-	-	white	solid
Parafin Wax	Guerowax -70	Guerowax -70	-	-	-	yellow	solid
Sorbitan Monooleate	Span 80	Span 80	-	-		yellow	liquid
Sorbitan Sesquioleate	Arlacel 83	Arlacel 83	-	-		yellow	liquid
Hollow Glass Microballons	Q-CEL 400	Q-CEL 400	-	0.11	0.21	white	solid

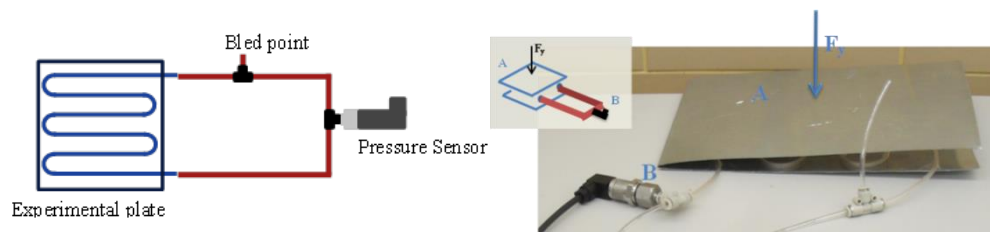
Table 5.2. Global characteristics of classic PETN explosive.

NAME	COM.	REF.	GLOBAL FORM.	DENS. [g/cm ³]		Melting point	Boiling point
	NAME			Bulk	Effective		
PentaErythritol TetraNitrate	Pentrite	PETN	C ₅ H ₈ N ₄ O ₁₂	0.69-0.74	1.77	142.9 C	180 C

The respective explosives were placed inside a balloon and fixed to the support structure for protecting them from the water. They also were placed in the middle of the respective containers.

A pressure mechanism was placed on the external wall of the container to measure the impact inflicted by the BWG. For the 25 litres container tests, it was placed between the ground floor and the water plastic container, and for the 1000 litres container, it was placed between the aluminum thin tube net grid and the container itself.

This mechanism consists in an assemble between a steel plate and the pressure sensor, connected in close loop with a tube (Figure 5.3). The steel plate was placed on the containers' external wall with a serpentine tube for a more homogeneous pressure distribution. This tube contains thin oil (pneumatic oil, Hyspin AWS 46, chosen because of his non compression properties) and is connected in a closed loop to a pressure transducer (Figure 5.3). Then the plate is pressed, and assuming the hydrostatic equilibrium of the fluid, the pressure is calculated by the compression force divided by the steel plate area being transmitted to the pressure sensor and registered on a periphery recording equipment, Tektronix TDS 320, oscilloscope. All the tube connections were properly sealed and a bled point was built on the circuit with the intuit of removing any possible air bubbles.

**Figure 5.3.** Experimental pressure set-up – hydrostatic pressure transmission.

Two pressure sensors were used, one with 0-10 bar range and other one with 0-16 bar range. The pressure devices measure the hydrostatic pressure level. Measured levels

justified the use of 4-20 mA Gems® Sensors & Controls (3100 series) (Figure 5.4). Both sensors were connected with a current output according to their specifications. The electrical circuit and its connections between the sensor and the periphery recording equipment are presented in Figure 5.4.

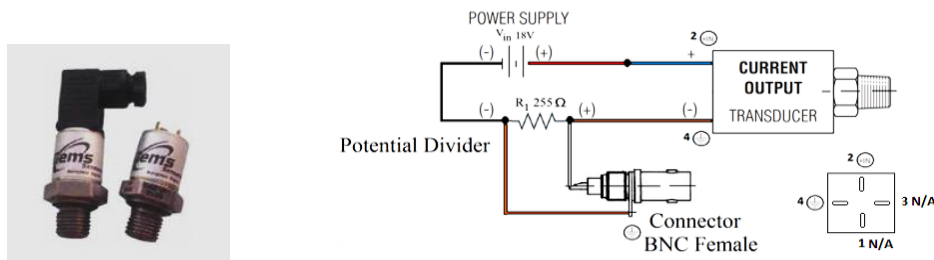


Figure 5.4. 3100 Series Pressure Transmitter, 4-20 mA and its connection circuit.

The sensors were calibrated for a source supply of 24 V_{DC} and a pressure level up to 6x10⁵ Pa of compressing air, using a oscilloscope, Tektronix TDS 320, as periphery recording equipment. Follow the specifications of both pressure sensors: power supply of 8-30 V, current of 4-20 mA and accuracy 0.25 %. The calibration curves are presented in the Figure 5.5. for the two pressure sensors. Where the sensor A correspond to the 0-10 bar pressure sensor (3100B0010G01B) and the sensor B correspond to the 0-16 bar pressure sensor (3100B0016G01B).

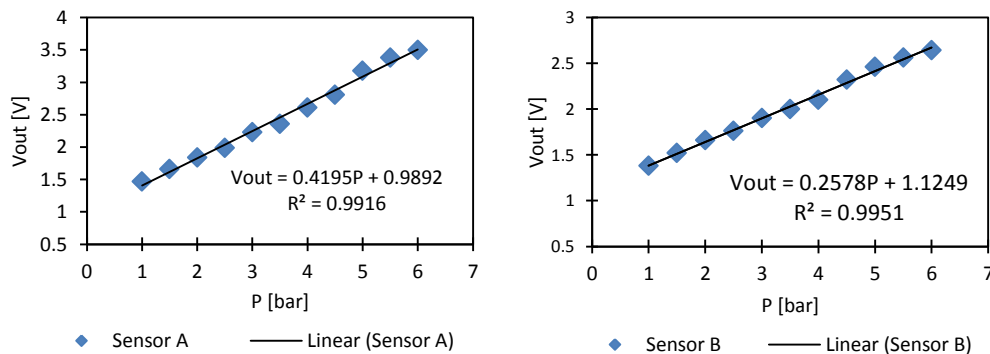


Figure 5.5. Pressure sensors calibration curves of Sensor A (left) and Sensor B (right).

The calibration curves procedure were done using a laboratory compressed air source adjusted with a pressure gauge connected to the tube of the pressure sensor system. The pressure variation was limited for 0-6 bar, the laboratory compressed air source range. In a closed system the pressure variations were registered on the oscilloscope, giving the curves represented on the Figure 5.5.

As was said before the pressure transducers systems were used for evaluate the outside container blast pulse, some experiments were performed with 25 litres plastic containers (Figure 5.6) and others in 1000 litres plastic container (Figure 5.12).

In the case of the 25 litres container, the explosive charge was placed in the center of the plastic container using a plate adapter, fixed in the open hole, or using a vertical plastic tube vertically fixed from the opening hole. The container was placed on top the pressure plate.



Figure 5.6. Plastic 25 litres container, charged with explosive, on the pressure set-up plate.

After the 25 litres container tests was detected a fault in the measure of the pressure, consisting of a damping signal before reaching the sensor itself. This damping is due to the elasticity and length of the tube (2 mm internal diameter polyethylene, 5 mm outside diameter and 2 m length) used. Therefore for the 1000 litres container test with PETN detonator cord charge the pressure set-up plate of both sensors was modified for one with two different kinds of plastic tube (Figure 5.7).



Figure 5.7. New experimental pressure set up – hydrostatic pressure transmission.

This new experimental pressure set-up was composed with a polyurethane 10 mm internal diameter inside the steel plate and with a blue polyamide rigid tube also with

10 mm internal diameter tube that connect the steel plate and the pressure sensor. The length of this last tube was also studied and verified an attenuation effect of the pressure wave transmission for up to a length of 1 m, and therefore the 1 m length was chosen, minimizing the attenuation signal. As was said before, for the PETN detonation cord charge positioned inside the 1000 litres container, this new experimental pressure set-up was placed between the container' wall and the tube net grid (Figure 5.12).

Given the security issues of explosion near historic buildings, was joined to the WBWG study of both explosives, a device that allows the measurement of the distance traveled by a certain reference point over time. For this approach, it was considered a wall [2.5 x 3 m], leaning against the water container, in which was identified 15 reference points in a [5 x 3] matrix (Figure 5.8 - left) and the time response of the wall movement of that 15 points for achieving a certain distances were study. And for each reference point was also assumed the ability to measure three different distances. For this proposes an electronic light circuit was design and built. Which switch is the very reference point and the measurement points correspond to three LEDs differentiated by colors (orange, green and red) for a better identification (Figure 5.8 - right). This mechanist consist on a light electrical circuit where the respectively terminal wires were placed at a certain distance from the container wall, and the wall itself switch on the light by pushing the electrical wires together closing the electrical circuit and with the help of a filming camera the time was recorded.

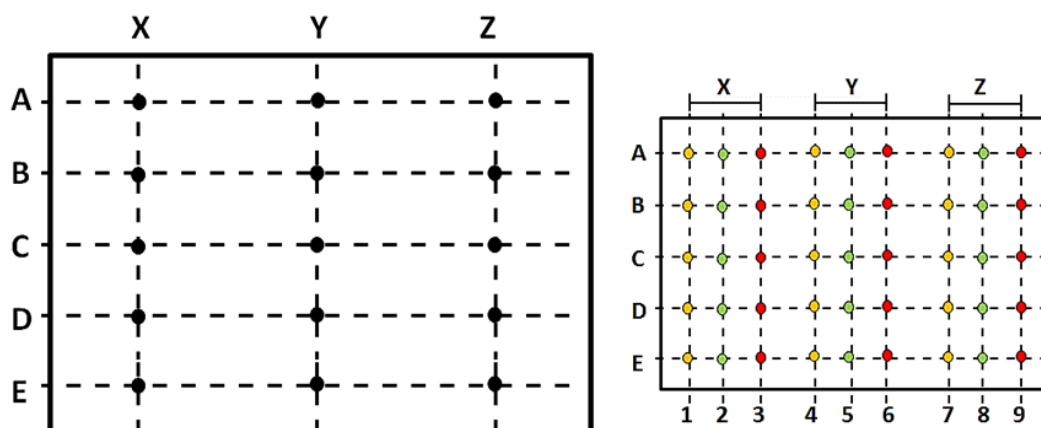


Figure 5.8. Scheme of the relation between the reference points of the wall, on the left, and the light electrical circuit measure points, on the right, to the experimental distance set up used.

The electrical circuit was composed by 45 LEDs (15 orange, 15 green and 15 red), with approximating 2.5 V and 10 Am, 15 capacitor with 2000 μF , for standing the electrical signal for a little time insuring some kind of power failure, 45 resistors of 470 Ω and 0.5 W for guaranty the adequate voltage for each LED, and a 12 V supply voltage. Each transistor was settle in parallel with a group of 3 different LEDs (1 orange, 1 green and 1 red) that correspond to a different distances in study. On the group of 3 different LEDs each LED had one resistor in series (Figure 5.9).

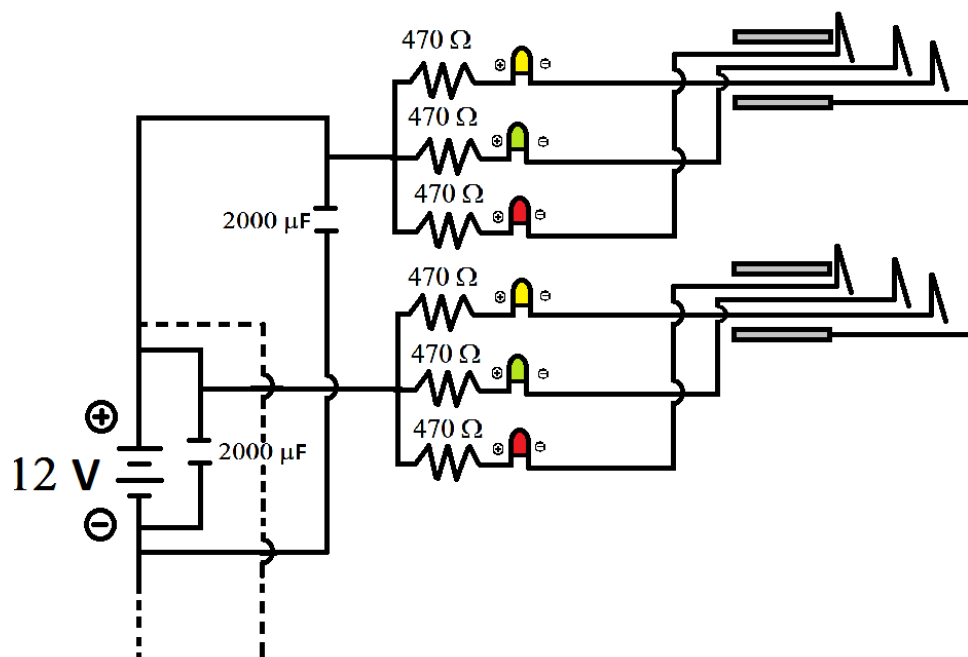


Figure 5.9. Scheme of the light electrical circuit of the experimental distance set up.

Although I have built a system for measuring the movement of 15 reference points of a wall, for the current work only the water wall container movement was study using only one reference point with three distances (one the contact, other the head start of 1 cm and another the final push of 2 cm). This means that was only needed one group of the different LEDs. The scheme used is represented on Figure 5.10.

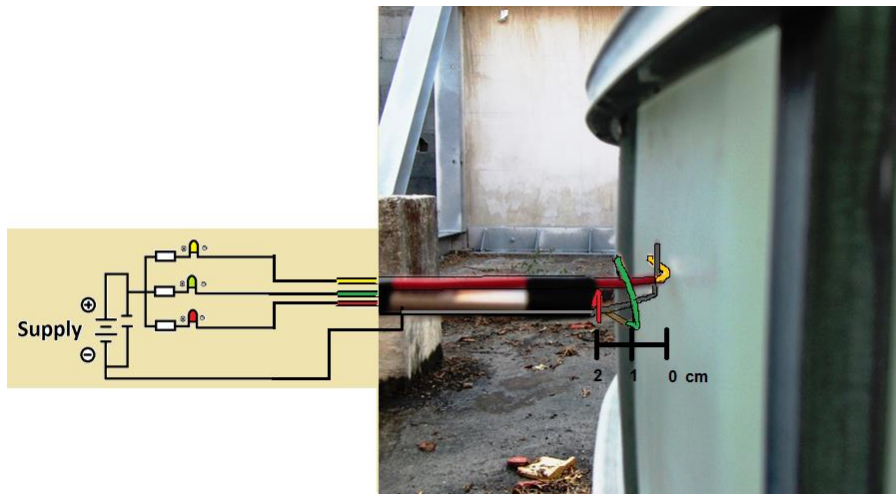


Figure 5.10. Scheme of the light electrical circuit of the experimental distance set up used.

The following picture represents the experimental light electrical circuit set up.

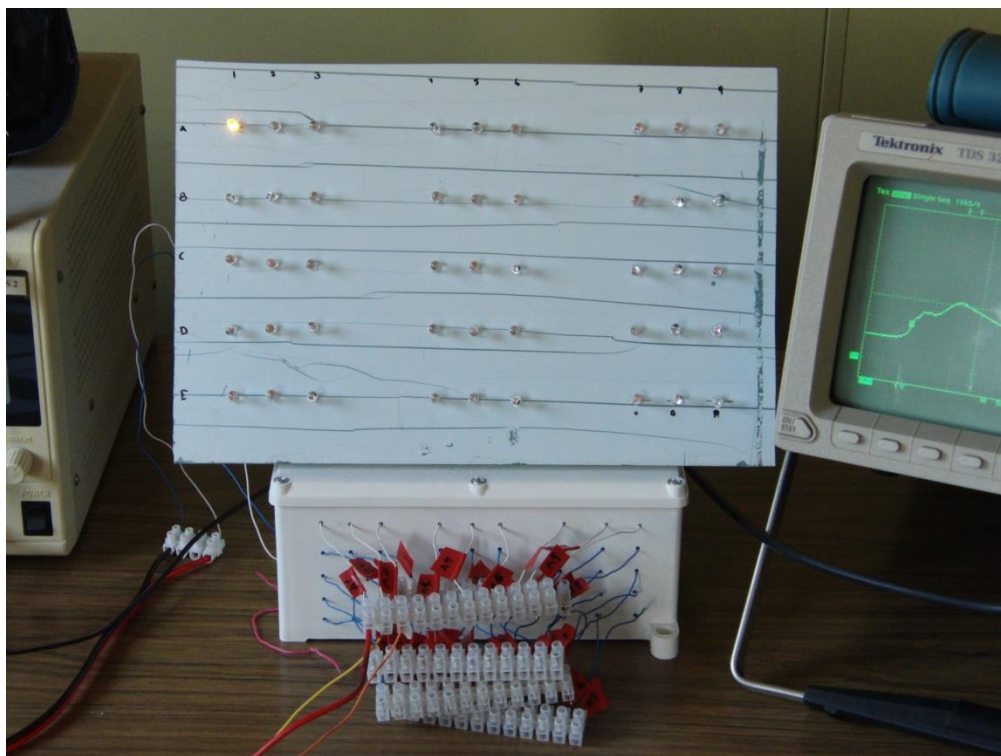


Figure 5.11. Experimental light electrical circuit set up.

The final experimental test for the 1000 litres setup using PETN charge was represented on the following figure where the explosive charge was already inside the container.



Figure 5.12. Plastic 1000 litres container, with the pressure set-up plate and the distance set-up.



Figure 5.13. Control room.

For a better understanding of the experimental tests done, i. e. the effect of the detonation of a determinate charge inside a container, follows an example of a blast type experiment using a 25 litres jerry can (25x27x38 cm) filled with water and an explosive charge of 20 cm PETN detonation cord (12 g / m) that correspond to 2.4 g. The explosive charge was initiated by a standard detonator No.8 that correspond proximally 0.8 g of PETN (0.6 g of PETN charge plus 0.2 g of primary explosive), triggered at the control room (Figure 5.13).

The container was laydown on the floor with a hole on the middle for placing the explosive charge. For placing it also in the middle of the container for a homogenous pressure distribution was used vertical plastic tube lined with a plastic wrap for serving as

support equipment and for protecting the explosive from the water. The recording was conducted with a fast camera under 420fps sequences. The camera was placed in the blasting zone inside a protective support. Follow the experimental results.



Figure 5.14. Blast type experiment – 2.4 g of PETN plus detonator No. 8 and 25L container.

At 2.4 ms the detonation takes place. We can observe the changing of the original size of the container to a spherical one deforming 0.4 cm to the front, 2.4 cm laterally and 2.8 cm to the top. We also observe the frontal section being cut when the detonation start, the detonation wave before the vertical plastic tube that contains the explosive charge, immediately following the flame wave from the interior of the plastic tube and finally the expansion of the DP of the explosive charge. At 4.8 ms there's the detonation wave breaking the container and a maximum DP release. At the final state the container walls are ruptured and also a frontal section projected (Figure 5.15).



Figure 5.15. Final state of the blast type experiment – 2.4 g of PETN plus detonator No. 8 and 25L container.

6. SIMULATIONS AND EXPERIMENTAL RESULTS

Before the experimental trials, was performed a detonation simulation for the two explosives using the program Autodyn. This simulation helps to determine the pressures that we are dealing with and the consequences of the surroundings for a specific quantity of the explosive used.

ANSYS ® AUTODYN ® software is an explicit analysis tool for modeling nonlinear dynamics of solids, fluids and gases as well their interaction. It is suited to the modeling of impact, penetration, blast and explosion events. AUTODYN-2D & 3D are explicit numerical analysis codes, sometimes referred to as “hydrocodes” where the equation of mass, momentum and energy conservation coupled with materials descriptions are solved. Finite difference, finite volume, finite element and meshless methods are used depending on the solution technique (or “processor”) being used. Some of the processors used:

- Lagrange processor, typically used for modeling solid continua and structures, provides rezoning algorithm which the grid moves with the material. It has the advantage of being computationally fast and gives good definition of material interfaces.

- Euler processor, typically used for modeling gases, fluids and the large distortion of fluids and large distortion of solids. Euler capability allows for multi-material flow and material strength to be included. Provides rezoning algorithm which material flows through a fixed grid. Although is computationally more expensive, is better suited to modeling larger deformations and fluid flow.

- ALE (Arbitrary Lagrange Euler) processor which can be used to provide automatic rezoning of distorted grids; ALE rezoning algorithms can range from Lagrangian to Euler.

- Mesh free SPH (Smooth Particle Hydrodynamics) processor is a Lagrangian method that is gridless/meshless, so the usual grid tangling processes that occur in Lagrange calculations are avoided, and the lack of a grid removes the necessity for unphysical erosion algorithms. It is best suited to the modeling of impact/ penetration problems.

The HE are modeled using the traditional JWL EoS considering the energy release from burning of HE particles after the explosives are detonated. Lee Tarver ignition and growth model can be used for more detailed explosive initiation studies (Fairlie, 1998).

Autodyn ANSYS code is an explicit software for nonlinear dynamics and uses the JWL EoS expressed in the classic form described in chapter 4, equation (4.2). This simulation allows the prediction of space/time/intensity of underwater shock wave and its multiple reflections at the external WBWG plastic wall. Results show clearly the evolution of pressure inside water container, as a function of explosive mass charges, and the consequent effect of reflections and wall deformation, dissipating expansion products energy. The experimental WBWG's are, basically, closed plastic cubic meter containers.

6.1. Autodyn simulations

For each explosive, ANFO emulsion and PETN, was performed an Autodyn ® (ANSYS, 2006) simulation. Each simulation is performed in two separated and complementary configurations. (i) detonation progression inside cylindrical charge of 2.5 cm and 10 cm long for ANFO emulsion and 2.5 cm diameter and 2.1 cm long for PETN both in 2D simulation (ii) expansion of detonation products of both explosives inside a cubic meter water tank in 3D simulation. The second visualization (3D) was performed according the following scheme (Figure 6.1), where it can be seen the placement the charge inside cubic water tank. The pressure lines were visualized, inside water, from the axial line of the charge.

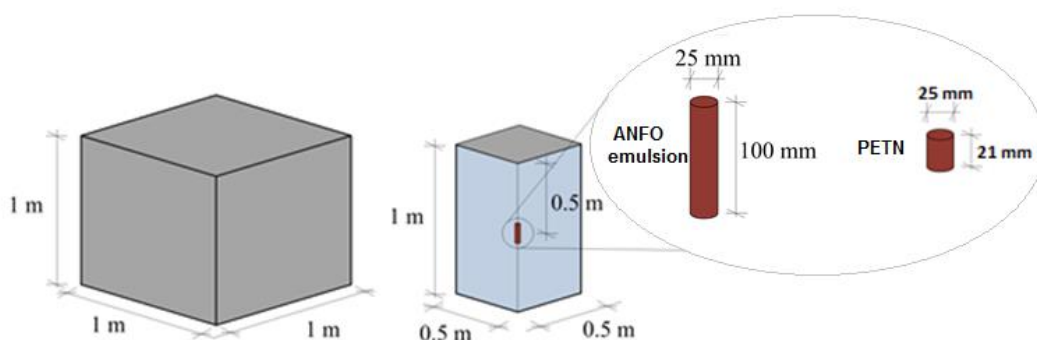


Figure 6.1. 3D Autodyn simulation scheme for both explosives – properties were visualized by the faces generated in the vertical axial line of the charge.

6.1.1. ANFO emulsion Autodyn simulations inside WBWG

For the next configurations the bibliographic data of the Autodyn doesn't has the JWL coefficients of the emulsion used, and so in order to validate the Autodyn data for the emulsion a complex method was established for the JWL coefficients calculation (Tavares, et al., 2012), starting by comparing the Autodyn bibliographic data for ANFO and the forecast data for ANFO using THOR simulation in the same way as described in chapter 4 (based in the evolution of adiabat and isentrope curves obtained by THOR code) in order to validate procedures. Once validated the previous procedure the JWL parameters for ANFO emulsion were calculated by THOR code and finally the approach to Autodyn code was made. Therefore was assumed, approximately, 58.3 g ANFO emulsion with a density of 1187 kg/m^3 and the JWL EoS with the corresponding parameters: $A = 46.75 \text{ GPa}$, $B = 97.57 \text{ GPa}$, $R_1 = 8.958$, $R_2 = 1.348$, and $\omega = 0.073$. At C-J point we have $D_{CJ} = 5509 \text{ m/s}$, $P_{CJ} = 7.85 \text{ GPa}$ and $E_{CJ} = 3.75E + 6 \text{ kJ/m}^3$.

Assuming a 2D configuration, it can be assumed that detonation wave travels through the emulsion material from left to right (Figure 6.2). The shock front is followed by the chemical reaction zone. Behind the reaction zone are located the dense and hot gases from the detonation products. The increase the volume of the gases of the products generates an increase of the pressure, generating a shock wave inside surrounding material (water).

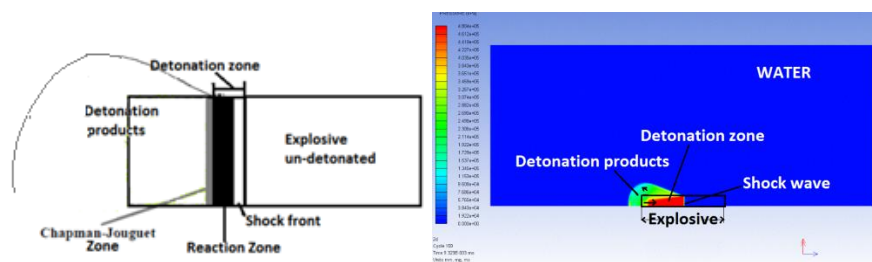


Figure 6.2. Simulation of propagation scheme of detonation of emulsion explosive.

The presentation of results concerns five particular instants: when detonation of explosive is at the end (2D simulation – Figure 6.3), when expansion products took the adimensional volume of 165 v/v_0 (3D simulation – Figure 6.4 left), when expansion products touch the wall of water tank (3D simulation – Figure 6.4 center) and when expansion products in moving to the corners (3D simulation – Figure 6.4 right).

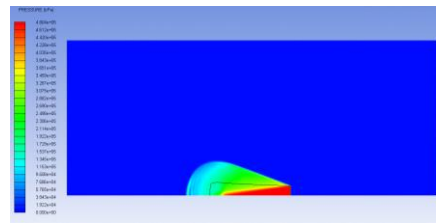


Figure 6.3. Simulation of detonation of emulsion explosive at its end (2D).

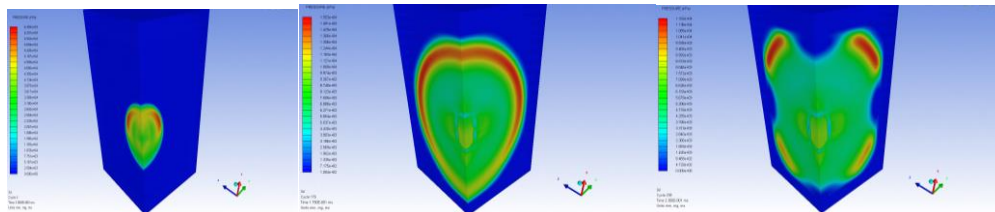


Figure 6.4. Simulation 3D of expansion products of detonation of emulsion explosive, when its adimensional volume reaches the value of 165 v/v₀ (3D simulation - left), when touch water tank wall (3D simulation - center) and when is moving to the corners zone (3D simulation - right).

According to predictions, when the wave reaches the lateral container wall, it is generated a reflection wave - the container plastic wall is then deformed according to a sinusoidal shape. However, when this wave reaches the center of the wall (and starts reflection), the corners are not yet attained by the original positive wave (Figure 6.5). The strong pressure drop only appears when the wave reaches the corners.

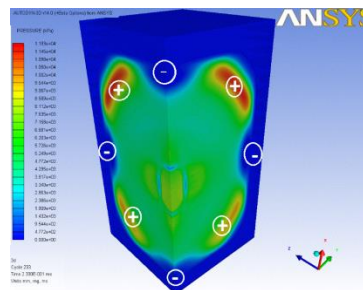


Figure 6.5. 3D simulation of pressure evolution inside water container.

Prediction pressure pattern shows:

- initial values of 0.48 GPa (at the end of detonation),
- 645.9E+5 Pa at expansion value of 165 v/v₀,
- 155.3E+5 Pa when pressure front touch water tank wall,
- 118.3E+5 Pa when it touch corner zone and
- 89.94E+5 Pa when starts reflection from the corner

With these Autodyn predictions of WBWG, using a cubic meter water container, we conclude the possibility of having emulsion charges without destruction of WBWG containers. Since water pressure levels, close to plastic walls, under maximum

admissible charges, are closed to 6 MPa. This simulation also proves the possibility of a new non-destructive method to collect detonation products of small charges.

6.1.2. PETN Autodyn simulations inside WBWG

For the next configurations was assumed, approximately, 15.46 g PETN with a density of 1.5 g/cm^3 and the JWL EoS with the corresponding parameters: $A = 625.3 \text{ GPa}$, $B = 23.29 \text{ GPa}$, $R_1 = 5.25$, $R_2 = 1.6$, and $\omega = 0.28$. At C-J point we have $D_{CJ} = 7450 \text{ m/s}$, $P_{CJ} = 22 \text{ GPa}$ and $E_{CJ} = 8.56E + 6 \text{ kJ/m}^3$.

Like was performed on the previous Autodyn simulation was assumed a 2D configuration, where the detonation wave also travels through the explosive material from left to right, (Figure 6.6). All the assumptions made to the emulsion 2D configuration are valid to PETN 2D configuration.

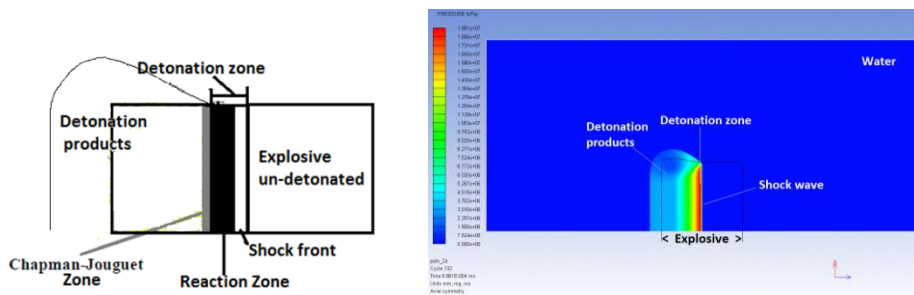


Figure 6.6. Simulation of propagation scheme of detonation of emulsion explosive.

The presentation of results concerns five particular instants: when detonation of explosive is at the end (2D simulation – Figure 6.7), when expansion products took the adimensional volume of 165 v/v_0 (3D simulation – Figure 6.9 left), when expansion products touch the wall of water tank (3D simulation – Figure 6.9 center) and when expansion products in moving to the corners (3D simulation – Figure 6.9 right). For both simulation, 2D and 3D, were measured the evolution at pressure in time at two specific points that are identify on the bottom of their simulations (2D simulation – Figure 6.8 measure at point #1 and #2; and 3D simulation – Figure 6.10 measure at point #3 and #4).

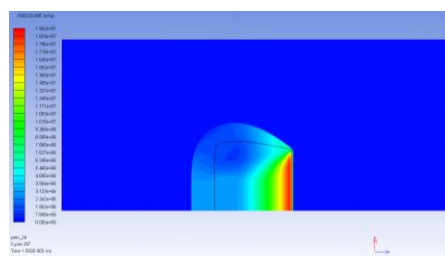


Figure 6.7. Simulation of detonation of emulsion explosive at its end (2D).

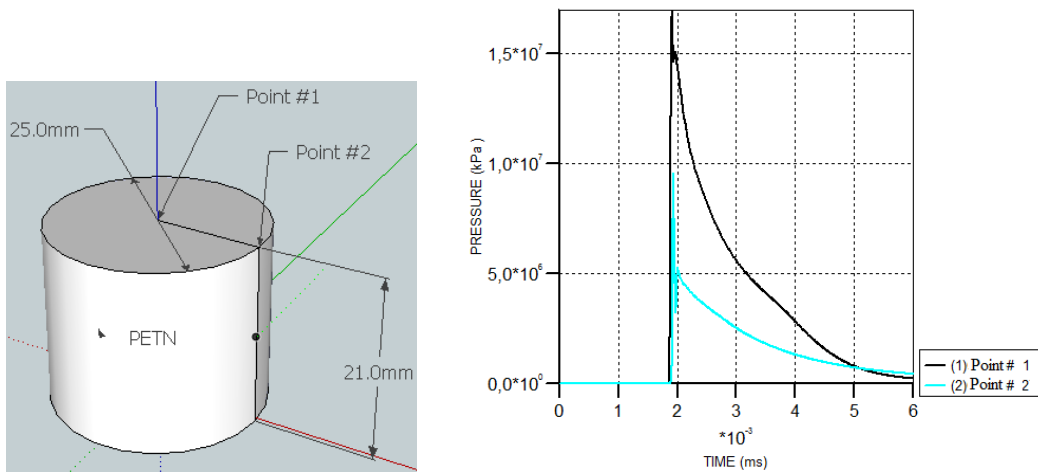


Figure 6.8. Pressure measurement at point #1 and #2 for the 2D simulation on the right. The points are identify on the left picture and correspond to the extrem of the explosive, one measure on the center, Point #1, and other on the edge, Point #2.

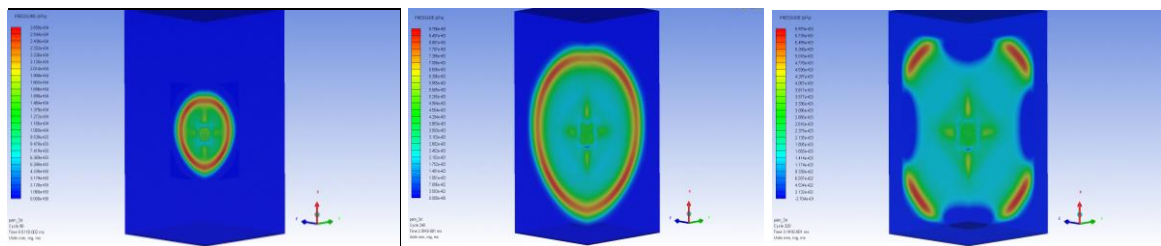


Figure 6.9. Simulation 3D of expansion products of detonation of emulsion explosive, when its adimensional volume reaches the value of 165 v/v₀ (3D simulation - left), when touch water tank wall (3D simulation - center) and when is moving to the corners zone (3D simulation - right).

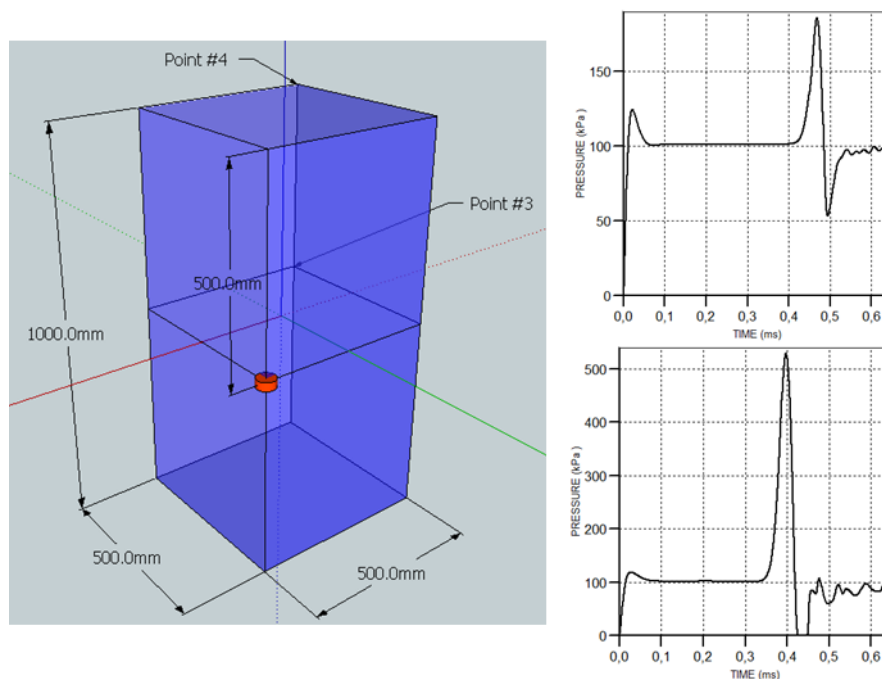


Figure 6.10. Pressure reflection measurements, at point #3 on the bottom and point #4 on the top for the 3D simulation. The points are identify on the center picture and correspond to the corner of the water container, one measure in the middle, Point #3, and other on the top, Point #4.

According to predictions, when the wave reaches the lateral container wall, it is generated a reflection wave - the container plastic wall is then deformed according to a sinusoidal shape. However, when this wave reaches the center of the wall (and starts reflection), the corners are not yet attained by the original positive wave (Figure 6.11). The strong pressure drop only appears when the wave reaches the corners.

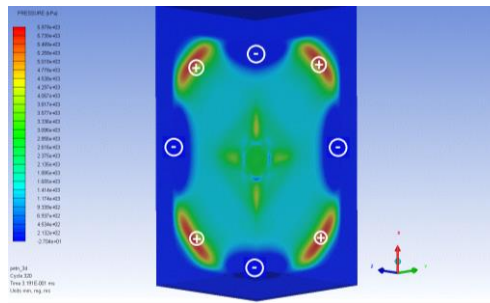


Figure 6.11. 3D simulation of pressure evolution inside water container.

Prediction pressure pattern shows:

- initial values of 19.52 GPa (at the end of detonation),
- 265E+5 Pa at expansion value of 165 v/v₀,
- 87.58E+5 Pa when pressure front touch water tank wall,
- 59.79E+5 Pa when it touch corner zone and
- 50.45E+5 Pa when starts reflection from the corner

And from the selected point above mentioned we have:

- maximum value of 17 GPa at point #1,
- maximum value of 9.5 GPa at point #2,
- maximum reflection value of 5.33E+5 Pa at point #3 and
- maximum reflection value of 1.89E+5 Pa at point #4.

With these Autodyn predictions of WBWG, using a cubic meter water container, we conclude the possibility of having PETN charges without destruction of WBWG containers. Since water pressure levels, close to plastic walls, under maximum admissible charges, are closed to 6 MPa. This simulation also proves the possibility of a new non-destructive method to collect detonation products of small charges.

6.2. Experimental results

6.2.1. ANFO emulsion experimental results

Experimental study shows the blast effect of 5 g, 10 g and 15 g study of ammonium nitrate-fuel oil emulsion explosive inside the cubic meter container (Figure 6.13). Explosive aluminium support tubes deformation (after detonations) gives an idea of the pressure level, as a function of charge radius distance (vd. Figure 6.12). Recorded movies, at 1000 frame/s, also presents external deformation of plastic container and observed reflections (vd. Figure 6.13).

The deformation of the aluminium supports tubes (that allow the explosive charges to be on center of the water container). These deformation indicate the zone where occurs the decrease of high pressure levels, as a function of explosive charge (Figure 6.12).



Figure 6.12. Deformed aluminium support tube, as a function of used charge (5 g left, 10 g center and 15 g right and their group).

The plastic confinement was enclosed inside an aluminum net structure (Figure 6.13) and selected explosive was an ammonium nitrate-fuel oil emulsion explosive. Three mass charges were fired: 5, 10 and 15 g. The value of initial mass (5 g) was obtained by the approach to the cubic root of 58.3 g ($58.3^{1/3}=3.88$) used in previous Autodyn simulations. The inlet opening of plastic cubic container was kept open, in order to have release opening pressure after initial shock and reflections (this cumulative process helps pressure decrease). Follows the fast video frame (at 1000 fps) of the respective tests presenting the external deformation of plastic container and observed reflections (vd. Figure 6.13).



Figure 6.13. External deformation of plastic container and observed reflections for the 3 tested charges (5 g left, 10 g center and 15 g right).

From these results it can be observed that:

- detonation of small charges generate elastic deformation of plastic wall, without any permanent deformation;
- four reflection shock movements of plastic container are clearly observed with 10 g charge; 15 g charge generates permanent deformation – all the other charges generate elastic deformation,
- keeping inlet open allows a dissipative pressure decreasing process, observed clearly under 15 g charge; it allows the non-destruction of container;
- the reflection wave, when shock front touch lateral wall and moves to the corners, generates a clear pressure decrease process,
- deformation of aluminium support tubes, as a function of used charge, show clearly the evolution of high pressure zone growing with increasing charges.

The non-destruction of cubic plastic container, designed for nominal pressure of 6 MPa, proves the validity of selected coefficients, design assumptions and simulation process.

6.2.2. PETN experimental results

Studying the underwater blast wave generated using PETN the shock polar was determined.

The water, according with data base tables, has the following characteristics, $\rho_0 = 998 \text{ kg/m}^3$, $c_0 = 1647 \text{ m/s}$, $s = 1.921$, so according with chapter 2 shock polar equations we have the water detonation equation, D ($D = U_s$) and the pressure, ΔP ($\Delta P = (P_1 - P_0)$), vs particle velocity, u_p , evolution:

$$D = c_0 + s \times u_p \tag{6.1}$$

$$\Delta P = \rho_0 \times D \times u_p \tag{6.2}$$

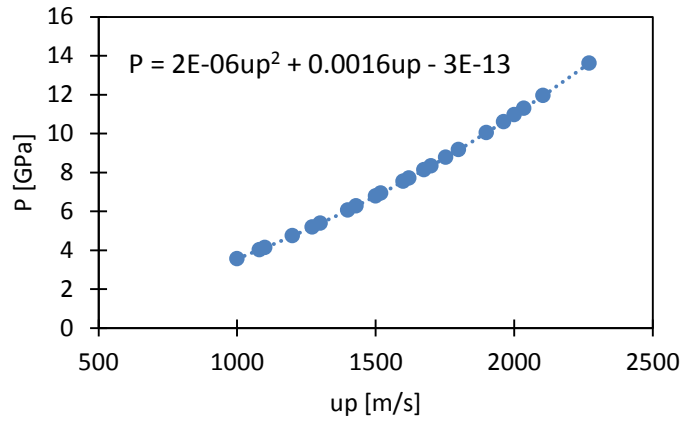


Figure 6.14. Prediction of the Water shock polar in P- u_p plane.

For the PETN properties was assumed proximally the same density as was used on THOR simulation, $\rho = 1170 \text{ kg/m}^3$ ($\rho_{THOR} = 1100 \text{ kg/m}^3$). The respectively shock polar properties for that density were unknown and that's why was needed to performed density approximation to the other data base densities.

By LASL, 1980, we know the PETN detonation products properties, calculated as a function of initial density allowing to the determining its detonation products shock polar. The detonation velocities given by LASL, 1980, were calculated using the $D = 1.608 + 3.933 \rho_0$ (D given in km/s and ρ_0 in kg/dm^3). Obtained experimental pressure P were the values presented by Francis Ree, 1984.

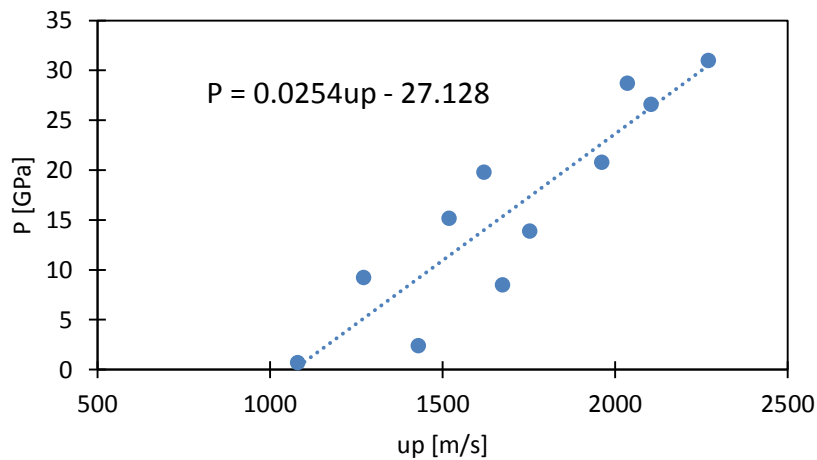


Figure 6.15. Prediction of the PETN shock polar in P- u_p plane. This prediction correlates different PETN densities from experimental data.

Knowing the shock polar of the water and the PETN was determined the shock deduced by the PETN in the water. And for that was constructed a symmetrical PETN line according with detonation conditions and until the water free surface on the collision point, that is assumed to be $2 \times u_p$. So for the same pressure values a new axes was settle $u_p' = 2 \times u_{p_{CJ\rho_0}} - u_p$. The intersection of this line with the water shock polar was recreated by using its trend line that gives the medium values of all PETN experimental values.

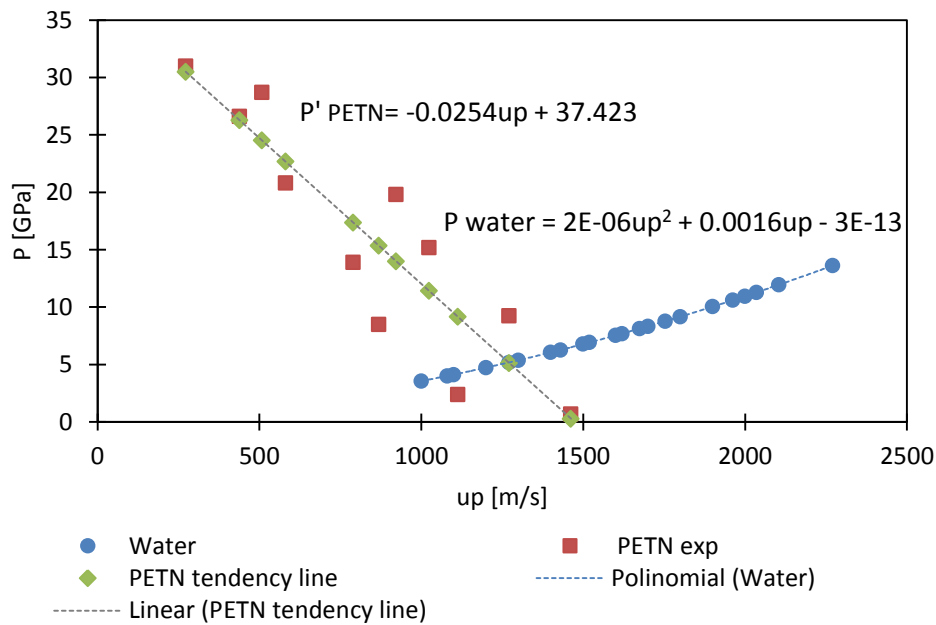


Figure 6.16. Prediction of the Water - PETN shock polar in $P-u_p$ plane.

This interaction approach from detonation products of PETN to the shock polar pressure of water allow the calculation of $A = 5.12 \text{ GPa}$ for the initial density of PETN of 1170 kg/m^3 . Applying the chapter 2 general equations preceding A value and the $\alpha = 1.5$ value it was possible to determine transmitted shock pressure inside water container, as a function of radius distance from central charge (Figure 6.17). The obtained results seem to show the possibility to reach low final pressure values ($P < 0.6 \text{ MPa}$) according to the previous experiments.

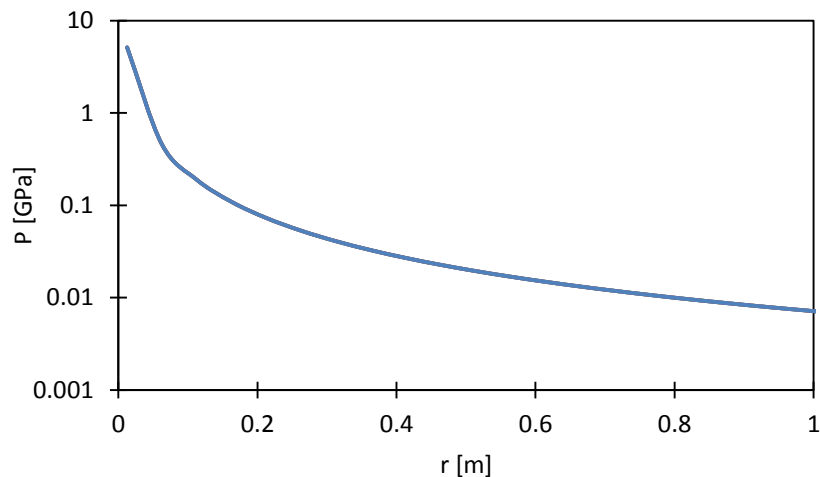


Figure 6.17. Peak pressure P [GPa] evolution as a function of radius r [m], from central charge – PETN vs Water.

After understanding the underwater blasting wave the experimental tests were conducted in two different containers forms, on a small container 25 litres and on a cubic meter container.

The experimental tests on the 25 litres container were performed for 2 classes of different explosive charges:

- using only the standard detonator (0.6 g PETN charge + primary explosive \Leftrightarrow 0.8 g of PETN) without any supplementary charge,
- using the same conditions of the previous test, but now adding 2.4 g PETN (from a detonating cord, 20 cm) to the standard detonator.

All the experiments were recorded with a fast camera under 420 fps or 1000 fps sequences. Pressure was also measured and recorded using 3100B0010G01B pressure sensor (0-10 bar). Pressure signal presents the classic pressure profile of this kind of experiments.

Fast video frames (at 420 fps sequence) of the first class of tests (only with the detonator charge) is presented in Figure 6.18.

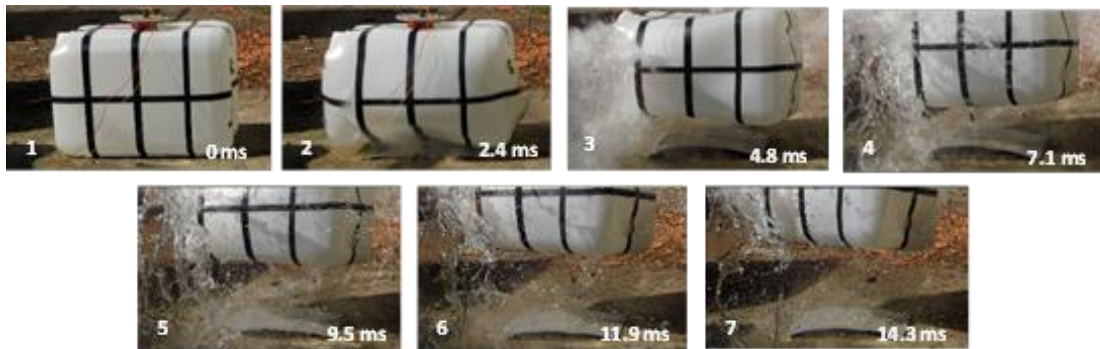


Figure 6.18. Video frames from first class of tests, using standard detonator as charge, inside a 25 litres water container.

For this first test we had a maximum lateral deformation of 2.2 cm and also a maximum frontal deformation of 2.2 cm approximately; on number 2 we can see the initial reflection with 7 cm; on number 7 the container jumps from the floor at a maximum high of 19.5 cm; according to the law of action-reaction pair, the force applied for the container rises 19.5 cm will be equal to an contrary force with the same value exerted on the steel plate, the $F = 35.242 \text{ kN}$ that correspond a $P = 5.65 \text{ bar}$ exerted on a steel plate area of 0.0624 m^2 . From number 1 to number 7 we had a time interval of 14.3 ms.

The pressure, like said before, was measured with the pressure sensor 0-10 bar and the periphery recording equipment used was an oscilloscope, Tektronix TDS 320. For this test we had the oscilloscope calibrated to single acquisition sequence, tigered at 1.32 V, at a vertical scale of 500 mV and a horizontal scale of 500 ms, (Figure 6.19).

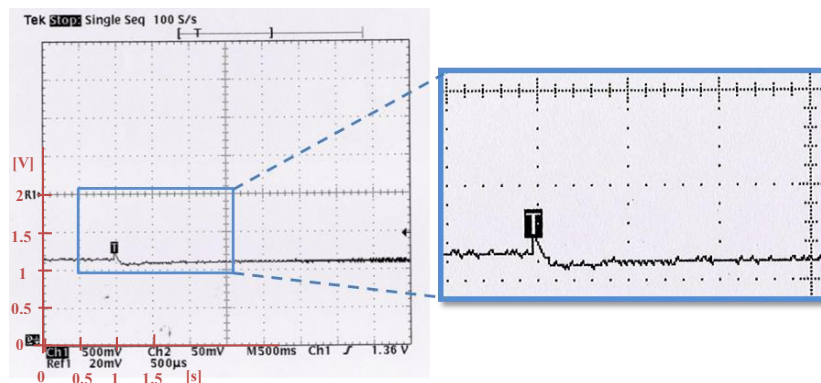


Figure 6.19. Measurement of the pressure of the first test conducted on 25 litres container. Signal obtained by using a pressure sensor 0-10 bar and a oscilloscope, Tektronix TDS 320, as his periphery recording equipment.

As can be observed at Figure 6.19 an initial value of 1.14 V, a maximum value of 1.33 V and a minimum value of 1.06 V. According with the calibration curve of the pressure sensor 0-10 bar we had an maximum pressure of $\Delta P = 0.45 \text{ bar}$. And the

intervale was 100 ms. This result proves the attenuation effect of the pressure wave inside the used oil tube.

Follows the second class of experimental tests performed. Fast video frames (sucessively at 420 fps and 1000 fps sequences) of the second class of tests (detonator more 2.4 g of PETN) are presented in Figure 6.20 and Figure 6.22.

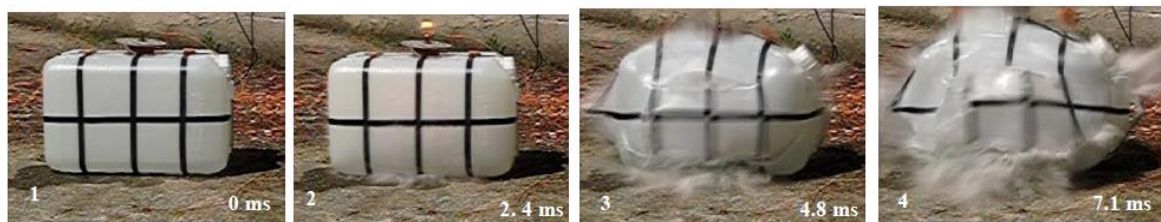


Figure 6.20. Video frames from second class of tests, using standard detonator more 2.4 g of PETN as charge, inside a 25litres water container (420 fps sequence).

For this test we observed a maximum lateral deformation of 3.5 cm and also a maximum frontal deformation of 2.2 cm approximately; on number 2 we observed the detonation products leaving the metal support tube; on number 3 we observed the deformation of the container changing from its original rectangular shape to a transient spherical one; and from number 1 to number 4 we had a time interval of 7.1 ms.

The pressure was measured with the 0-10 bar pressure sensor and the periphery recording equipment used was an oscilloscope (Tektronix TDS 320). The oscilloscope was calibrated to single acquisition sequence, tiggered at 1.32 V for the two tests at a vertical scale of 500 mV and a horizontal scale of, 250 ms (Figure 6.21).

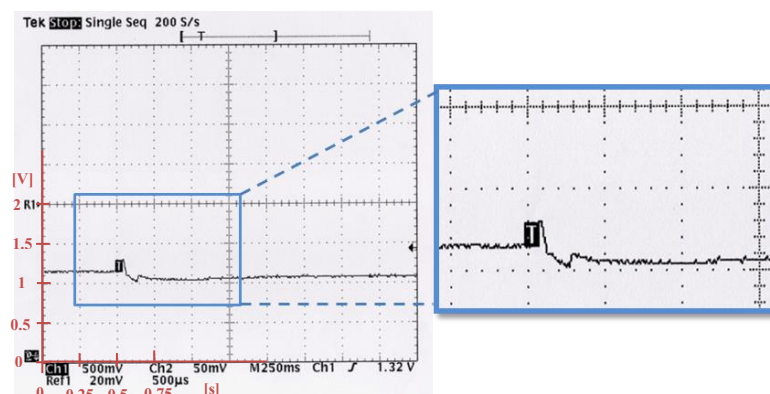


Figure 6.21. Measurement of the pressure of the second class of tests conducted on 25 litres container. Signal obtained by using a pressure sensor 0-10 bar and a oscilloscope, Tektronix TDS 320, as his periphery recording equipment.

As can be observed at Figure 6.21 we have an initial value of 1.14 V; a maximum value of 1.33 V; and a minimum value of 1.02 V. According with the calibration curve of the 0-10 bar pressure sensor we had an maximum pressure of $\Delta P = 0.45 \text{ bar}$. And the intervale was 150 ms. It was observed the attenuation effect of pressure wave transmission.

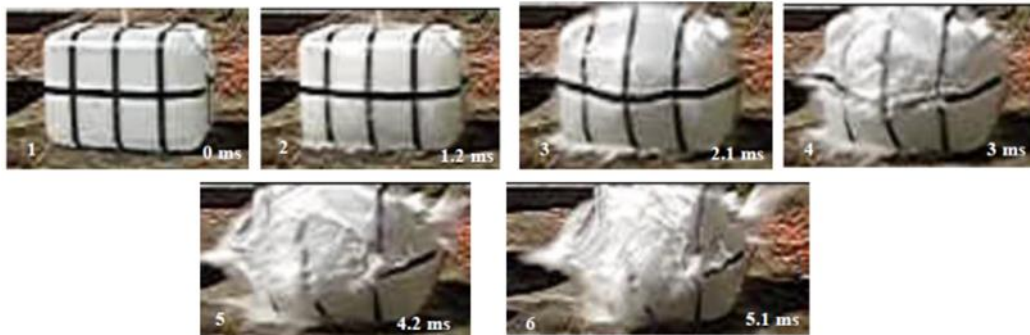


Figure 6.22. Video frames from second class of tests, using standard detonator more 3 g of PETN as charge, inside a 25litres water container (1000 fps sequence).

For this new test with the same conditions as the previous one at 1000 fps sequece we could observe a maximum lateral deformation of 2.6 cm and also a maximum frontal deformation of 3.5 cm approximatelly; at number 3 we observed the deformation of the container changing from its original rectangular shape to a transient spherical one; at number 4 took place the equatorial break of the container and from number 1 to number 6 we had a time interval of 5.1 ms.

Obtained results prove the validity of simulations, confirming central blasting phenomena process for the generation of an exterior blast generator. Main blast wave expands initially according an “equatorial” disc. The blast process, later on, is expanding for all directions. Sinusoidal shapes of lateral walls were observed. Measured pressure levels are lower than theoretical expected values, the reasons of this were mentioned on the Chapter 5, and that’s will the previous pressure set-up with 5 mm diameter polyethylene tube was changed for the next cubic meter experimental test. Plastic 25 litres containers are ruptured at final, but not destroyed, confirming predicted values. Follow the final images of the tested containers.



Figure 6.23. Final images of the 25 litres container – on the left the first class of tests and on the center and right the second class of the tests respectively.

The deformation and blasting of 1000 litres container was performed for a standard detonator (0.6 g PETN charge + primary explosive \Leftrightarrow 0.8 g of PETN) with 7.2 g PETN (60 cm from a detonating cord, 12 g / m). Like the previous experimental test with the emulsion the plastic confinement was enclosed inside an aluminum net structure and the inlet opening of plastic cubic container was kept open, in order to have release opening pressure after initial shock and reflections (this cumulative process helps pressure decrease). The value of 7.2 g was obtained by the approach to the cubic charge of the explosive equivalent length by the cylindrical volume formula and by the following correlation $m/V = 1170 \text{ kg/m}^3$. Since the small container, 25 litres, for 3 g PETN (20 cm detonation cord) correspond an equivalent length, $L_{eq} = 5.2 \text{ mm}$ then for 9 g PETN correspond to $L_{eq} = 15 \text{ mm}$. Since 60 cm of detonating cord (12 g/m) correspond to 7.2 g PETN, and then 7.2 g PETN plus standard detonator, 0.8 g PETN, gives 8 g PETN proximally the charge used was 7.2 g PETN.

The recording was conducted with a fast camera under 420 fps sequences. Pressure was also measured and recorded using 3100B0016G01B pressure sensor (0-16 bar). Pressure signal presents the classic pressure profile of this kind of experiments (Figure 6.26). When the charge explodes the container enlarges his original size, and so 1 cm and 2 cm of that expansion were measured and recorded in time. For that one light circuit was built, where the respectively light switches correspond to the distances covered by the wall. Through the filming (at 420 fps sequence) of the light plate was recorded the times that the container wall took to achieve these distances. Taking as zero position the yellow circuit light, green circuit light 1 cm and red circuit light 2 cm.

Fast video frames (at 420 fps sequence) of test (detonator charge plus 7,2 g PETN) is presented in Figure 6.24 and Figure 6.25.



Figure 6.24. Video frames from the external deformation of plastic container on the detonation initial states, using 7.2 g PETN plus standard detonator as charge, inside a 1000 litres water container (initial point left, detonation point right).



Figure 6.25. Video frames from the external deformation of plastic container on the final states before the water comes out, using 7.2 g PETN plus standard detonator as charge, inside a 1000 litres water container.

From the initial and final frames we can determine that the container wall enlarge 4.3 cm and the container itself full of water moves to left proximally 2 cm. The non-destruction of cubic plastic container, designed for nominal pressure of 6 MPa, proves the validity of selected coefficients, design assumptions and simulation process.

The measurement of the test pressure is presented in Figure 6.26. The oscilloscope record signal was conducted at the scale 5 ms and 1 V, to single acquisition sequence, triggered at 1.72 V.

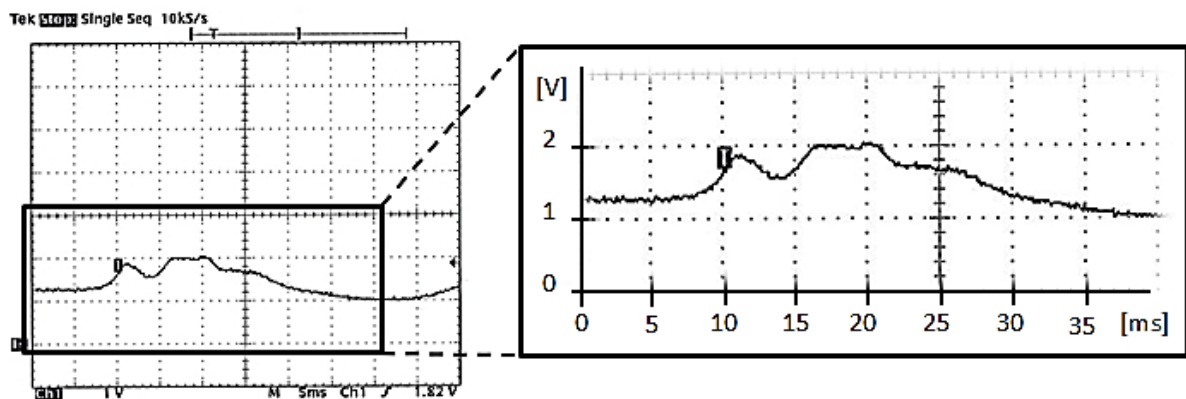


Figure 6.26. Measurement of the pressure of 7.2 g PETN on 1000 litres containers. Signal obtained by using a pressure sensor 0-16 bar and a oscilloscope, Tektronix TDS 320, as his periphery recording equipment.

The pressure peak represents an indicative value. Using the calibration curve of the 0-16 bar sensor we have for the 2 V given by the oscilloscope $\Delta P = 3.5 \text{ bar}$. From this recording we can know that detonation took proximally 18 ms. Under this conditions, increasing oil tube from 5 mm to 10 mm, the pressure attenuation effect was strongly reduced (vd. Figure 6.26)

The non-destruction of cubic plastic container designed for nominal pressure of 6 MPa, using 7.2 g the PETN plus standard detonator proves show the possibility of having PETN charges without destruction of WBWG containers.

Fast video frames (at 420 fps sequence) of test distance vs time is presented in Figure 6.27.

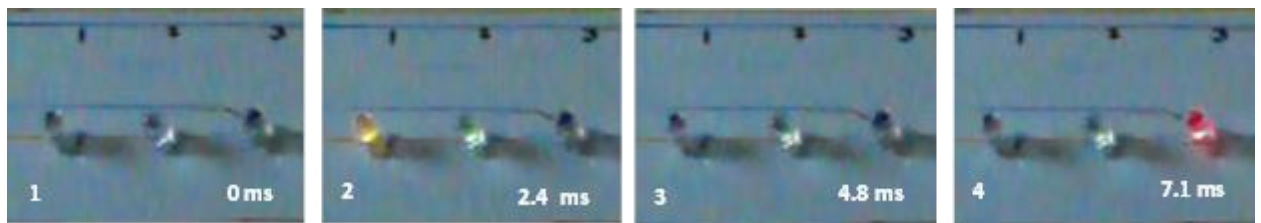


Figure 6.27. Video frames from the light panel , using 7.2 g PETN plus standard detonator as charge, inside a 1000 litres water container.

From only one reference point of the water container wall was recorded the time lines of the contact point, represented by the orange LED, the head start of 1 cm represented by the green LED and the final push at 2 cm represented by red LED.

The response time to the container wall move 1 cm was 2.4 ms (represented by green LED) and for move 2 cm was 4.7 ms (represented by red LED). This new distance measurement prove to be viable. However, the time line between the contact point and the 1 cm distances couldn't be recorded because the camera was not fast in of to capture it (could be achieved using 1000 fps sequence).

For posterior works in order to improve the distance-time set up the switch mechanism could be improved and the time recorded could to be improved as well by changing it to a faster camera 1000 fps.

7. SYNTHESIS AND CONCLUSIONS

The present study shows the behavior of WBWG, based in two different water plastic containers (25 litres and 1000 litres), having in the center a detonator inside a cylindrical explosive charge. The explosive charges used were ammonium nitrate with fuel oil (ANFO) emulsion and pentaerythritol tetranitrate (PETN) detonating cords (12 g/m). The explosives detonation properties were predicted using a thermochemical computer code, named THOR. For the expansion of the detonation products of the explosives was applied JWL EoS. Good adjustment (between the theoretical adiabatic and isentropic curves, from CJ point, obtained by THOR code, and predicted expansion curve using JWL equations) allow to define and optimize JWL parameters to a minimum difference with an auxiliary quadratic function, under different restricted conditions and a function of the Microsoft Excel ®:

- the Grüneisen coefficient from the exponential of the adiabatic curve;
- the Grüneisen coefficient from the exponential of the isentrope curve at a limit adimensional volume;
- the Grüneisen coefficient from the exponential of the total expansion of isentrope curve and, at last;
- the Grüneisen coefficient and the parameter C of JWL deduced by Caroline (Handley, 2011). (This final assumption reveals to be not suitable).

The best results were obtained using the Grüneisen coefficient from the exponential of the total expansion of isentrope curve, which were $\omega = 0.328$; $C = 3.6 \text{ GPa}$; $A = 90 \text{ GPa}$; $R_1 = 5$; $B = 90 \text{ GPa}$; $R_2 = 2.9$ for ANFO emulsion and $\omega = 0.356$; $C = 2 \text{ GPa}$; $A = 2343.6 \text{ GPa}$; $R_1 = 7.9$; $B = 47.6 \text{ GPa}$; $R_2 = 2.4$ for PETN.

The dimensions and design configurations of the experimental WBWG suffers a few alterations on the pressure plate setup since to the experimental WBWG within the 25 litres container shows a strong attenuation effect of pressure wave inside the used oil tube. Therefore the original tube of 5 mm inside the steel plate was changed to one with 10 mm plus the connection tube from the steel plate and the pressure sensor to one also with 10 mm and more rigid. The PETN experimental WBWG within the water plastic cubic meter proves a strongly reduced of the attenuation effect using this new pressure setup.

A blast type experiment was described and shows and demonstrate the time line of detonation wave until reaches the plastic wall, using 3 g of PETN (detonator No. 8 plus 2.4 g charge of PETN detonation cord), less than 2.1 ms, and also shows the flame wave and expansion gases from the detonation.

Autodyn 2D and 3D simulation of WBWG were performed using a cubic meter water container (1000 litres) for both explosive. The obtained results show the possibility of having these explosive charges without destruction of WBWG containers. Since water pressure levels, close to plastic walls, under maximum admissible charges, are closed to 6 MPa. This simulation also proves the possibility of a new non-destructive method to collect detonation products of small charges.

At last, experimental results were performed to:

- 5 g, 10 g and 15 g charge of ANFO emulsion using a cubic meter container;
- 0.8 g charge of PETN corresponding to the standard detonator No. 8 within the 25 litres container;
- detonator No. 8 plus 2.4 g charge of PETN detonation cord also within the 25 litres container, and;
- 7.2 g charge of PETN plus the standard detonator within the 1000 litres container.

Experimental results within the cubic meter container validate simulations non-destructive method to collect detonation products. It is always observed the elastic deformation of containers wall, under the water shock reflections, changing from its original cubic shape to a transient spherical one. Obtained results prove the validity of simulations, confirming central blasting phenomena process for the generation of an exterior blast generator.

REFERENCES

Ambrósio, J. Ferreira, R. Mendes, R. and Campos, J. "Prediction and experimental results of confined underwater blasting generators". *44rd International Annual Conference of ICT*. 2013.

Ambrósio, J., Gois, J., Campos, J., Santos, P., Duarte, B., Oliveira, N., Pereira, J. and Lourenço, P. "Shock and Blast Behavior of Confined Underwater Blasting Generators". *EFEE - 7th world conference on explosives & blasting*, 2013.

ANSYS. "ANSYS ® AUTODYN ® Explicit Software for Nonlinear Dynamics". 2006

Baudin, G. and Serradeill, R. "Review of Jones-Wilkins-Lee equation of state". *EPJ Web of Conferences*. 2010, Vol. 10 00021, pp. 1-4.

Durães, L. and Campos, J. "Thermodynamic predictions of pollutants using a new equation of state". *3rd International Conference on Combustion Technologies for a Clean Environment*. 1995, Vol. II, pp. 116-123

Durães, L., Campos, J. and Gois, J. C. "New equation of state for the detonation products of explosives". *Proceedings of the conference of the American Physical Society topical group on shock compression of condensed matter*. 13-18 de Aug de 1995, pp. 385-388

Fairlie, G. E. "The numerical simulation of high explosives using AUTODYN - 2D & 3D". *Explo'98, Institute of Explosive Engineers 4th Biannual Symposium*, 1998

Fried, L. and Souers, P. "CHEETAH: A Next Generation Thermochemical Code". 1994.

Gibbs, T. and Popolato, A. "LASL explosive property data". *Los ALAMOS series on Dynamic material Properties*. 1980. ISBN: 0-520-04007-4.

Handley, Caroline A. "Numerical modelling of two HMX-based plastic-bonded explosives at the mesoscale". *Thesis submitted for the degree of Doctor of Philosophy of the University of St Andrews*. 2011.

Henderson, Leroy F. "General Laws for Propagation of Shock Waves through Matter". [book auth.] Gabi Ben-Dor, Ozer Igra and Tov Elperin. *Handbook of Shock Waves*. s.l. : Academic Press, 2001, Vol. I, 2, pp. 143-169.

Kerley, G. and Christian-Frear, T. "Prediction of Equations of Explosive Cylinder Tests Using State from the PANDA Code". 1993.

Marsh, S. "LASL Shock Hugoniot Data". *Los ALAMOS series on Dynamic material Properties*. 1980. ISBN: 0-520-04008.

Morley, J. "Shock compression of water and solutions of ammonium nitrate". *Thesis Submitted for the Degree of Doctor of Philosophy*. June 2011

MSC.Software.. "MSC.Dytran 2005 Release Guide". 2005.

Nadykto, B.A. "Equation of state of HE detonation products". *EPJ Web of Conferences*. 2010, Vol. 10 00008, pp. 1-7.

Plaksin, I. and Campos, J.. "Blast Wave Generator Based on PBX Enclosed in Water Container". [ed.] Fraunhofer-Institut für Chemische Technologie. Proc. of the 5th European Symposium on Non-Lethal Weapons, 2007.

Simões, P., Carvalheira, P., Portugal, A., Campos, J., Durães, L. and Gois, J. "Characterization of 2-oxy-4,6-dinitramine-s-triazine". [ed.] D. W. S. Werbeagentur e Karlsruhe Verlag GmbH. *27th International Annual Conference of ICT*. 25.28 de June de 1996, p. 136.1.136.13.

Suceska, M. "Detonation". [ed.] Fraunhofer-Institut für Chemische Technologie. *Proc. of 4th Workshop on Pyrotechnics Combustion Mechanisms*, 2007.

Tarver, C. and Urtiew P. "Theoretical and Computer Models of Detonation in Solid Explosives". *Lawrence Livermore National Laboratory*. 1997. UCRL-JC-128755.

Tang, P. K. "Modeling PBX 9501 overdriven release experiments". *Los Alamos National Laboratory, Los Alamos, New Mexico 87545*. November 01, 1997, Vols. LA-UR-97-2855 ; CONF-970707, pp. 1-5.

Tavares, Bruno and Campos, J. "Prediction and experimental results of confined underwater blasting generators". 2012.

Complementary reference:

Clark Souers, P. "JWL Calculating". *Lawrence Livermore National Laborator*. 2005, UCRL-TR-211984.

Durães, L. "Simulação e análise de sistemas gasosos decorrentes da decomposição de materiais energéticos". *Dissertação para obtenção do grau de Mestre em Engenharia Química*. 1999.

Durães, L. Campos, J. and Portugal, A. "Thermodynamical prediction of combustion and detonation properties using modified THOR code". 1995

Durães, L., Campos, J. and Portugal, A. "Reaction path of energetic materials using THOR code". *AIP - The Journal of Chemical Physics*. 1997.

Dunnett, J. Swift, D. and Braithwaite, M. "Comparison of Williamsburg and JWL Equations of state for Nitromethane". *Proceedings, Eleventh International Detonation Symposium*. 1998.

Fickett, W. and Scherr, L. "Numerical Calculation of the Cylinder Test". *Los Alamos National Laboratory*. 1975. LA-5906, UC-32 and UC-45.

Fomin, V. Kraus, E. and Shabalin, I. "A few-parameter equation of state of the condensed matter and its application to the impact problems". *EPJ Web of Conferences*. 2010.

GEMS Sensors & Controls. "3100 Series Compact High Pressure OEM Pressure Transmitter". GEMS Sensors & Controls catalog.

GEMS S Sensors & Controls. "3100 Series and 3200 Heavy Duty Series". GEMS Sensors & Controls catalog.

GEMS Sensors & Controls. "Operating & Installation Instructions - Series 3100/3200". GEMS Sensors & Controls catalog.

Green, L. and Lee, E. "Detonation pressure measurements on PETN". *13th International Detonation Symposium*. 2006. URCL-CONF-222433.

Hamashima, H. Itoh, S. Sumiya F. and Kato, Y. "Numerical Calculation of Detonation Phenomenon for Emulsion Explosives". 2006.

Headquarters, U.S. army materiel command. "Explosives series properties of explosives of military interest". *Engineering design handbook*. 1971.

Headquarters, U.S. army materiel command. "Principles of explosive behavior". *Engineering design handbook*. 1973. AD900260.

Itoh S. and Hamashima H. "Determination of JWL parameters from underwater explosion test". *Detonation Symposium*, 2002.

Kato, H. Kaga, N. Takizuka, M. Hamashima, H. and Itoh, S. "Research on the JWL Parameters of Several Kinds of Explosives". *Materials Science Forum*, Vols. 465-466 (2004) pp 271-276. 2004.

Liu, Zhi-Yue. "Chapter 2 - Basics of detonation theory and numerical calculation". *Kumamoto University PhD-Thesis*, 2001.

Liu, Zhi-Yue. "Chapter 3 - Equation of state for explosives at overdriven detonation regime". *Kumamoto University PhD-Thesis*, 2001.

Mader, C. Johnson, J. and Crane, S. "Los ALAMOS explosives performance data". *Los ALAMOS series on Dynamic material Properties*. 1982. ISBN: 0-520-04007-4.

Meyer, R. Kohler, J. and Homburg, A. "Explosives". WILEY-VCH. 2002.

NTIS. "Engineering design handbook. Explosives series. Explosive trains". *NTIS - National Technical Information Service*. 1974. AD 777 482.

APPENDIX A - THOR EXECUTION PROCEDURE

The THOR operation system has an execution procedure, follows an example that illustrate the THOR platform and the steps taken. The simulation interfaces will be conducted only for one explosive in study, the PETN, as an example.

For the first step was needed to specify the reagents of the base mixture in study, i. e., explosive plus water, and then the possible products of the chemical reaction. Follows the composition of the mixtures used on THOR:

Table A.1. Composition of the mixtures used on the THOR code.

	Mixture	Designation	Mol/kg
emulsion ANFO	$H_4N_2O_3$	Ammonium nitrate	2
	$C_{10}H_{17.963}$	Fuel Oil	0.05
	$N_{1.5788}O_{0.4212}$	Air	0.002
	H_2O	Fresh Water	0.9
PETN	$C_5H_8N_4O_{12}$	PETN	10
	$N_{1.5788}O_{0.4212}$	Air	0.046

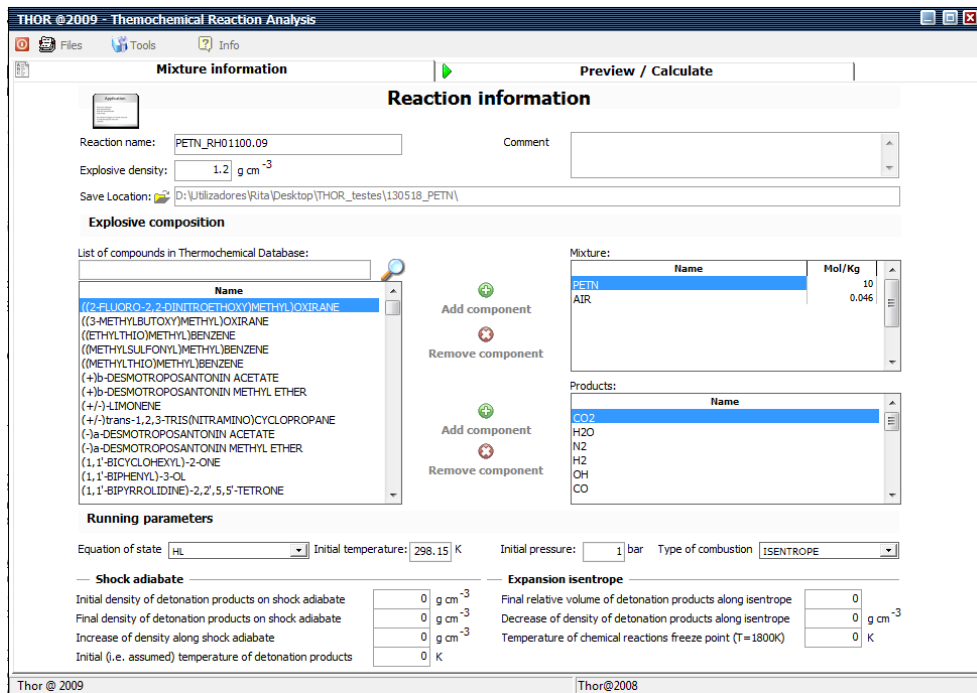


Figure A.1. An example of the interface of the reaction information of the program THOR using PETN.

The THOR code relies on a thermochemical database where all the properties of the compounds are described, as their Gordon & McBride polynomial coefficients. This thermochemical database can be visualized by clicking in Tools (Tools) then on thermochemical database.

The screenshot shows the 'Thermochemical Database' window. On the left, a search bar contains 'petn' and a list of compounds is shown, with 'PETN' highlighted. The main area displays the chemical structure of PETN, $C_5H_8N_4O_{12}$, and its properties. The properties table is as follows:

Property	Value	Units
Molecular Weight	316.138	g
Oxygen Balance	-10.12	%
Phase	Gas	
State	Solid	
Class	Energetic fillers	
Enthalpy	-532.2048	$kJ\ mol^{-1}$
Entropy	7376.392	$J\ mol^{-1}\ K^{-1}$
C_p	339.95	$J\ mol^{-1}\ K^{-1}$
Density	1778	$kg\ m^{-3}$
Enthalpy	-127.202269248	$kcal\ mol^{-1}$
Entropy	1763.03145192	$cal\ mol^{-1}\ K^{-1}$
C_p	81.2514495	$cal\ mol^{-1}\ K^{-1}$

Below the properties table, there is a section for 'Known Properties' with a table:

property	Value	Units	Remarks	Source
density	1778	$kg\ m^{-3}$		63
difference enthalpy-energy	-7.1	$kcal/Mol$		528
enthalpy of formation	-128.8	$kcal/Mol$		C
enthalpy of formation	-127.2	$kcal/Mol$		STB
enthalpy of formation	-126.8	$kcal/Mol$		121
enthalpy of formation	-121.03	$kcal/Mol$		88

The 'Literatura' section lists: R. Weinheimer (Chairman, IPS Wall Chart Committee) Properties of Selected High Explosives Proceedings of the Eighteenth International Pyrotechnics Seminar.

Figure A.2. An example of the interface of the thermochemical database of the program THOR – selecting PETN.

When the compound doesn't have Gordon & McBride polynomial coefficients, they can be found at the NASA Thermo Build site ([http:// www.grc.nasa.gov/ WWW/ CEAWeb/ ceaThermoBuild.htm](http://www.grc.nasa.gov/WWW/CEAWeb/ceaThermoBuild.htm)) or JANAF thermochemical tables.

As was mentioned above, in this methodology the THOR needs the information of possible products of the reaction. They also can be achieved by NASA Thermo Build site. For a correct determination of the reaction products we must identify all the possible products compounds of the reaction (20 compounds in the maximum) and in the correct order of formation. The product compounds formed and at a larger fraction must be identified primarily for a correct simulation of the THOR code. This first compounds are the determiner factor for the explosive chemical reaction, the other products that follows are the consequence of that first reaction. The products compounds that are formed at a larger fraction are CO_2 , H_2O and N_2 , so they must be identify in first. The next table shows the products compounds that were predicted to be formed on the chemical reaction for both explosives. Only the four first products are formed at a larger fraction the others products that follows are the consequence of that first reaction, so his order is less important.

According with the reagents of the reaction the NASA platform can provide the different combinations that can be formed and we select the more suitable ones for our conditions.

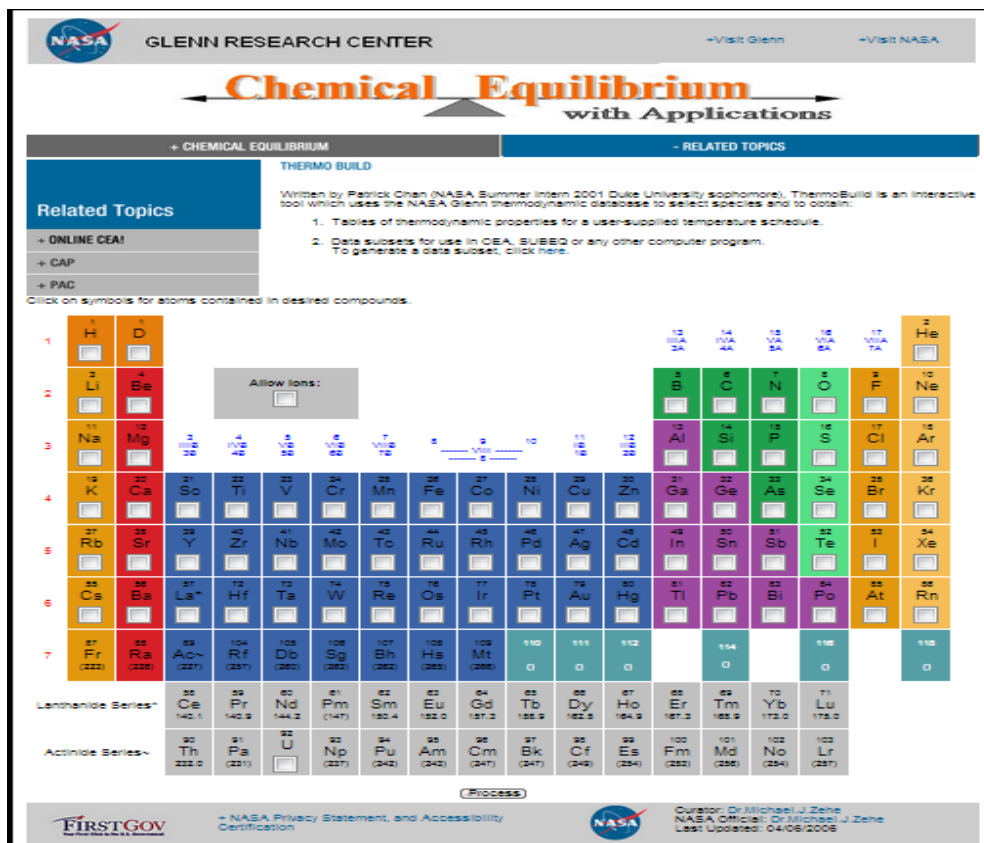


Figure A.3. NASA Thermo Build interface.

Both explosives used a system of C, H, N and O. On the NASA platform we select that compounds and it process all the combinations. According with the provide data we chose the most viable ones for our reaction. And since the THOR code need the Gordon & McBride polynomial coefficients, this web site also can provide that information only need to know is the compound that we are looking for and the thermal conditions that we are working with.

After we determined the mixture and the products, the next step is running the THOR program. Assuming the H_L equation of state, the thermochemical reaction was study for different conditions (type of combustion), CJ detonation, adiabatic dynamic and isentrope.

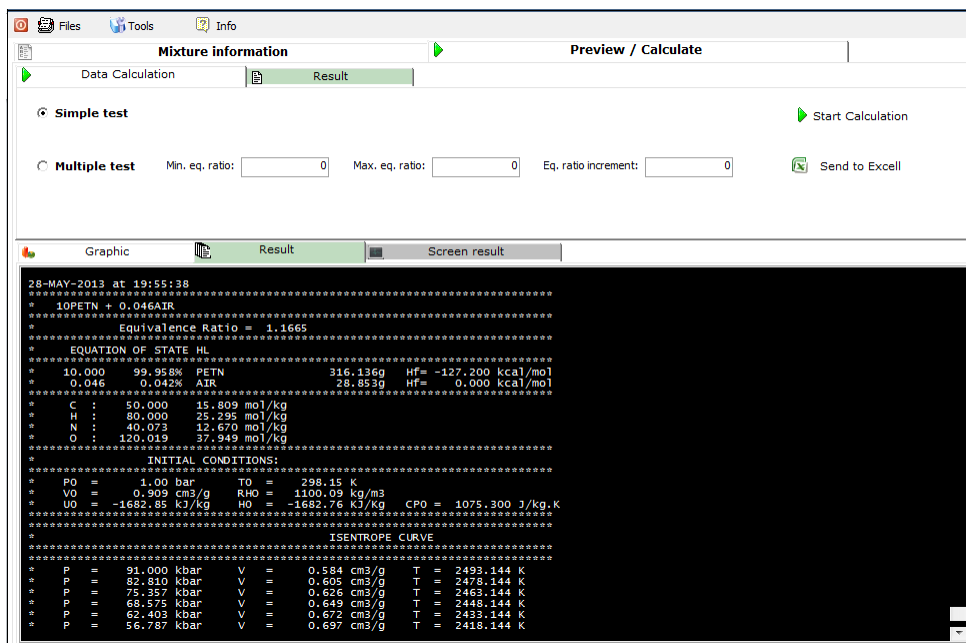


Figure A.4. An example of the interface of the Preview / Calculate of the program THOR – for PETN in the isentropie condition.

All the data given by the program THOR code after running it is automatically transferred and saved for a folder of the computer.

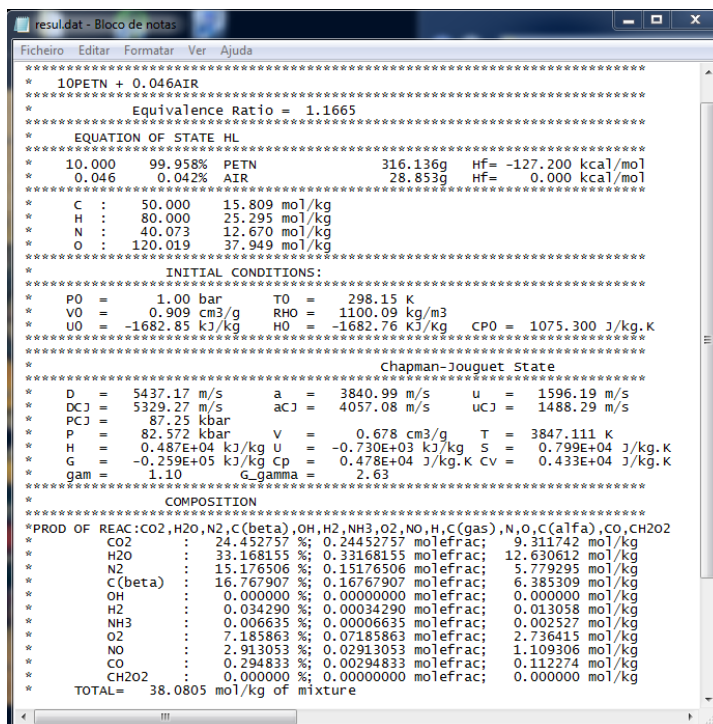


Figure A.5. An example of the interface of the data given by the THOR – for PETN in the detonation condition.

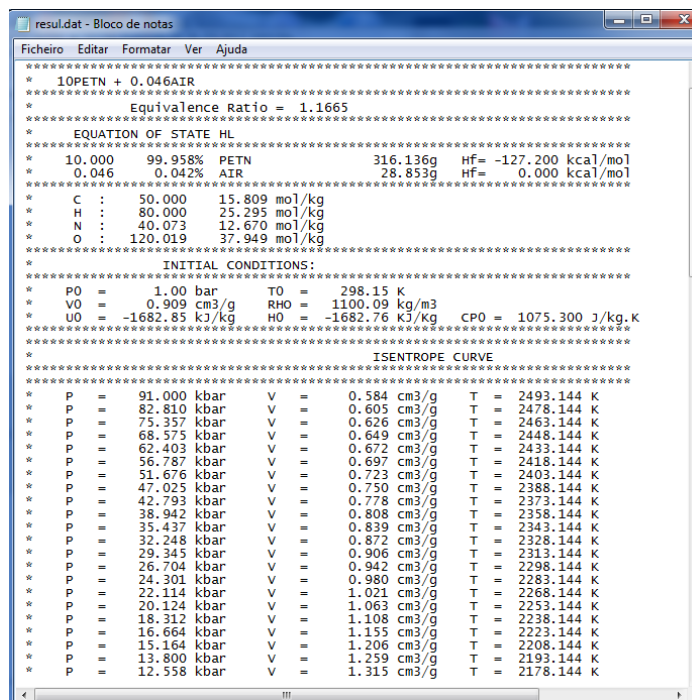


Figure A.6. An example of the interface of the data given by the THOR – for PETN in the isentropic condition.

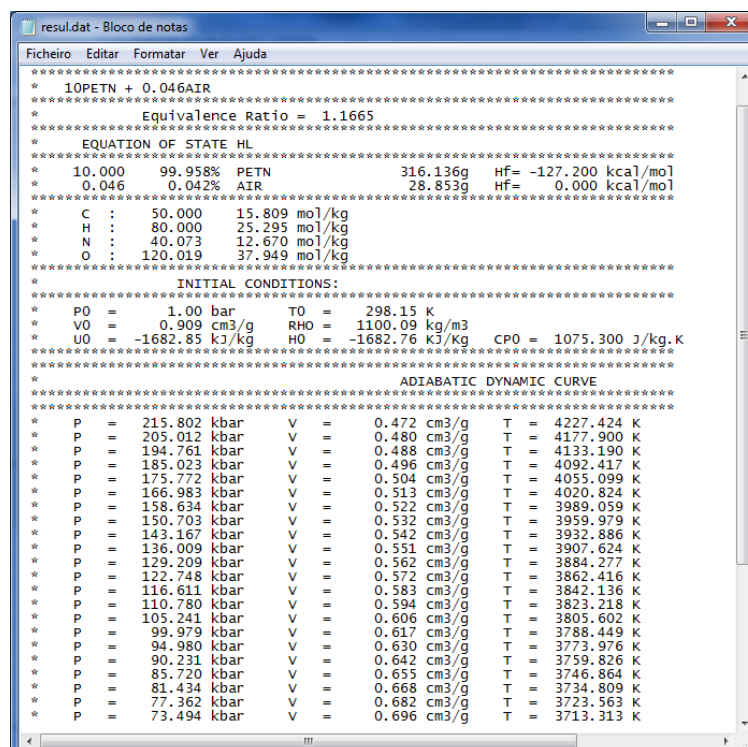


Figure A.7. An example of the interface of the data given by the THOR – for PETN in the adiabatic dynamic.

APPENDIX B - MICROSOFT EXCEL SOLVER EXECUTION PROCEDURE

All the experimental data about the CJ detonation, adiabatic dynamic, and isentropic regimes achieved from THOR was transferred to Microsoft Excel. In this new platform all the database was treated in order to find the JWL parameters.

The Excel Solver is used to optimize linear and nonlinear problems. In this work this supplement of the Microsoft Excel is used for minimize the difference between theoretical and experimental curves in order to match both of them, with an auxiliary quadratic function that correlates the difference values of both functions points. And so, the Solver is going to minimize that difference providing an optimized values for the JWL parameters.

This tool Solver is a “supplement” of the Microsoft Excel, and couldn’t be available on the menu “data” and so is need to be activated. For that go to the menu “file” and submenu “options”:

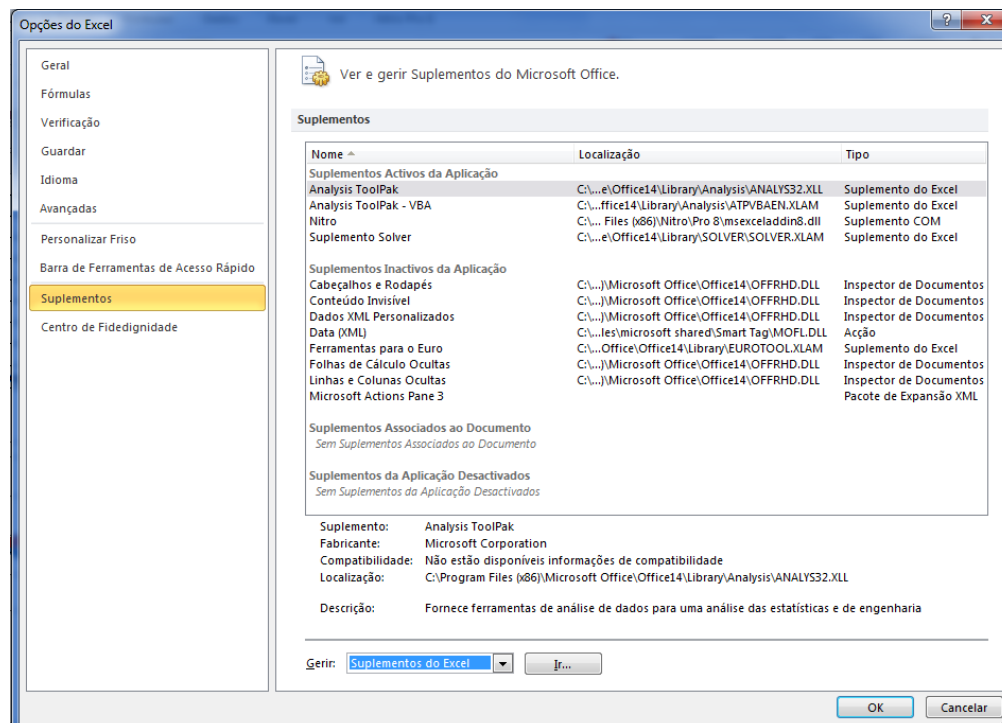


Figure B.1. Interface of the Excel options of the menu "file".

At the “supplements” click in manage Excel supplements and then enable supplement Solver.

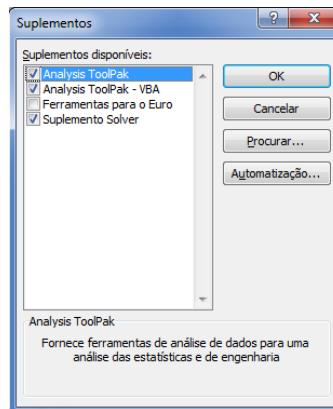



Figure B.2. Supplement menu of the interface Excel options from the menu "file".

After the command “Solver” ( Solver) be available on the menu “data” we can proceed for the optimization of the minimum deflection of both curves, theoretical and experimental, changing the variables of experimental curve, the JWL parameters (A , B , C , R_1 , R_2 and ω).

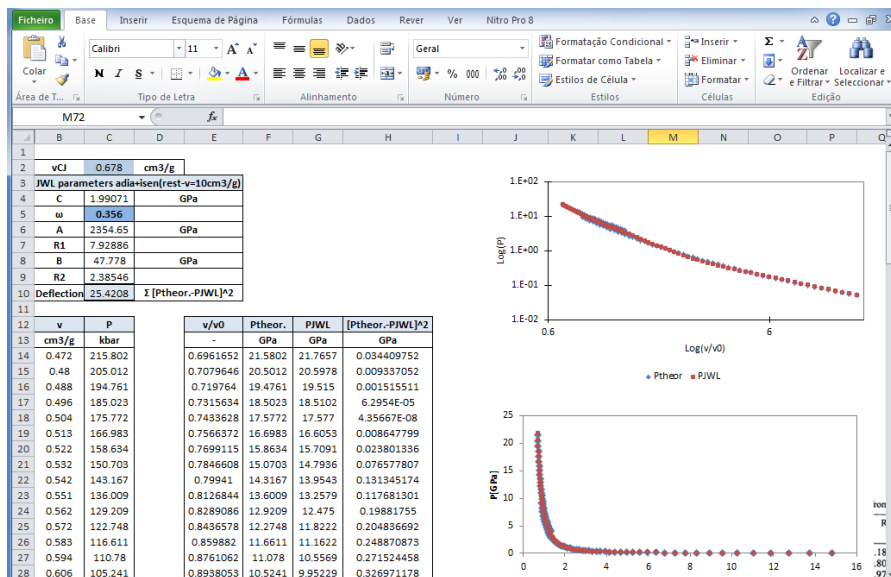


Figure B.3. Interface of the Microsoft Excel – JWL parameters calculation.

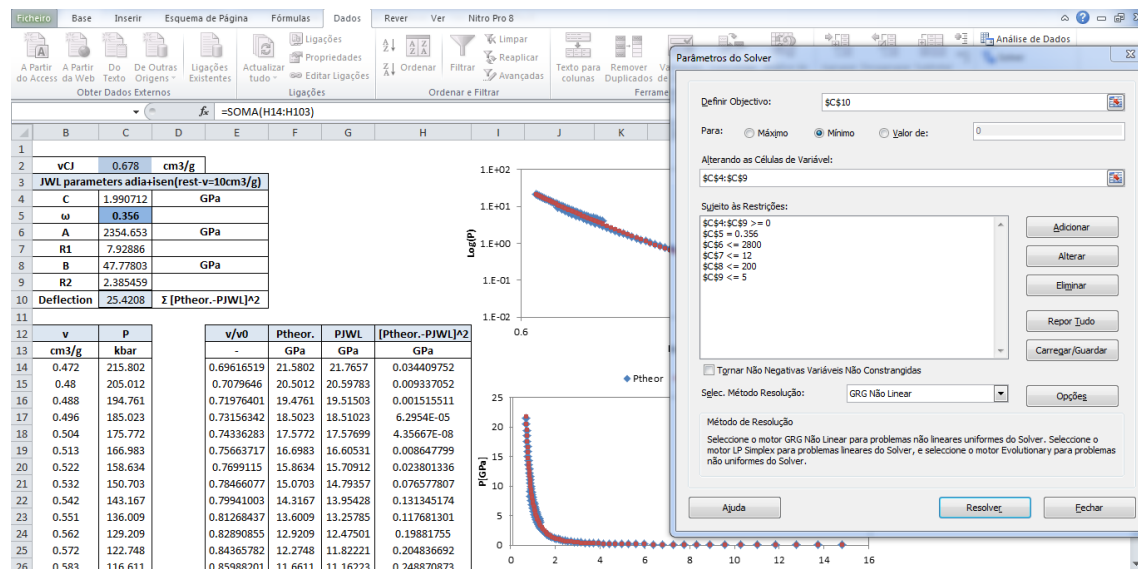


Figure B.4. Interface of the Solver implementation.

The Solver needs to identify the locations (cells) of objective function, decision variables, nature of the objective function (maximize/minimize/value) and constraints. And so, since the objective is to match the experimental curve, P_{JWL} , with the theoretical curve, P_{theor} , a quadratic function is created to measure the deflection between each Pressure point as $[P_{theor} - P_{JWL}]^2$ and minimized it, therefore the objective function that the Solver needs minimize is the sum of all the deflection values ($\sum [P_{theor} - P_{JWL}]^2$). Defining as the objective function of the Solver the sum of all deflection values allows it to minimize all the different points related to the experimental pressure. Then the variables that are going to be changed for minimizes the deflections of both curves are the JWL parameters. The previous image shows an interface of a possible way to calculate the JWL parameters using the Solver. For Solver simulation can be used constrains in order to optimize the JWL parameters values to more accepted and real values like is shown on the following image, for example an exactly value for one of the parameters of the JWL equation and limits for the remained ones.

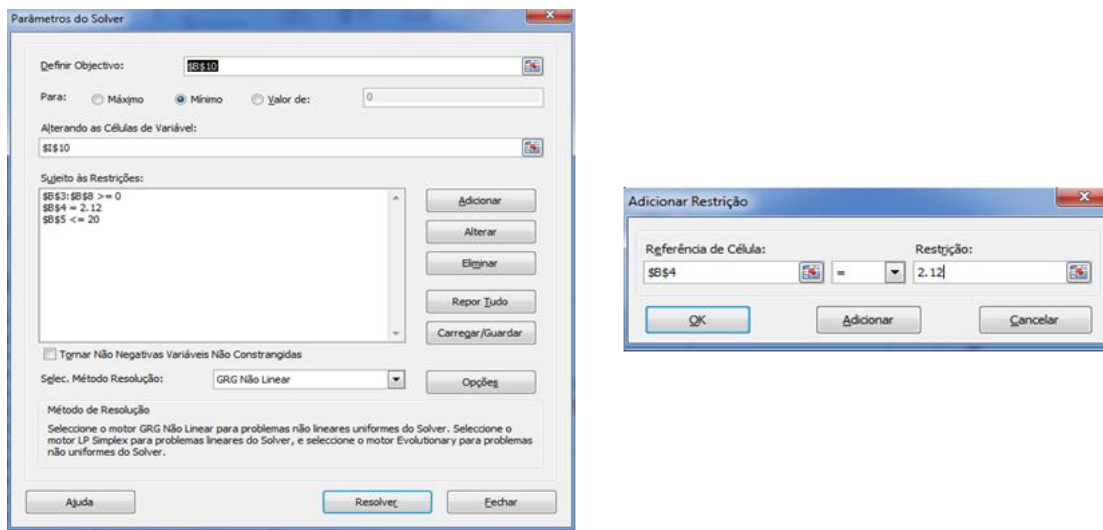


Figure B.5. Interface of an example of the possible restrictions used on the Solver parameters box.

As the previous images shows, the theoretical curve of the detonation products created by the union of the evolution of isentrope and adiabat curves obtained by THOR code is compared with the experimental curve, i.e., is compared to the JWL EoS for the same adimensional volume points, and using the previews function of the Excel, the Solver, the JWL parameters were achieved.

For the JWL parameters were used different approaches:

1. The first one is related to the adiabatic evolution obtained by THOR code. Using a double logarithmic $Y = Y(x)$ plot, as was shown on the previous graphics, the global approach of a power trend line shows a linear evolution of the curve. At a double logarithmic $Y = Y(x)$ plot approach to the adiabatic and isentrope evolution curves, we can verify an increasing slope on the adiabatic curve;
2. The second one is related to the isentrope evolution for two assumptions, one for a limit interval of adimensional volume values from the expansion reaction, and the other was for all the values obtained by THOR simulation program representing an longer expansion and a lowest exponential value;
3. The last one is based on Caroline assumption only for detonation products on the isentrope evolution with an appropriate value for the parameter C of the JWL EoS (Handley, 2011). (This final assumption reveals to be not suitable).

APPENDIX C - AUTODYN MATERIAL DATA INPUT

Follow an example of the interface of the Autodyn material data input for PETN charge simulation.

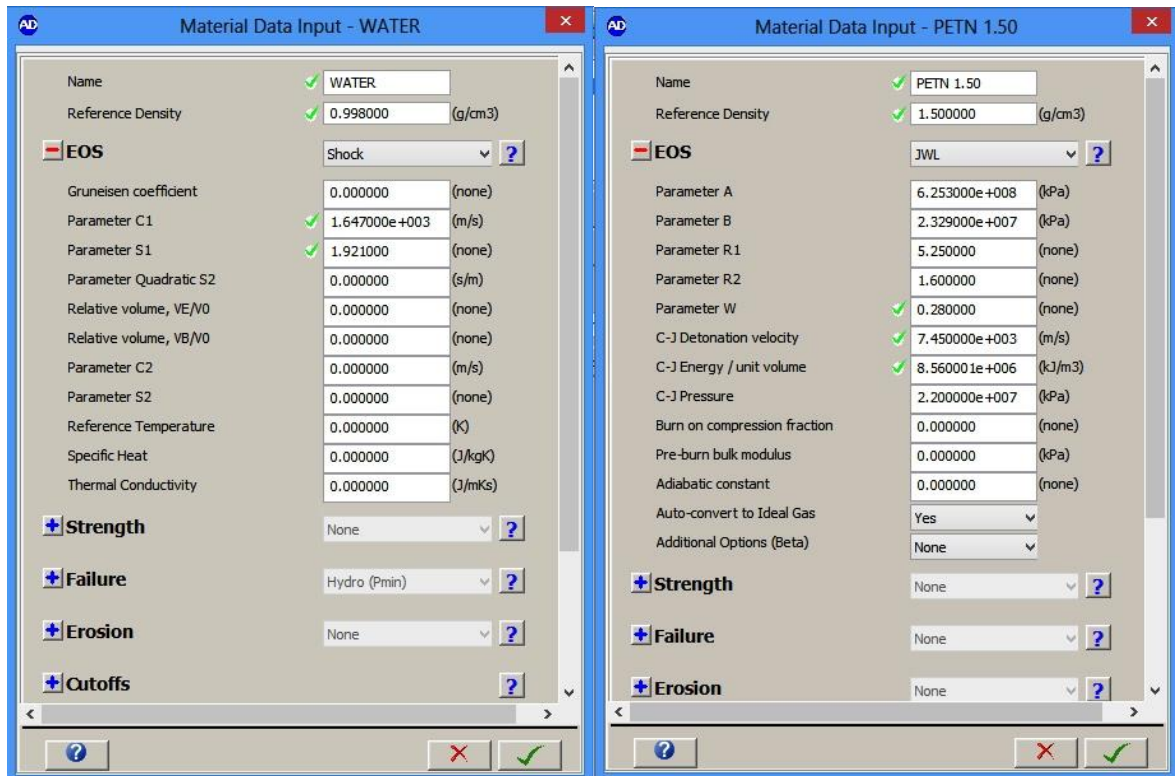


Figure C.1. Interface of the Autodyn material data input – water in the left and PETN on the right.

